Lateral Torsional Buckling of Timber Built-up Beams

by

Robabeh Robatmili

Thesis submitted to the University of Ottawa

in partial Fulfillment of the requirements for the degree of

Master of Applied Science

in Civil Engineering

Under the auspices of the Ottawa-Carleton Institute for Civil Engineering

uOttawa

Department of Civil Engineering

Faculty of Engineering

University of Ottawa

Abstract

Built-up timber beams consist of individual lumber laminations connected together using mechanical fasteners such as nails, bolts and screws. Lateral torsional buckling (LTB) is an important failure mode that needs to be considered in deep beams with long spans and insufficient lateral supports. Due to the mechanical connectors, built-up beams are expected to have a lower moment capacity compared with solid beams with similar dimensions. The behaviour of built-up beams is greatly affected by the stiffness of the fasteners joining the individual laminations and determining the level of partial composite action attained in the beam. The current research aims to investigate the buckling behaviour of timber built-up beams. This is done by initially investigating the important parameters that play a role in the behaviour through an extensive sensitivity analysis. The focus of the analysis is on the contribution of the connections, since the buckling behaviour of individual solid timber beam element has been relatively well-established. Input parameters for the connection properties are obtained from joint level experimental tests. Finally, recommendations for specific fastener patterns and accompanying reduction factors on the buckling capacity relative to equivalent solid sections are developed and proposed.

Acknowledgments

I would like to acknowledge and give my warmest thanks to my supervisor, Dr. Ghasan Doudak, for his advice and financial support through all stages of this research. His dynamism, vision and motivation have deeply inspired me and taught me to carry out the research and present it as clearly as possible. I am extremely grateful for what he has taught me.

I would like to thank my colleague, Mr. Yang Du, for teaching me, always being available to help, and patience from the very first step of this research. Your knowledge and expertise helped me solve problems every time I got stuck during this research.

The help of my fellow graduate student, Mr. Esmaeil Morshedi, in lab was extremely appreciated. Thanks for all your assistance throughout the project.

I would like to give a special thanks to my husband, Hamed Masoumi, and my son, Hami Masoumi, and my parents as a whole for their continuous support and understanding when undertaking my research. Your prayer was what sustained me this far.

Table of Contents

List of Tables

List of Figures

Notation

Symbol	Definition
a	the maximum purlin space
A	lamination cross-section area
C_b	the equivalent moment factor
C_e	load eccentricity factor
C_w	the warping constant
d	beam depth
E	modulus of elasticity
E_L	modulus of elasticity along the longitudinal direction
E_R	modulus of elasticity along the radial direction
E_T	modulus of elasticity along the tangential direction
F	concentrated load applied at each node in FEM
G	shear modulus
G_{LR}	shear modulus about longitudinal and radial direction
G_{LT}	shear modulus about longitudinal and tangential direction
G_{RT}	shear modulus about radial and tangential direction
I_y	moment of initial in weak axis
I_z	moment of initial in strong axis
J	Saint Venant torsion constant
K_{across}	lateral stiffness of mechanical fasteners in across-longitudinal direction per unit length

K_{along}	lateral stiffness of mechanical fasteners in longitudinal direction per unit length
K_{ser}	lateral stiffness of mechanical fasteners based on Eurocode 5
K_E	elastic stiffness matrix
K_{Par}	lateral stiffness of mechanical fasteners, parallel to grain direction
K_{Per}	lateral stiffness of mechanical fasteners, perpendicular to grain direction
K_w	Withdrawal stiffness of mechanical fasteners
K_G	geometric matrix
L	beam length
L_e	the effective length of beam
L_u	the unbraced length of beam
M_{end}	end moment
M_u	the critical moment of simply supported beam under constant moment
M_{cr}	critical moment of beam
M_{FEM}	critical moment of beam achieved by FEM
M_{an}	Critical moment of beam achieved by analytical model
N_x	number of nodes in a single ply along x axis
N_y	number of nodes in a single ply along y axis
N_z	number of nodes in a single ply along z axis
P	magnitude of concentrated load applied on the mid-span of beam
P_{cr}	critical load of beam
U	internal strain energy
V	load potential energy gain
β	rotation about longitudinal direction
μ	Poisson's ratio
μ_{LR}	Poisson's ratio for deformation along the radial axis caused by stress along the longitudinal axes

μ_{LT}	Poisson's ratio for deformation along the tangential axis caused by stress along the longitudinal axes
μ_{RL}	Poisson's ratio for deformation along the longitudinal axis caused by stress along the radial axes
μ_{RT}	Poisson's ratio for deformation along the tangential axis caused by stress along the radial axes
μ_{TL}	Poisson's ratio for deformation along the longitudinal axis caused by stress along the tangential axes
μ_{TR}	Poisson's ratio for deformation along the radial axis caused by stress along the tangential axes
u	shear centre displacement along lateral direction
π_p	total potential energy
ρ_m	wood density
λ_i	eigenvalues
υ_i	buckling mode shapes

CHAPTER 1- Introduction

1.1. General introduction and research needs

In timber engineering, beam elements can be efficiently constructed by combining joist elements using mechanical fasteners in order to obtain larger cross-section and bridge longer spans. The use of smaller dimension joist elements instead of solid sawn beams is mainly attributed to their availability and cost efficiency. Such built-up beam elements typically consist of two to five plies of the same depth (CSA O86, 2019). Common mechanical fasteners used to connect the joist elements include nails, screws, bolts and split-rings. Figure 1.1 illustrates a 4-ply built-up beam fastened by screws.

Due to the discrete connections between the built-up beam plies and the fact that these connections have limited stiffness, the capacity of built-up beams are expected to be smaller than that of solid sawn beam with the equivalent cross-section. As a consequence of the non rigid nature of the connections, significant slip may occur between the beam lamination especially at large beam displacements or once buckling failure occurs. This in turn affects the geometrical properties, such as moment of inertia and torsional rigidity, compared to those obtained for solid members (Challamel and Girhamar, 2012).

Lateral torsional buckling is a probable failure mode in long-span and deep built-up beams that are not laterally restrained. The buckling failure load is significantly affected by the level of composite action between the plies comprising the built-up beam, which in turn is determined by the connections. In case of no composite action between the plies, each ply behaves individually,

and the buckling capacity of the beam can be obtained as the sum of the buckling capacities of the individual plies.

Any connectivity between the plies will produce a case with partial composite action, where the capacity of the beam is expected to be between the cases of full composite action and no composite action.

(a)

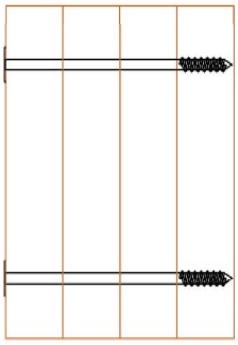

(b)

Figure 1.1 4-Ply built-up beam fastened by screws (a). 3D view; (b). Beam section

Although the Canadian wood design standard (CSA O86, 2019) includes detailed provisions for built-up columns, its built-up beam clause is not comprehensive in terms of the type and the

geometry of necessary fasteners to achieve a level of composite action. Some provisions on built-up beams are available in the National Building Code of Canada Clause 9.23.8.3 (NBCC, 2015); however, these provisions are limited to Part 9 buildings and are based on prescriptive requirements rather than engineering design. This lack of consistency in the design code has resulted in some designers simply assuming full composite action in design scenarios where it is not warranted, while others may completely ignore the connections between the individual plies of the beam and assume no composite action, which may be too conservative.

Within the above context, the reduction in capacity, caused by the partially rigid connections between the beam laminations when lateral torsional buckling failure is considered, will be investigated in this research through experimental testing on connections and numerical modelling representing the beam behaviour. The primary objective of the current research is to identify parameters affecting lateral torsional buckling capacity of built-up beams and examine the levels of composite action for different connection configurations. It is anticipated that the outcome of this study will help develop clear design guidelines and detailing for the buckling capacity of built-up beams.

1.1.1. Wood material properties

It is well-established that variability exists in wood's mechanical properties due to the nature of its growth conditions. Notably, this affects the strength and stiffness characteristics in relation to the grain direction. As such wood is considered to be an anisotropic material; however, when considering the orientation of the fibres, wood may be classified as orthotropic material with directions that are perpendicular to one another along the longitudinal axis (L), radial axis (R) and tangential axis (T), as illustrated in Figure 1.2.

The longitudinal axis is parallel to the grain; the radial axis is perpendicular to both the grain direction and the growth rings, whereas the tangential axis is perpendicular to the grain direction and tangential to the growth rings.

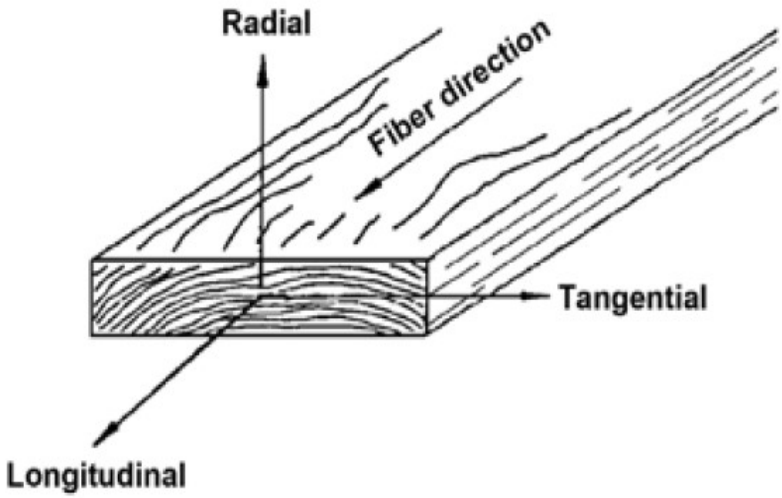

Figure 1.2 Three principal axes of wood (FPL, 2010)

In order to describe the orthotropic elastic behavior of wood, twelve mechanical properties are defined, including three moduli of elasticity (E), three shear moduli (G) and six Poisson's ratios (μ). The three moduli of elasticity are denoted as E_L, E_R and E_T, where the subscript refers to the longitudinal, radial and tangential directions, respectively. While E_L is derived from bending tests, E_R and E_T are typically obtained from the compression test (FPL, 2010). The Poisson's ratios include $\mu_{LR}, \mu_{RL}, \mu_{LT}, \mu_{TL}, \mu_{RT}$ and μ_{TR} which are the deformation perpendicular to loading direction divided by the deformation parallel to loading direction. For instance, μ_{RL} is the Poisson's

ratio in longitudinal direction originated by stress along the radial direction. The relationship between the moduli of elasticity (E) and the Poisson's ratio is shown in Equation (1.1).

$$\frac{\mu_{ij}}{E_i} = \frac{\mu_{ji}}{E_j},\ i \neq j, i, j = L, R, T \tag{1.1}$$

Moreover, the shear moduli are defined by G_{LR}, G_{LT} and G_{RT} and represent the elastic constant in LR, LT and RT planes, respectively.

1.1.2. Lateral torsional buckling behaviour of timber beams

Lateral torsional buckling is a failure mode in beams that occurs when members are not equipped with proper bracings to prevent lateral deflection and twisting (Ziemian, 2010). Figure 1.3 illustrates a reference case for lateral torsional buckling of a simply supported doubly symmetric beam with elastic behaviour under uniform end moments in the y-z plane.

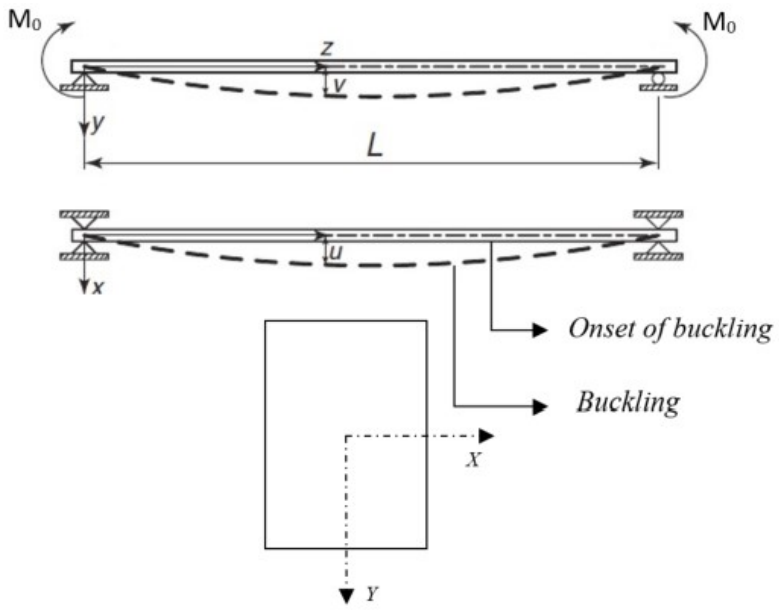

Figure 1.3 Lateral Torsional Buckling Reference Case (Galambos & Surovek, 2008)

The beam considered in the study illustrated in Figure 1.3 is subjected to a moment at each end about the strong axis, M_0. Accordingly, it undergoes vertical in-plane deformation in the y-direction, v, as shown in Figure 1.4.

By increasing the applied moment by a factor λ, from M_0 to λM_0, the beam would be at the onset of buckling (Figure 1.4), and the moment is therefore referred to as the critical moment, M_{0cr}. Beyond this point the beam is expected to buckle, and out-of-plane deformation, defined by the lateral displacement, u, and angle of twist, β, will cause instability in the beam. In addition, the beam may warp; however, such warping is typically insignificant in rectangular sections. Figure 1.4 shows the deformations of a simply supported rectangular section under end moments prior to and after lateral torsional buckling.

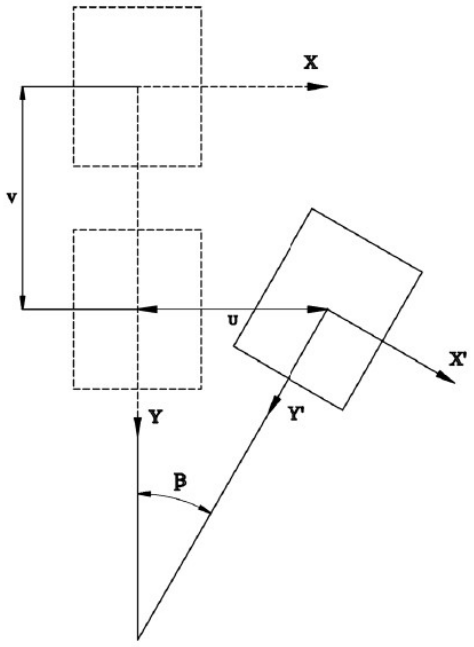

Figure 1.4 Cross-section deformation of beam before and after buckling

One of the lateral torsional buckling solutions for a simply-supported rectangular solid beam under uniform moment is obtained by applying the principle of stationary potential energy (Trahair, 1993). In the energy-based solution, the total potential energy of a beam, π_p (Equation (1.2), is expressed as the sum of internal strain energy U, Equation (1.3), and load potential energy V, Equation (1.4).

$$\pi_p = U + V \tag{1.2}$$

$$U = \frac{1}{2}\int_0^L EI_y u''^2 dz + \frac{1}{2}\int_0^L EC_w \beta''^2 dz + \frac{1}{2}\int_0^L GJ\beta'^2 dz \tag{1.3}$$

$$V = \int_0^L M_x(z)\beta(z)u''(z)dz \tag{1.4}$$

Where L is the unbraced length of the beam, defined as the distance between points providing lateral and torsional restraint. E is the modulus of elasticity, G is the shear modulus, u is the lateral displacement of the cross-section centre along the X-axis, β is the angle of twist about the z axis, C_w is the warping constant, J is the Saint Venant torsional constant, I_y is the moment of inertia about the weak axis and $M_x(z)$ is moment about the X-axis along the beam length.

By substituting Equation (1.3) and Equation (1.4) into Equation (1.2) the total potential energy can be expressed as follows:

$$\pi_p = \frac{1}{2}\int_0^L EI_y u''^2 dz + \frac{1}{2}\int_0^L EC_w \beta''^2 dz + \frac{1}{2}\int_0^L GJ\beta'^2 dz + \int_0^L M_x(z)\beta(z)u''(z)dz \tag{1.5}$$

By applying the principle of stationary potential energy $\delta\pi = \delta(U + V) = 0$, Equation (1.6) can be achieved:

$$\delta\pi_p = \int_0^L (EI_y u'' + M\beta)''\delta u dz + \int_0^L [(EC_w\beta'')'' - (GJ\beta')' + Mu'']\delta\beta dz + \left[\left(EI_y u'' + M\beta\right)\delta u'\right]_0^L - \left[\left(EI_y u'' + M\beta\right)'\delta u'\right]_0^L + \left[(EC_w\beta'')\delta\beta'\right]_0^L - \left[((EC_w\beta'')' - GJ\beta')\delta\beta\right]_0^L = 0 \quad (1.6)$$

By applying the stationary potential energy condition, Equation (1.6), and the boundary condition of the simply-supported beam according to Equations (1.7) and (1.8), the classical solution in Equation (1.9) is recovered.

$$u(0) = u''(0) = u(L) = u''(L) = 0 \quad (1.7)$$

$$\beta(0) = \beta''(0) = \beta(L) = \beta''(L) = 0 \quad (1.8)$$

$$M_u = \frac{\pi}{L}\sqrt{EI_y GJ + (\frac{\pi E}{L})^2 I_y C_w} \quad (1.9)$$

As mentioned earlier, the warping effect for a rectangular section can be considered insignificant. Equation (1.10) shows the simplified classical solution for a rectangular simply supported beam under uniform moment.

$$M_u = \frac{\pi}{L}\sqrt{EI_y GJ} \quad (1.10)$$

Another method of achieving the closed-form classical solution is assuming a displacement function for the lateral displacement and twisting angle. Based on the simply-supported boundary condition and uniform moment, assuming $u = Asin\left(\frac{\pi z}{L}\right)$ and $\beta = Bsin(\frac{\pi z}{L})$, by substituting the displacement fields in the Equation (1.5) one obtains:

$$\pi_p = \frac{1}{2}\int_0^L EI_y \left[Asin\left(\frac{\pi z}{L}\right)''\right]^2 dz + \frac{1}{2}\int_0^L EC_w \left[Bsin\left(\frac{\pi z}{L}\right)''\right]^2 dz + \frac{1}{2}\int_0^L GJ \left[Bsin\left(\frac{\pi z}{L}\right)'\right]^2 dz +$$

$$\int_0^L M\left[Bsin\left(\frac{\pi z}{L}\right)\right]\left[Asin\left(\frac{\pi z}{L}\right)\right]'' dz \quad (1.11)$$

By deriving the energy expression with respect to A and B and equating those to zero $(\partial\pi)/(\partial A) = 0$ and $(\partial\pi)/(\partial B) = 0$, the following matrix is obtained:

$$\begin{bmatrix} a_{11} & a_{12} \\ a_{21} & a_{22} \end{bmatrix} \begin{Bmatrix} A \\ B \end{Bmatrix} = \begin{Bmatrix} 0 \\ 0 \end{Bmatrix} \quad (1.12)$$

By setting the determinant of the above matrix to zero, one recovers the same classical solution as that presented in Equation (1.9).

The formula presented above is valid for simply-supported beams under uniform moments. In order to extend Equation (1.10) to different boundary conditions and loading patterns, either the effective length approach or equivalent moment factor method can be used, since no closed-form solution exist to calculate the critical moment for those cases.

1.1.3. Effective length approach

The effective length method was adopted by Hooley and Madsen (1964) and proposed as basis for the Canadian timber design approach to lateral torsional buckling design for single-span and cantilevered beams under several loading conditions. The authors also conducted experimental testing on glue-laminated beams to verify the proposed approach. In this method, the unbraced length of the beam is substituted by the effective length, as presented in Equation (1.13) (AFPA, 2003).

$$M_{cr} = \frac{\pi}{L_e}\sqrt{EI_y GJ} \quad (1.13)$$

Where L_e is the effective length of the beam, which is a function of the unsupported length, l_u, and the loading type.

In the case of no intermediate support, the unsupported length is taken as the distance between points of bearing or the length of the cantilevered. If the compressive edge of a bending member is prevented from lateral displacement, the unsupported length is then considered as the maximum spacing between lateral support points. The Canadian wood design standard (CSA O86, 2019) provides effective length for bending members for common cases of loading and support conditions, as presented in Table 1.1.

Table 1.1 Effective length, L_e, for bending members (CSA O86:19)

	Intermediate support	
Type of load	**Yes**	**No**
Beams		
Any loading	1.92 a*	1.92 lu**
Uniformly distributed load	1.92 a	1.92 lu
Concentrated load at centre	1.11 a	1.61 lu
Concentrated load at 1/3 points	1.68 a	-
Concentrated load at 1/4 points	1.54 a	-
Concentrated load at 1/5 points	1.68 a	-
Concentrated load at 1/6 points	1.73 a	-
Concentrated load at 1/7 points	1.78 a	-

Concentrated load at 1/8 points	1.84 a	-
Cantilevers		
Any loading	-	1.92 lu
Uniformly distributed load	-	1.23 lu
Concentrated load at free end	-	1.69 lu

*maximum length purlin space
**unsupported length, the distance between points of bearing or the length of the cantilever

1.1.4. Equivalent moment factor

Based on this method, the critical moment of a beam, M_{cr}, under any loading is calculated by multiplying the equivalent moment factor C_b by the critical moment of the reference case M_u, as expressed in Equation (1.14).

$$M_{cr} = C_b M_u \tag{1.14}$$

Where C_b is obtained by dividing the critical moment of the beam by the reference case (Equation (1.9).

The critical moment can be calculated using the energy method for different load and boundary conditions, and the equivalent moment factor is used to convert any loading scenario into an equivalent simply supported beam under bending moments at its ends.

1.2. Research objectives

In this study the lateral torsional buckling behavior of timber built-up beams in the linear domain will be analysed through a commercially available software using Finite Element Method (FEM).

Also, the parameters that influence the lateral torsional buckling capacity of built-up beams will be investigated.

The objectives of current study are as follow:

- Determine the parameters that can affect the Lateral Torsional Buckling (LTB) behaviour of built-up beams
- Conduct joint level experimental testing to establish typical stiffness of the mechanical fasteners used to join individual plies in built-up timber beams
- Evaluate the partial composite action of built-up beams through finite element modelling based on fastener stiffness obtained experimentally.
- Propose recommendations to the Canadian wood design standard on the levels of composite action for built-up beams based on specific fastener types, sizes and patterns.

1.3. Research methodology and scope

In order to establish an understanding of the parameters that affect the LTB capacity of built-up beams, a finite element model (FEM) was developed in ABAQUS (Simulia, 2014). The fasteners stiffness are obtained through joint level experimental approaches and used as the input in the FEM. This includes parameters related to lateral and withdrawal stiffness. The developed FEM is compared to the classical solution and to full-scale tests obtained from the literature on solid sections. In addition, the FEM of built-up beams will be compared with the analytical model proposed for built-up beams in the literature. Once the model is validated, a variety of configurations are investigated, and design provisions are developed and presented. The timber built-up beams analyzed in this study are limited to 2- to 4-ply beams consisting of Spruce-Pine-

Fir (SPF) lumber or laminated veneer lumber (LVL) laminations that are connected by common nails or screws.

1.4. Outline of the thesis

Chapter 1 provides the basic solutions for lateral torsional buckling of timber beams, current design approaches, as well as objectives and research methodology.

Chapter 2 provides a literature review on past studies on lateral torsional buckling of beams from the analytical and experimental perspective, with a focus on studies dealing with built-up beams.

Chapter 3 includes the finite element model description for built-up beams and the results from the sensitivity analysis related to the fasteners' stiffness and layout pattern and FEM validations.

Chapter 4 describes the experimental connection test setup and presents the results on lateral and withdrawal stiffness of the mechanical fasteners.

Chapter 5 presents analysis results for the level of composite action based on experimental inputs on fastener stiffness and specific recommendations for fastener types, sizes and layout patterns and corresponding levels of composite actions for the built-up beams in comparison with the equivalent solid sections

Chapter 6 presents the major conclusions of the present study and provides recommendations for future research.

CHAPTER 2- Literature Review

2.1. General

The lack of access to large dimension timbers have necessitated the introduction of built-up beams which have two types of vertical and horizontal laminations. Although the focus of this research is timber built-up beams with vertical laminations, it is worth mentioning the application of horizontal timber built-up beams which involved the construction of a deep beam by, for example, connecting small laminations through shear keys for a bridge girder (Jacob Leupold 1726). It was recognized that the capacity of the laminated built-up beams was significantly smaller than solid beams with the same dimension. Mahan (1886) and Rankine (1889) introduced built-up beams with multiple layers with inter-connected laminations. Miller (2009) developed an inter layer slip model to analyse any n-layer built-up beam connected with shear keys.

With increasing demand for timber built-up beams in construction specifically in railroad industry and bridges, researchers attempted to optimize the design of such beams through improving the lamination connection and decreasing the interlayer slip. Notable examples include work by Snow (1895) who suggested the use of steel shear keys for built-up girders. Parameters that may affect the composite action of the built-up beams have been explored by Forchheirmer (1982), where it was reported that the effect of the shear key orientation and size as well as clamping were influential to the capacity of the built-up beam.

The remaining of this chapter presents analytical and experimental research on the lateral torsional buckling of both solid and composite beams. Analytical research on LTB behaviour and the behaviour of composite beams will be discussed in Section 2.2 with highlights on a closed-form

solution for LTB capacity of timber built-up beams. In Section 2.3, literature on experimental testing of LTB of solid wood beams is presented. Finally, Section 2.4 summarizes all the experimental and analytical research discussed in this chapter and highlights the research needs.

2.2. Analytical research on lateral torsional buckling behaviour of solid and composite beams

2.2.1. Analytical research on solid beams

Zahn (1973) used energy-based solutions to develop formula that governs the equilibrium conditions for timber beams with rectangular cross-section and continuous lateral bracing along the beam length. The shear stiffness provided by the deck system was taken into account to provide a closed-form solution for investigating different load and support conditions. Zahn (1984) further investigated the effectiveness of lateral and torsional reinforcements in beam-deck systems under gravity loads.

AFPA (2003) investigated the effects of various parameters, including beam slenderness, load types, load heights and partial torsional restraints at beam ends. A formulation for lateral torsional buckling of a simply-supported beam with rectangular cross-section was presented for uniform moment loading. In addition, the formula for beams under different loading and boundary conditions were presented through the equivalent moment factor method or the effective length method.

Du (2016) studied the lateral torsional buckling behavior of wooden beam-deck systems. Closed-form solutions, energy-based approximate solutions and finite element solutions for the sway and non-sway models of beam-deck systems were formulated.

Hu et al. (2017a, 2018) developed an energy-based solution to investigate the effect of midspan lateral support on the LTB behaviour of wooden beams under two loading conditions including uniformly distributed load and midspan point load. In addition, the parametric study was performed to analyse the effect of lateral bracing and load height on LTB capacity of the beams. Also a FEM was used to model the beams that was in a good agreement with the analytical model.

2.2.2. Analytical research on composite beams

Early research on the behaviour of partially composite beams and columns under static loading have been undertaken by Stussi (1947), Granholm (1949), Newmark et al. (1951) and Pleshkov (1952). Their models were used as a foundation for future research on the behaviour of composite beams with interlayer slip which have been investigated by Amana and Booth (1967).

A closed-form solution was also formulated by Sapkas and Kollar (2002) for simply supported and cantilevered composite beams. Thin walled, open section, orthotropic composite beams subject to concentrated end moments, concentrated loads and uniformly distributed loads, including the effect of shear deformation, were analyzed.

Girhammar and Pan (2007) extended the model developed by Girhammar and Gopu (1993) through variational methods to propose differential equations for the deflection and internal actions of partially composite Euler-Bernoulli beams and beam-columns. The model included analysis of the structural elements under several static loading scenarios such as transverse and axial loading through first and second order analyses. The exact closed- form characteristic equations and their corresponding buckling length coefficient for composite beams with interlayer slip for four Euler

boundary conditions were derived. A maximum potential range for the relative bending stiffness for beams and beam-columns with partial interaction was developed.

Machado (2010) proposed an analytical solution for the lateral stability of cross-ply laminated thin-walled beams with large displacements and rotations induced by axial loading and bending. The study also considered the nonlinear pre-bucking geometrical deformations of the beams. By comparing the results with the classical solutions, it was demonstrated that the capacity derived from the classical solution was conservative.

Amadio and Bedon (2010) developed models to analyze the out-of-plane behaviour of laminated glass elements under flexural loads. The effects of crucial parameters to buckling capacity included degradation of the mechanical properties of the interlayer, load time variations and the degree of the initial imperfections.

The static buckling and free vibration of laminated composite plates were analyzed by Admin et al. (2016) through a refined shear deformation theory. The parabolic distribution of transverse shear stresses with no shear stresses on the top and bottom surfaces of the plates was considered.

Girhammar and Challamel (2012) derived a closed-form solution for the LTB capacity of vertically laminated beams. Figure 2.1 shows a 2-ply built-up beam with different material properties and geometry. The flexibility of fasteners caused slippage in longitudinal direction (Δu) in Figure (2.1.d), and transverse direction (Δv) of the laminations in Figure (2.1.b). Figure (2.1.c) illustrates the horizontal free-body diagram of a built-up beam, where M_z and V_y are the total moment and shear applied to the beam, and M_{z1}, M_{z2}, V_{y1} and V_{y2} are the moment, and shear, in lamination 1 and 2, respectively.

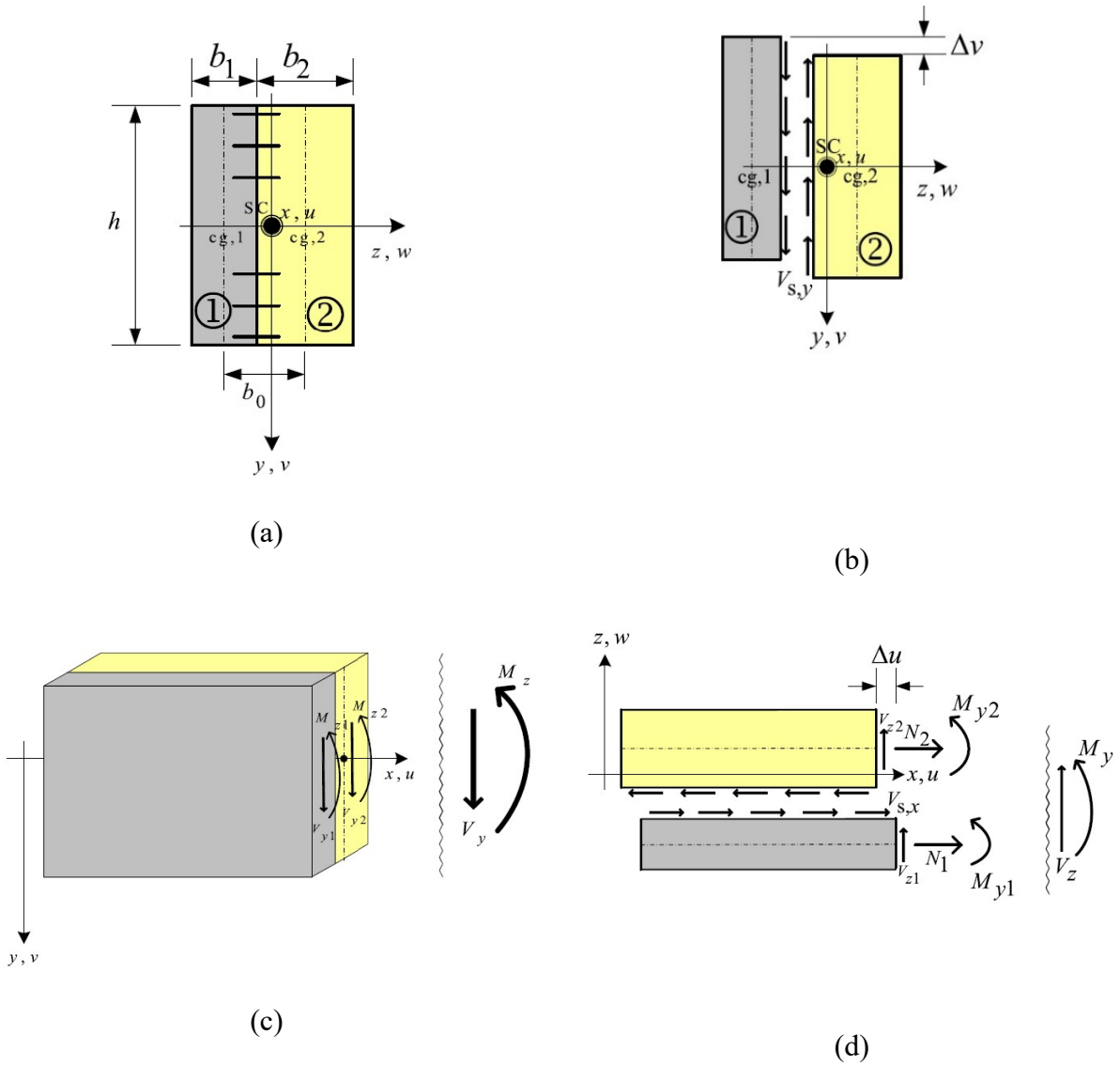

Figure 2.1 (a). Geometric parameters of partial vertically connected composite beam (x,y,z= coordinates; u,v,w= displacements; cg,1,cg,2=centroid (center of gravity) of sub-element 1 and 2, respectively, and SC=shear center); (b). Slip forces in the cross-longitudinal or vertical direction (the element is shown in non-deformed state with respect to rotation); (c). Horizontal and (d). Vertical view of beam element with transverse forces and moments defined positive as shown, including slip forces in the longitudinal or horizontal direction (the element is shown in non-deformed state with respect to lateral deflection); $h_1=h_2=h$; $b_0=(b_1+b_2)/2$. (Challamel & Girhammar, 2012)

The study proposed a formulation for the buckling capacity of a pinned-pinned partial composite built-up beam subjected to end moments, as shown in Figure (2.2.a), while considering the axial deformation, longitudinal and across-longitudinal slippage of the laminations. The deformed shape of the composite cross-section under lateral torsional bucking is shown in Figure (2.2.b).

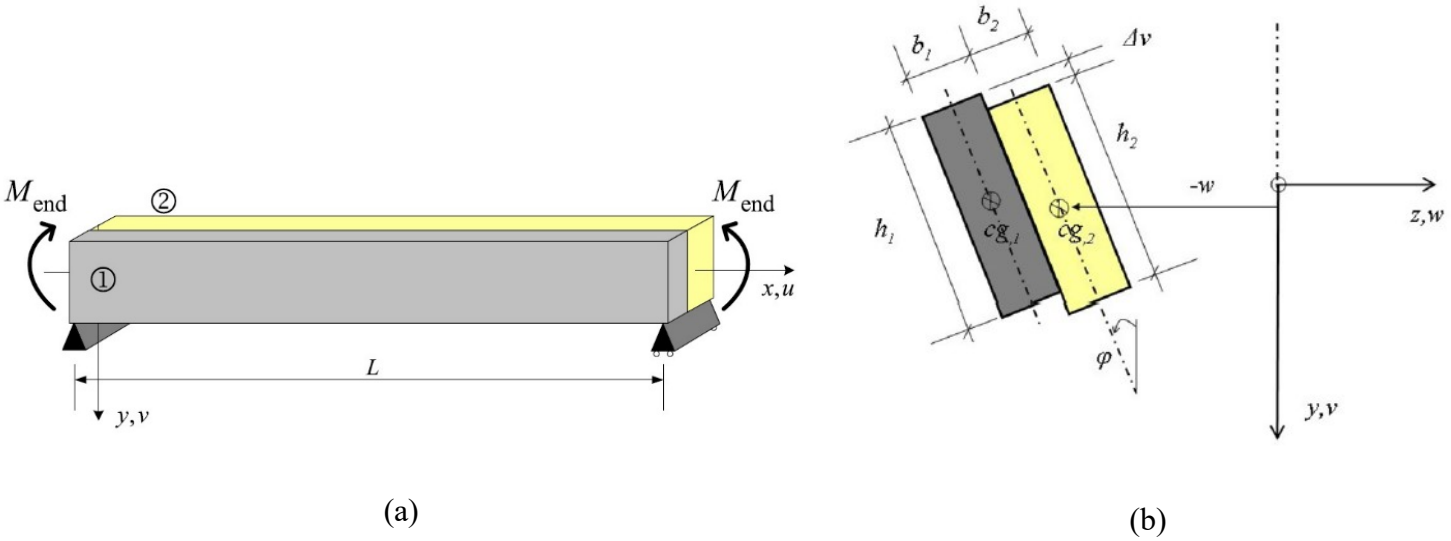

(a) (b)

Figure 2.2 (a). A simply supported partially composite beam under end moments; (b). A Partially composite cross-section after LTB

The lateral torsional buckling behaviour of thin-walled anisotropic laminated composite beams with rectangular cross-section was investigated by Ahmadi (2017). An effective lateral-torsional-coupling stiffness matrix was developed based on the classical laminated plate theory for simply supported and cantilevered beams both under bending and concentrated loading through.

2.3. Lateral torsional buckling tests related to wood members

Hooley and Madsen (1964) validated existing lateral torsional buckling theory for wood with anisotropic material models. Twenty-seven tests on simply supported and cantilever glulam beams

were conducted in the elastic range and six tests in the inelastic range. A formulation for the allowable stress in glulam beams was derived and verified with test results.

Hindman et al. (2005a) studied the lateral torsional buckling behavior of dimension lumber including machine stress rated lumber (MSR), laminated veneer lumber (LVL), parallel strand lumber (PSL) and laminated strand lumber (LSL) to investigate the difference of their behaviour with solid wood. The study concluded that differences could be attributed to the difference in the elastic constant ratios and torsional rigidity between visually graded sawn lumber and structural composite lumber.

Hindman et al. (2005b) investigated the behaviour of I-joists by testing unbraced cantilever beams and compared the results with predicted values by design standard and elastic beam buckling theory. The comparison showed that current design standard for I-joists, which assumed the compression flange acting as a column restrained in the direction of the web, and the elastic beam buckling theory underestimate the critical buckling load of the beams.

Burow et al. (2006) conducted lateral torsional buckling tests on twenty-two composite wood I-joists including cantilever and simply supported beams. The test results were compared with theoretical models that are based on Load and Resistance Factor Design (LRFD), Euler elastic buckling (EEB), equivalent moment factor (EMF), and Nethercot models. Comparing the test results with the theoretical models indicated that EMF model is more adaptable than EEB model for analyzing the LTB behaviour of various composite wood I-joists, and LRFD model was found to be very conservative in predicting the LTB capacity of composite wood I-joists.

Suryoatmono and Tjondro (2008) tested rectangular simply supported beams under concentrated load at the mid-span. The measured values were compared with that of classical lateral torsional buckling solution and a finite element model. The finite element analysis was performed for the beams assuming the material as either isotropic or orthotropic. The classical solution matched well with the isotropic finite element predictions but were higher than the orthotropic finite element results.

Xiao et al. (2017) studied the elastic lateral torsional buckling capacity of wood beams through experimental testing and finite element modelling. Through a sensitivity analysis by a finite element model on the orthotropic material properties of the wood, it was concluded that the LTB capacity is sensitive to the longitudinal modulus of elasticity and the transverse shear modulus. In order to verify the FEM results, full-scale lateral torsional buckling tests on the simply-supported rectangular beams under concentrated load at mid-span were conducted. The comparison showed good agreement between the experimental and analytical results.

St. Amour and Doudak (2017) conducted full-scale lateral torsional buckling tests on wood I-joists. Also, numerical analysis was conducted through FEM by inputting the material properties obtained from the experimental program. The experimental results were also compared with the American design standard for wood construction (NDS, 2018) and the classical solution, and it was concluded that the NDS underestimates the buckling capacity while the classical solution was found to provide adequate prediction.

Wang et al. (2017) investigated the buckling and post-buckling behaviours of composite laminates variable stiffness with fiber curvatures and compared experimentally and analytically the results with the composite laminations with constant stiffness with no curvatures. Based on the analytical

results, the buckling capacity of the composite laminates with variable stiffness was found to be higher than the composite laminations with constant stiffness

Pelletier and Doudak (2019) investigated the lateral torsional buckling performance of various commercial wood I-joist. The study also investigated the effect of reinforcement of the web-to-flange connection on the lateral torsional buckling capacity. A 3D FEM was developed in ABAQUS to predict the lateral torsional buckling capacity of wood I-joists and their associated mode shapes which were compared with the experimental results. It was concluded that the increase in the rotational connection as a result of reinforcement at the web-to-flange joints had a positive influence on the buckling resistance of the I-joists.

2.4. Summary

The lateral torsional buckling behavior of solid and partially composite beams has been the subject of several past studies. Challamel and Girhammar (2012) derived a closed-form solution for the lateral torsional buckling capacity of the vertically laminated elements. This is applicable to partially composite beams under uniform bending moment and both longitudinal and vertical slip of laminations due to lateral deflection are considered. Although it is the most relevant study to the scope of this research, the type of fasteners and its effect on the LTB capacity of built-up beams were not investigated.

Several studies investigated the LTB behaviour of solid and composite beams under different loading and boundary conditions. AFPA (2003) offered a closed-form solution to predict the LTB capacity of simply-supported solid beams with rectangular cross-section. Hindman et al. (2005a), Hindman et al. (2005b), Burow et al. (2006) and Xiao (2014), Xiao et al. (2017) studied the ability

of the Canadian and American code design provisions to predict the buckling load through experimental program. The results achieved by Suryoatmono and Tjondro (2008) and Xiao et al. (2017) were compatible with the classical solution offered by AFPA (2003). Zahn (1973) and Du (2016) focussed on the bracing action to prevent the buckling failure. These studies are limited to LTB behaviour of solid beams and consider the bracing affects while the current study is developed to investigate the LTB behaviour of vertically laminated unbraced built-up beams.

The LTB behaviour of composite beams has been studied numerically and experimentally by other researchers, including Sapkas and Kollar (2002), Gara et al. (2006), Machado (2010), Admine et al. (2016) and Wang et al. (2017). These studies have not investigated the composite beams built with mechanical fasteners which the purpose of this study.

The horizontally laminated timber built-up beam has been investigated experimentally by Tredgold (1820), including Trautwine (1862), Mahan (1886) and Rankine (1889). Mahan (1886) and numerically by Miller (2009). Since the focus of this study is vertically laminated timber built-up beams, these studies were not covered in details, although, a comprehensive review of the associated literature can be found in Miller (2009). The main finding obtained from these studies relate to the reduction in capacity associated with the partial composite action brought forth by the connections between the beam laminations.

In summary, a number of studies have been conducted on composite beams including timber-concrete, steel-FRP, LVL and etc., although very limited work specifically focused on the lateral torsional buckling for mechanically-jointed timber built-up beams. The focus of the current study is on investigating the LTB behaviour of mechanically-jointed timber built-up beams and to compare the buckling capacity obtained with those from equivalent solid beams, using FEM. The

study also presents experimental joint level testing that could be used directly as input in FEMs to establish a realistic level of stiffness obtained from typical connectors. The focus on nail and screw connections is motivated by the fact that the vast majority of built-up beams used in construction are built using these types of connectors. Timber design standards assume that stiffness of nails and screws can be approximated to be the same in the parallel and perpendicular to grain directions. The current study provides test results for both directions. The study also provides a direct contribution to the design provisions in the Canadian timber design standard (CSA O86) that would facilitate the design of built-up beams in a safe manner. Also, this study provides critical information on the sensitivity of certain key parameters, including the fasteners stiffness both in the shear and withdrawal directions on the LTB capacity of built-up beams, in addition to the contribution of number and pattern of mechanical fasteners. Finally, prescriptive fastening detail recommendation on reduction factors to be used in design of built-up beams with specific fastener layouts is provided.

CHAPTER 3- Finite Element Model

3.1. General

In order to determine the reduction factor of the LTB capacity of built-up beams, a finite element model (FEM) based on the commercially available software ABAQUS (Simulia, 2014) is presented. All the analyses in this study are conducted with ABAQUS Scripting Interface (ASI) that is based on PYTHON Programing Language, and then the LTB analysis are performed with ASI. A sample of input file is provided in Appendix B.

This chapter includes a description of the model in Section 3.2, including the mechanical properties of wood laminations and fasteners, types of elements used in the model, loading and boundary conditions. In Section 3.3, the FEM is validated by comparing the LTB results of a solid rectangular beam with the classical solution and experimental results obtained from the literature (Xiao 2014). In addition, a built-up beam with almost rigid connectors is compared with its equivalent solid beam. A comparison between FEM of built-up beams with the analytical solution offered in the literature (Challamal and Girhammar, 2012) is performed in Section 3.4., and finally, the results of the sensitivity analysis on the fasteners stiffness and configurations on LTB capacity is presented in Section 3.5.

3.1.1. Convention used for the laminations and the mechanical fasteners

The principal axes of the built-up beam laminations used throughout the FEM are shown in Figure 3.1. The longitudinal direction is represented by the Z axis, whereas the lateral and transverse directions are denoted by the X and Y axes, respectively.

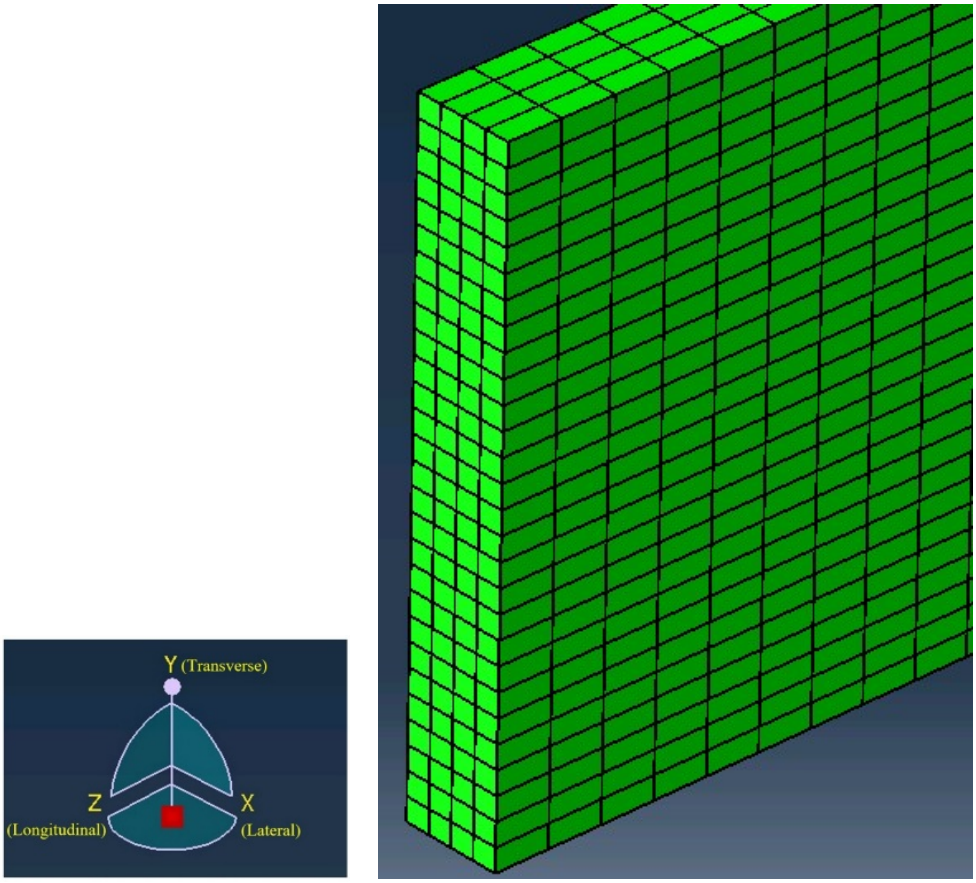

Figure 3.1 Principal axes of wood laminations

The fastener properties are defined by their stiffness in each of the three principal axes, including lateral stiffness parallel to grain (Z-axis), lateral stiffness perpendicular to grain (Y-axis) and withdrawal stiffness (X-axis). Figure 3.2 illustrates the finite element model with fasteners represented by discrete spring elements between built-up beam laminations.

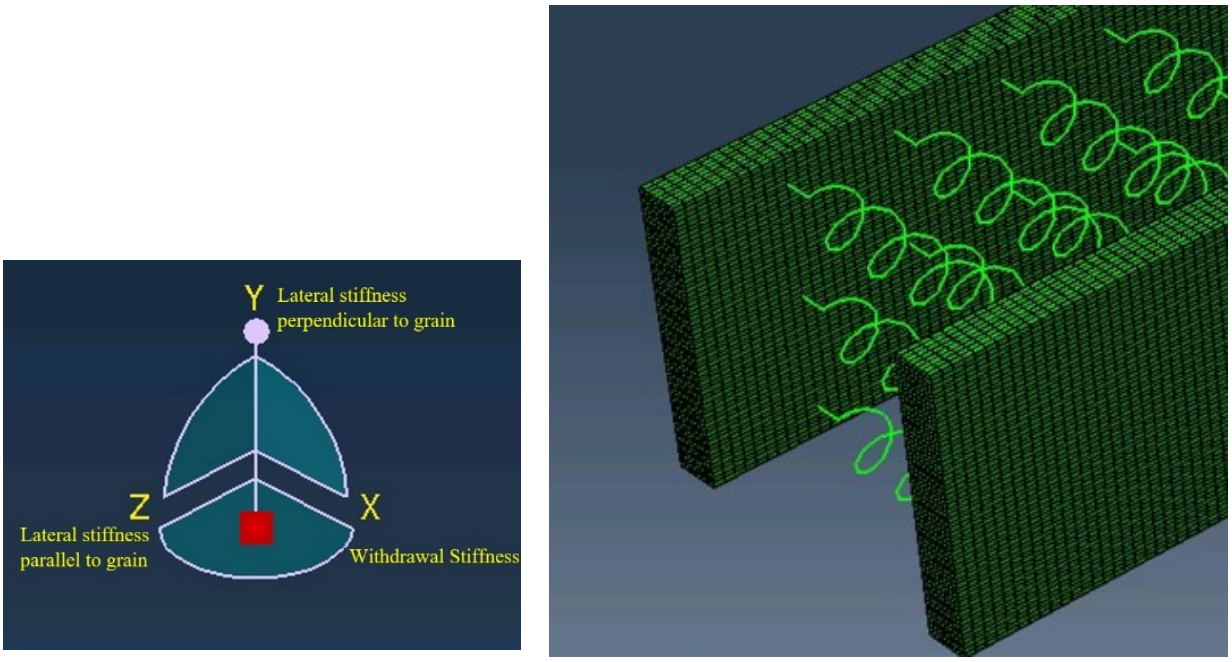

Figure 3.2 Convention used for the fasteners

3.2. Model description

An eigenvalue buckling analysis has been conducted in this study to evaluate the elastic LTB capacity of built-up beams through the ABAQUS software.

3.2.1. Laminations and mechanical fasteners properties

A built-up beam typically consists of two or more individual laminations of dimension lumber (CSA O86, 2019). Two types of wood material are analyzed in this study, including No.1/No.2 grade Spruce-Pine-Fir (S-P-F) and 2900F_b-2.0E grade laminated veneer lumber (LVL). As mentioned in Chapter 1, the choice of material was based on those most typically used in light frame wood construction where built-up beams are commonly used. The analyses are performed

for 2, 3, and 4-ply built-up beams with the lamination thickness of 1.5" and 1.75" for SPF and LVL, respectively.

For mechanical fasteners, wood screws and nails are chosen to connect the individual plies of built-up beams. The size of the fasteners used for each built-up beam differs depending on the number of plies. Specifically, for 2-ply and 3-ply built-up beams, 3" and 3-1/2" common nails are used for SPF and LVL, respectively. For 4-ply built-up beams, 6" and 6-3/4" wood screws are selected for the SPF and LVL, respectively.

3.2.2. Element types for laminations and mechanical fasteners

The element chosen in the model is an 8-node brick-type C3D8 element from the ABAQUS library (Simulia, 2014) which is a first-order element and uses linear interpolation in each direction.

As illustrated in Figure 3.3, each element has 8 nodes, each with 3 translational degrees of freedom (DOF) and a total of 24 DOFs for the element. This element has been successfully used by other researchers to investigate the LTB behaviour of wood beams (e.g., Xiao et al. 2017).

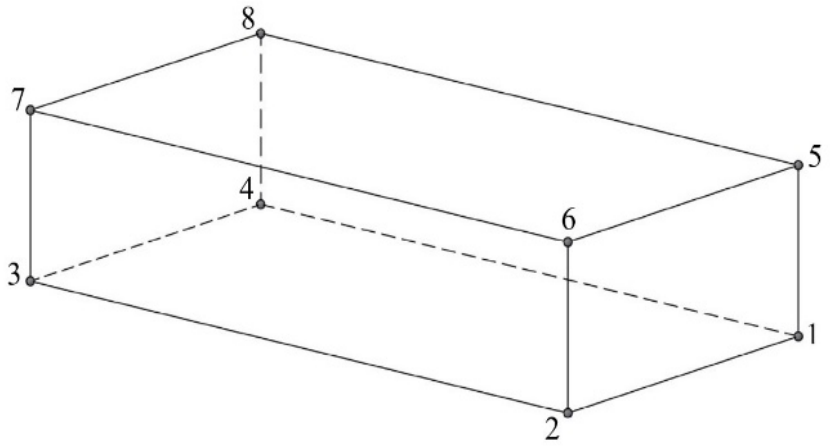

Figure 3.3 C3D8 Element

In order to model the interactions between built-up beam laminations in the FEM, connecting elements are created to simulate the fasteners behaviour. Among different elements in the ABAQUS library, two-node SPRING2 element is selected to model fastener stiffness in each of the three principal axes between two nodes (Figure 3.4). This element can provide partial restrain between beam laminations by connecting two nodes of the laminations with three stiffness values of the fasteners which can be assigned in each of the orthogonal directions. Therefore, three SPRING2 elements are needed at each fastener location to represent the withdrawal stiffness in the X direction and lateral stiffness in both Y and Z directions.

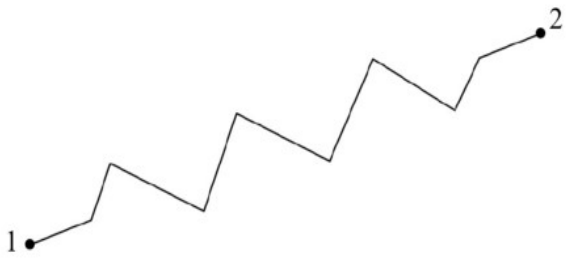

Figure 3.4 SPRING2 element

3.2.3. Mechanical properties of laminations and mechanical fasteners

As discussed in Section 1.1.1, wood is an anisotropic material but can generally be considered as orthotropic (FLP, 2010), with different mechanical properties in each principal axis. This includes three moduli of elasticity (E_L, E_R and E_T), three moduli of rigidity (G_{LR}, G_{LT} and G_{RT}) and six Poisson's ratios (μ_{LR}, μ_{RL}, μ_{LT}, μ_{TL}, $\mu_{RT,}$ and μ_{TR}). Among these twelve constants, nine of them are independent and the other three are dependent which can be achieved by Equation (1.1).

Lodgepole Pine, which falls under the SPF species combination, and 2900Fb-2.0E grade LVL will be analyzed in this study. The mechanical properties of SPF from the CSA O86 Standard (2019) and Wood Handbook (FPL, 2010) are shown in Table 3.1.

It should be noted that μ_{RL} and μ_{TL} are not provided in the references, however, it has been demonstrated that these variables have no effect on LTB capacity (Xiao, 2014). In modeling, only nine independent mechanical properties of the lumber are used as input.

Table 3.1 Mechanical properties of Lodgepole Pine sawn lumber (CSA O86:19, FPL, 2010)

Mechanical Property	**Value**
E_L (MPa)	9500
E_T (MPa)	646
E_R (MPa)	969
G_{LR} (MPa)	466
G_{LT} (MPa)	437
G_{RT} (MPa)	47.5
μ_{LR}	0.316
μ_{LT}	0.347
μ_{RT}	0.469
μ_{TR}	0.381

Xiao (2014) performed a sensitivity analysis on the material properties of a simply supported rectangular beam elements under uniform moment. The effects of the material properties on the LTB capacity were investigated by decreasing and increasing the mechanical properties by 50% and 150%, respectively. It was concluded that among all the mechanical properties only the modulus of elasticity in longitudinal direction (E_L) and shear moduli in transverse planes (G_{LT}, G_{LR}) affect the LTB capacity of the beam.

As the difference in magnitude of shear moduli in radial and tangential directions can be considered negligible, they are considered as one parameter denoted as the shear modulus about the transverse direction G_T ($G_{LT} = G_{LR} = G_T$). The moduli of elasticity in radial and tangential axes, shear modulus G_{RT} and the Poisson's ratios have little effect on the LTB capacity of the beam.

Table 3.2 summarizes the mechanical properties used in the FEM for the beam with SPF laminations.

Table 3.2 Mechanical properties used in FEM

Mechanical Property	**Value**
E_L (MPa)	9500
E_T(MPa)	646
G_T (MPa)	437
G_{RT} (MPa)	47.5
μ_T	0.347
μ_{RT}	0.469

For beams with LVL laminations, the longitudinal modulus of elasticity (E_L) is taken as 13790 (MPa) (LP SolidStart LVL), and the shear modulus G_T is assumed to be $E_L/16$ (CSA O86, 2019). As the other mechanical properties of the wood have negligible impact on the LTB capacity of the beam, they are considered the same as values used for SPF beams.

For the purpose of the sensitivity analysis in this chapter, the withdrawal stiffness of the nails is taken 500 N/mm, based on values obtained from the literature (Winistorfer & Soltis, 1994). The lateral stiffness is predicted based on the Eurocode 5 (CEN, 2004) given by the Equation (3.1).

$$K_{ser} = \frac{\rho_m^{1.5} d^{0.8}}{30} \quad (3.1)$$

Where K_{ser} (N/mm) is the slip modulus per nail per shear plane, ρ_m (kg/m^3) is the wood density and d (mm) is the diameter of the nail.

By taking the mean relative density of SPF equal to 420 (kg/m^3) and the diameter of 3'' common nail equal to 3.76 mm (CSA O86, 2019), the slip modulus is 810 (N/mm). This number is rounded to 900 (N/mm) for the analysis.

A different approach is used when the stiffness values for nails and screws used in the FE analysis of built-up beams for chapter 5 where the lateral and withdrawal stiffness are obtained from testing rather than code equations which are described in Chapter 4.

3.2.4. Boundary conditions

As mentioned earlier, the beam considered in the FEM has simply supported boundary condition. To simulate this boundary condition, the displacement along the x and y axes and rotation about the z axis are restrained. Accordingly, nodes along horizontal axes at the mid-height of the beam-ends (lines AB and AABB in Figure 3.5) are restrained from movement in the vertical direction. In addition, nodes along lines CD and CCDD are restrained from movement in the lateral direction.

The centroid at each end of the beam is denoted as nodes E and EE, respectively. At node E, all three translational DOFs are restrained; however, node EE is restrained in X and Y directions but free to translate in Z direction.

By restraining the displacements as mentioned above, simply supported conditions is achieved at beam-ends. It should be noted that in the case of built-up beams, the same boundary condition is applied to all individual plies.

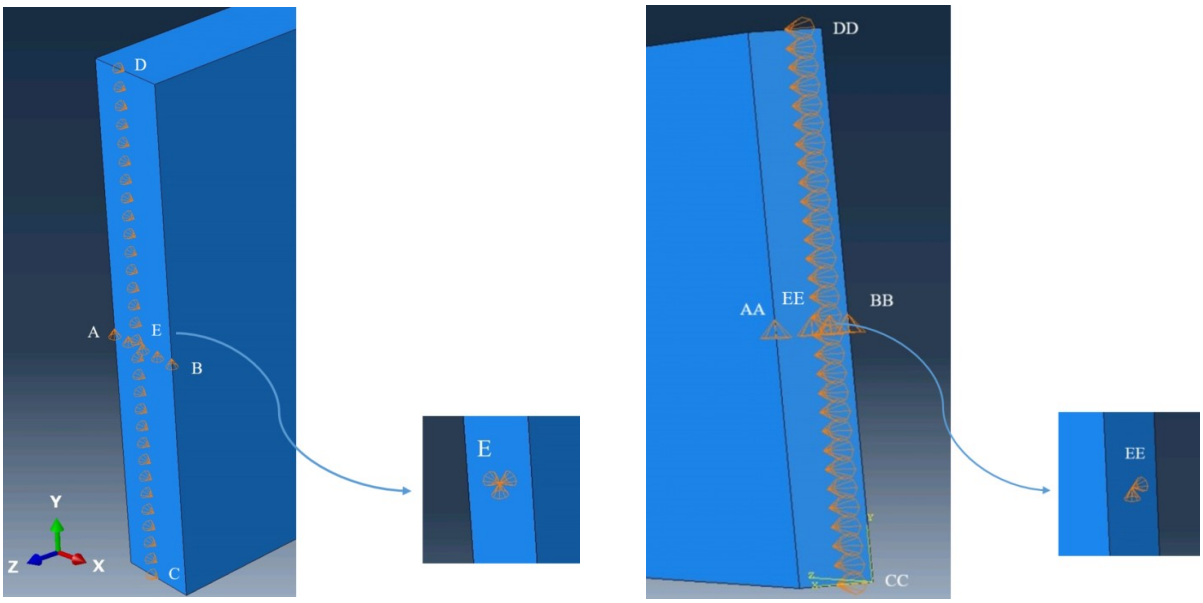

(a) (b)

Figure 3.5 Boundary condition at (a). left end of the beam; (b). right end of the beam

3.2.5. Load application

The loads applied in the FEM are assumed to be end moments about the strong bending axis. To apply end moments, horizontal lines denoted as FG and FFGG are defined in the top edges of the cross-section, lines HI and HHII are defined in the bottom edges of the cross-section at the beam left and right end, respectively (Figure 3.6). Concentrated loads along the beam longitudinal axis are applied at nodes along the FG axis and in opposite direction at nodes in HI axis. This procedure is repeated for the right end of the beam except the direction of the concentrated loads at the FFGG

and HHII lines are reversed. The same loading is applied to all individual plies of the built-up beam.

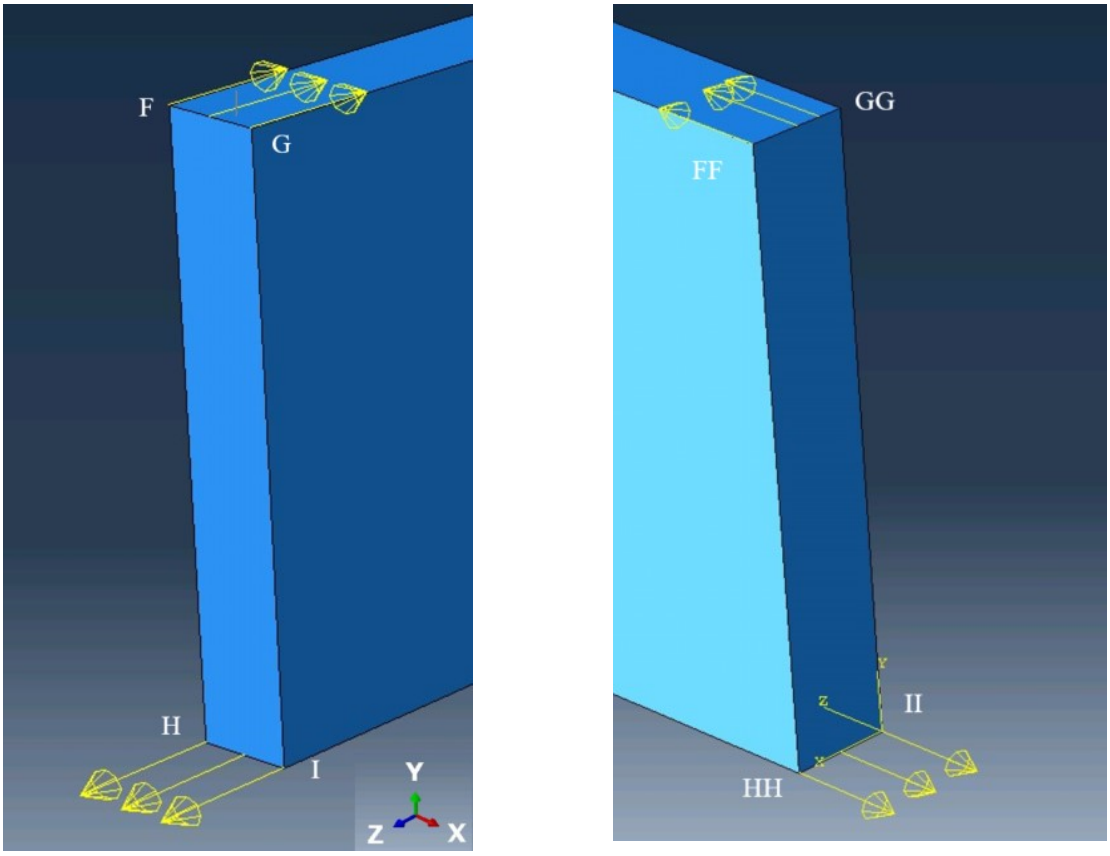

Figure 3.6 Load application at (a). Left end; (b). Right end of the beam in FEM

These loads create a uniform moment M_x, as provided in Equation (3.2).

$$M_x = N_x \times F \times d \times n \quad (3.2)$$

Where N_x is number of nodes in a single ply along the X axis, F is the concentrated load applied to each node, d is the depth of the cross-section and n is the number of plies in the built-up beam.

3.2.6. Eigenvalue buckling analysis

In the ABAQUS model, an eigenvalue buckling analysis is used to evaluate the LTB capacity which is obtained by Equation (3.3).

$$([K_E] + \lambda_i[K_G])\{v_i\} = 0 \quad (3.3)$$

Where $[K_E]$ is the elastic stiffness matrix, $[K_G]$ is the geometric matrix and λ_i denotes the i^{th} eigenvalue corresponding to the buckling mode shapes$\{v_i\}$.

The critical load, typically corresponding to the first mode, is calculated as the applied load multiplied by the eigenvalue λ.

3.2.7. Mesh sensitivity analysis

The mesh sensitivity analysis is conducted for a single ply of the built-up beam and will be used as the mesh for all plies. As the reference case, the present study considers a simply supported SPF sawn lumber with 38 x 286 mm^2 cross-section and 5144 mm in length under uniform moment. The mesh sensitivity analysis was conducted for six mesh densities, as shown in Table 3.3. In each mesh analysis, the element dimension in the longitudinal direction is kept at approximately twice the other two dimensions (Xiao, 2014).

As illustrated in Table 3.3, the critical moment converges to a value for the critical moment of 3.19 kN·m in Case 3, with 4 elements along the section width (N_X=4), 24 elements along the section depth (N_Y=24) and 256 elements along the beam length (N_Z=256). The mesh size is approximately 10×10×20 (mm^3). Beyond Case 3 with increasing mesh density, no changes are observed in the

critical moment of the beam. Hence, the mesh size in Case 3 is selected as the optimum size for the rest of this study.

Table 3.3 Mesh sensitivity analysis

Case	N_X	N_Y	N_Z	Eigen-value	Critical Moment (kN.m)	Element size in X direction (mm)	Element size in Y direction (mm)	Element size in Z direction (mm)
1	1	8	68	4.35	2.49	38.1	35.8	75.6
2	2	14	128	3.5915	3.08	19.1	20.4	40.2
3	4	28	256	2.2302	3.19	9.5	10.2	20.1
4	6	44	396	1.5951	3.19	6.4	6.5	13.0
5	8	58	512	1.3066	3.19	4.8	4.9	10.0
6	10	76	682	1.014	3.19	3.8	3.8	7.5

3.3. Verification and validation of finite element model

The verification of the finite element model was performed in two stages. First, the LTB capacity obtained from FEM of a single lamination under mid-span concentrated load is compared against the analytical LTB solution in Equation (3.8), adapted from the classical solution in Equation (3.4), and the full-scale tests conducted by Xiao (2014). Secondly, the LTB capacity from the FEM for a 2-ply built-up beam with near rigid connections is compared with the classical solution for uniform moment.

As mentioned in Chapter 1, the classical solution for calculating the LTB capacity of a simply supported beam under uniform moment is given in Equation (3.4).

$$M_u = \frac{\pi}{L}\sqrt{E_L I_y G_T J + (\frac{\pi E_L}{L})^2 I_y C_w} \quad (3.4)$$

Where C_w is the warping constant and the other parameters have been defined in Section 1.1.2.

The section properties I_y, J and C_w are calculated as follows:

$$I_y = db^3/12 \quad (3.5)$$

$$J = \frac{(1-0.63\frac{b}{d})}{3} db^3 \quad (3.6)$$

$$C_{w=} \frac{b^3 d^3}{144} \quad (3.7)$$

In the experimental testing conducted by Xiao (2014), the beams were subjected to a mid-span load applied at the beam top face. To account for the loading conditions, the critical moment obtained from the classical solution is multiplied by the equivalent moment factor C_b and the load eccentricity factor C_e (AFPA, 2003) as shown in Equation (3.8).

$$M_{cr} = M_u \times C_b \times C_e \quad (3.8)$$

Where M_{cr} is the LTB capacity of a simply supported beam under mid-span load applied at its top face. The load eccentricity factor C_e can be calculated by Equation (3.9) and (3.10).

$$C_e = \sqrt{\eta^2 + 1} - \eta \quad (3.9)$$

$$\eta = \frac{Kd}{2L_u}\sqrt{\frac{EI_y}{GJ}} \quad (3.10)$$

Where K is a constant depending on loading conditions from Table 3.4 and d is the depth of the beam.

The equivalent moment factor C_b and parameter K are given in Table 3.4 for simply supported boundary conditions and single span beams subjected to different loading conditions (AFPA, 2003). The critical load (P_{cr}) is obtained by using Equation (3.11) to compare it with the critical load estimated by the FEM.

$$P_{cr} = \frac{4M_{cr}}{L} \quad (3.11)$$

Table 3.4 C_b and K for simply supported beam subjected to different loading conditions (AFPA, 2003)

Loading Condition	Laterally Braced at point of loading	Laterally Unbraced at point of loading	
	C_b	C_b	K
Concentrated Load at Centre	1.67	1.35	1.72
Concentrated load at 1/3 points	1.00	1.14	1.63
Concentrated load at 1/4 points	1.11	1.14	1.45
Concentrated load at 1/5 points	1.00	1.14	1.51
Concentrated load at 1/6 points	1.05	1.14	1.45
Concentrated load at 1/7 points	1.00	1.13	1.47
Concentrated load at 1/8 points	1.03	1.13	1.44
Eight or more equal concentrated loads at equal spacing	1.00	1.13	1.46
Uniformly distributed load	1.00	1.13	1.44
Equal end moments (opposite rotation)	1.00		
Equal end moments (same rotation)	2.3		

Three simply supported rectangular beams with material properties experimentally obtained by Xiao (2014), and geometries shown in Table 3.5 are analyzed by the FEM.

Table 3.5 Material properties and beam geometries selected for verification study (Xiao, 2014)

Case	Beam dimension	E_L (MPa)	G_T (MPa)	I_y (m^4)	J (m^4)	C_w (m^6)
1	2’’×8’’×14’	9022	614	8.49E-07	2.95E-06	2.40E-09
2	2’’×10’’×12’	9745	535	1.08E-06	3.89E-06	4.98E-09
3	2’’×12’’×14’	5491	720	1.32E-06	4.83E-06	8.98E-09

The load eccentricity factors from Equation (3.9) and (3.10) are C_e= 0.93, 0.88 and 0.92 for Cases 1, 2 and 3, respectively. Based on Table 3.4, the equivalent moment factor for mid-span concentrated load is C_b=1.35. Table 3.6 shows an acceptable compatibility of the FEM results with both the classical solution and the experimental results. The ratio of the critical loads estimated by the FEM to the classical solution is close to unity. In addition, the ratio of the critical loads estimated by the FEM to the test results is around 0.9, which again indicates that the FEM values are in reasonable agreement with the test results.

Table 3.6 Comparison of FEM with classical solution and Xiao (2014) tests

Beam dimension	**Critical load by analytical solution (kN)**	**Critical load by Xiao test (kN)**	**Critical load by FEM (kN)**	**FEM/analytical solution**	**FEM/test**
2’’×8’’×14’	3.23	3.72	3.25	1.007	0.873
2’’×10’’×12’	5.28	5.67	5.16	0.976	0.909
2’’×12’’×14’	4.30	4.53	4.24	0.986	0.938

In addition to the above validation for single ply, a 2-ply SPF built-up beam is modelled to validate the developed FEM for built-up beams. In this model the fasteners are located such that they provide continuum connection between the plies and their withdrawal and lateral stiffnesses are considered near infinity (i.e., set in the model equal to 1E+11 N/mm for withdrawal stiffness and 2E+14 N/mm for lateral stiffness). In other words, all nodes of the individual plies are connected with spring elements.

It is expected that the LTB capacity of the built-up beam modelled with this connection be the same as its equivalent solid beam. Accordingly, the critical moment of the built-up beam estimated by the FEM is compared to the critical moment of its equivalent solid beam from the classical

solution given in Equation (3.4). Table 3.7 shows the beam geometries and the critical moments of a 2-ply SPF built-up beam. The value of the critical moment as obtained by the FEM is equal to 25.33 kN.m while the value obtained for an equivalent solid section is equal to 24.89 kN.m. This comparison in part verifies the accuracy of the FEM model for built-up beams.

Table 3.7 Comparison of a 2-ply SPF built-up beam with its equivalent solid section

Ply dimension	**No. of Plies**	**$M_{cr,B}$ of built-up beam by FEM (kN.m)**	**$M_{cr,S}$ of equivalent solid beam by classical solution (kN.m)**	**$\frac{M_{cr,B}}{M_{cr,S}}$**
2''×12''×16'	2	25.33	24.89	1.02

3.4. Comparing built-up beam FEM with analytical model

As mentioned in Chapter 2, one of the key references addressing the topic of LTB capacity of vertically laminated beams is that by Girhammar and Challamel (2012) where a closed form solution was proposed. The study accounts for built-up beams with different material properties and geometries; however, in the current study the same properties are assumed for all laminations. Key to the analytical solution is that it accounts for the flexibility of fasteners which are assumed to cause slip in both the longitudinal and transverse directions of the laminations. The case with a built-up beam having pinned-end conditions and subjected to end moments is used to compare the analytical solution with the FEM results from the current study. The motivation for such comparison is partly to further verify the FEM, but also to establish potential differences between the analytical and numerical models since such comparison was not found in the literature.

The LTB moment can be expressed as shown in Equation (3.12).

$$\bar{M}_{end}^2\left[E_1I_{z1}E_2I_{z2}\left(\frac{n\pi}{L}\right)^4+K_{across}EI_{z,0}\right]\left[E_1A_1E_2A_2\left(\frac{n\pi}{L}\right)^2+K_{along}EA_0\right]$$

$$=\left(\frac{n\pi}{L}\right)^2\left\{GJ_0E_1I_{z1}E_2I_{z2}\left(\frac{n\pi}{L}\right)^4+K_{across}\left[GJ_0EI_{z0}+b_0^2\left(\frac{n\pi}{L}\right)^2E_1I_{z1}E_2I_{z2}\right]\right\}$$

$$\times\left[EI_{y,0}E_1A_1E_2A_2\left(\frac{n\pi}{L}\right)^2+K_{along}(EI_{y,0}EA_0+b_0^2E_1A_1E_2A_2)\right]$$

(3.12)

Where,

$$GJ_0=G_1J_1+G_2J_2$$

$$EI_{y0}=E_1I_{y1}+E_2I_{y2}$$

$$EI_{z0}=E_1I_{z1}+E_2I_{z2}$$

$$EA_0=E_1A_1+E_2A_2$$

In Equation (3.12), M_{end} is the end moment, indices 1 and 2 refer to parameters associated with laminates 1 and 2, respectively, E is the longitudinal modulus of elasticity, G is the shear modulus in transverse direction, I_z and I_y are the moment of inertia about the strong and weak axis, respectively, A is the cross-section area, L is the beam length, n is the mode shape number, which for global buckling is assumed to be 1 for the first mode shape.

The analytical formulation assumes that the beam laminations are connected together by a weak shear layer, which produces uniformly distributed slip forces with a constant slip modulus per unit length. This is represented in Equation (3.12) by variable K_{along} [N/m^2], with respect to bending in the lateral direction, and K_{across} [N/m^2], with respect to torsion (i.e., slip in the across-longitudinal

or vertical direction). To calculate these values, the stiffness of the connection, which could be obtained from test results or code formula (in N/mm), is divided by the nail spacing in the longitudinal and transverse directions, respectively.

All input parameters for Equation (3.12) are provided in Table 3.8 and Table 3.9 for the cases analyzed in this section. These cases are described in more details in Section 3.5.

Table 3.8 Geometric and material properties of laminations

L (m)	**b_1 (m)**	**d_1 (m)**	**I_{y1} (m4)**	**I_{z1} (m4)**	**J_1 (m4)**	**E_1 (N/m2)**	**G_1 (N/m2)**
5.144	0.0381	0.286	1.32E-06	74.27E-06	4.83E-06	9500E+06	465.5E+06

Table 3.9 Stiffness and spacing of the mechanical fasteners joined built-up beam laminations

Cases	**Kser (N/mm)**	**spacing parallel to grain (mm)**	**spacing perpendicular to grain (mm)**	**K_{along} (N/mm/mm)**	**K_{across} (N/mm/mm)**
Reference Case	900	600	93	1.50	9.68
A	450	600	93	0.75	4.84
B	1350	600	93	2.25	14.52
E	900	300	93	3.00	9.68
F	900	150	93	6.00	9.68

Table 3.10 provides the results and comparison between the analytical solution provided by Girhammar and Challamel (2012), $M_{an.}$, and those obtained through the FEM analysis presented in this study, M_{FEM}.

Table 3.10 Comparison between analytical and FEM

Case	$M_{an.}$ (kN.m)	M_{FEM} (kN.m)	$\frac{M_{an}}{M_{FEM}}$
Reference Case	7.29	7.98	0.91
A	6.97	7.36	0.95
B	7.58	8.44	0.90
E	7.84	10.12	0.77
F	8.65	10.63	0.81

Based on the results obtained in Table 3.10, it can be observed that the analytical model provides inconsistent results relative to the FEM for different cases with difference nailing pattern. It should be noted that even for the reference case, where the nailing pattern is maintained and only the value of stiffness is varied, some discrepancies and inconsistences could be observed between the two models. It can also be observed that the values obtained by the analytical model is generally lower than those from the FEM analysis. Considering this observation from a design point of view, and assuming that the observation can be generalised, the analytical equation seems to provide a conservative estimate of the LTB moment. It is not possible given the limited number of cases used in this comparison to draw general conclusions and provide plausible explanations on the cause of the discrepancy.

The work presented in this section provides a general overview of the validity of the analytical solution available in the literature for estimating the buckling moment of built-up beams with flexible joints. The preliminary results seem to indicate a need for more analytical approaches to be developed since the solution proposed by Girhammar and Challamel (2012) does not match well with the FEM. This in-depth investigation of the existing analytical model and future development of enhanced models is subject for future studies.

3.5. Connection sensitivity analysis

In order to investigate the fastener parameters that can affect the LTB capacity of built-up beams, a sensitivity analysis on the stiffness of mechanical fasteners connecting the individual plies is performed. In addition, the effects of the fastener spacing on the LTB capacity are analyzed by comparing the LTB capacities of built-up beams with same mechanical fasteners but varying spacing.

3.5.1. Sensitivity analysis on connection stiffness

A 2-ply built-up beam with material properties and dimensions defined as the reference case in Section 3.2.6 is chosen for the sensitivity analysis on the fastener stiffness. The laminations are assumed to be fastened together with 3'' common nails following the pattern shown in Figure 3.7. As illustrated in Figure 3.7, there are three rows of nails with equal spacing in the perpendicular to grain direction, 600 mm spacing parallel to grain, 300 mm end distance parallel to grain and 50 mm edge distance perpendicular to grain.

Figure 3.7 Nailing Pattern for sensitivity analysis

A total of five runs are conducted where the first run is taken as the reference case. In the other runs, one stiffness is increased by a factor of 1.5 and decreased by a factor of 0.5, one at a time, while the other stiffness is kept the same.

As illustrated in Table 3.12, the critical moment of the built-up beam does not change significantly when the fasteners' withdrawal stiffness is changed. This may be expected since the withdrawal stiffness of the fastener needs to simply keep the laminations together so they can buckle in the same direction. However, the LTB capacity is observed to be marginally sensitive to the lateral stiffness of the fasteners. In fact, the LTB capacity decreases by 8% when the lateral stiffness is decreased by a factor of 0.5 and increases 6% when the lateral stiffness is increased by a factor of 1.5.

Table 3.11 Sensitivity analysis of built-up beam to fastener stiffness by FEM

Case	$\frac{\mathbf{K_{ser}}}{\mathbf{K_{ser-ref}}}$	$\frac{\mathbf{K_{w}}}{\mathbf{K_{w-ref}}}$	**Critical Moment (kN.m)**	$\frac{\mathbf{M_{cr}}}{\mathbf{M_{cr-ref}}}$
Reference Case	1	1	7.977	1.00
A	0.5	1	7.362	0.92
B	1.5	1	8.443	1.06
C	1	0.5	7.977	1.00
D	1	1.5	7.977	1.00

K_{ser} is the lateral stiffness
K_w is the withdrawal stiffness

3.5.2. Sensitivity analysis on connection number

It can be hypothesized that not only the fastener stiffness can affect the LTB capacity of a built-up beam, but the fasteners' configuration may also play a role. In order to investigate the effect of fastener configurations on the LTB capacity of built-up beams, three 2-ply beams are analyzed.

All beam and fastener properties are assumed to be the same as the beams analyzed in Section 3.5.1, except the fastener patterns, as demonstrated in Figure 3.8.

The reference case is the same as one used in the sensitivity analysis (Figure 3.7). In the second case the number of fasteners is twice the reference case by decreasing the fasteners space along the length of the beam by half. In the second configuration, the fastener spacing in direction parallel to grain is 150 mm (6 in) and the end and edge distances are 150 mm (6 in) and 50 mm (2 in), respectively. In this case, the number of fasteners is more than four times that of the reference case due to decreasing the end distance and the longitudinal spacing of the fasteners.

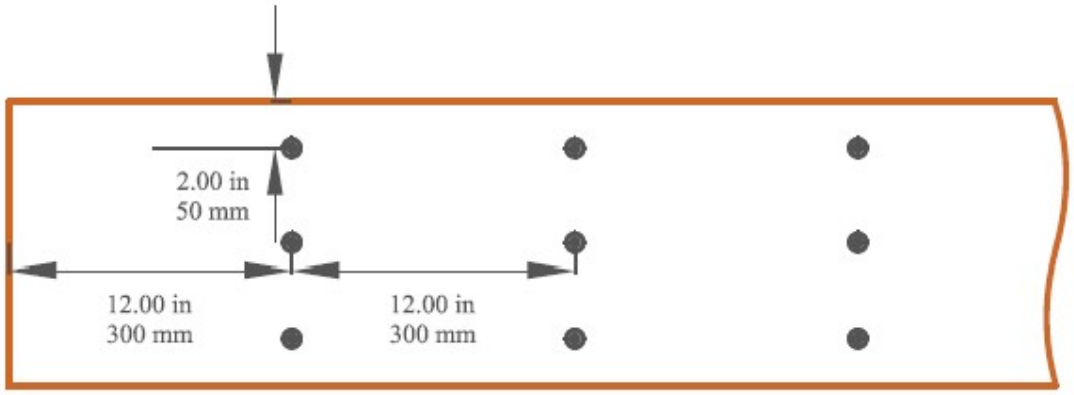

(a)

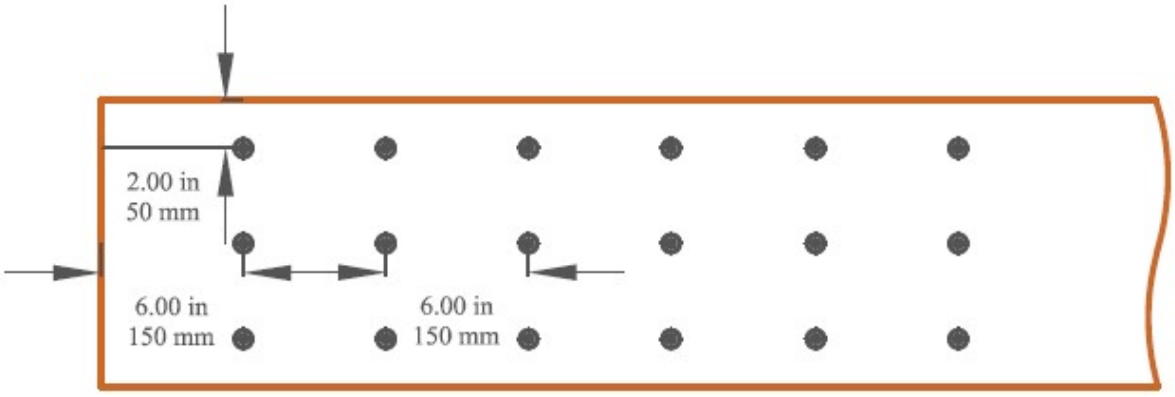

(b)

Figure 3.8 Nailing patterns for LTB capacity (a). Pattern 1; (b). Pattern 2

As shown in Table 3.13, by increasing the number of fasteners to about two times and four times that of the reference case, the LTB capacity increases by 13% and 33%, respectively. It can be concluded that the LTB capacity is sensitive to fastener spacing, although the increase is not proportional to the number of fastener or change in stiffness.

Table 3.12 Pattern contribution on LTB capacity by FEA

Cases	**Spring Pattern**	$\frac{\textbf{\# Nails}}{\textbf{\# Nails of the reference case}}$	**Buckling Load (kN)**	**Critical Moment (kN.m)**	$\frac{\mathbf{M_{cr}}}{\mathbf{M_{cr-ref}}}$
Reference Case	Reference Case	1	2.79	7.98	1.00
E	1	2	3.14	8.99	1.13
F	2	4.4	3.72	10.63	1.33

CHAPTER 4- Joint Level Tests and Results

4.1. Introduction

The objective of conducting the joint level tests is to provide realistic values for the lateral and withdrawal stiffness of the connections used in common construction cases for built-up beams and intended to be used as input for the model described in Chapter 3. These values are important because they are not currently provided in the timber design standard for all types of mechanical fasteners (CSA O86, 2019). Stiffness values provided in the Eurocode 5 (CEN, 2004) are also evaluated against those obtained experimentally; however, these expressions may not be specifically appropriate for the purpose of being used in conjunction with LTB analysis. It should be noted that this discussion is wider than can be addressed as part of the current study as more joint testing and evaluation against full-scale beam testing results are required.

In this chapter, Section 4.2 describes the fasteners tested and the testing apparatus and instrumentations, while Sections 4.3 and 4.4 describe the lateral and withdrawal test setup and procedures, respectively. The calculation method of the stiffness is described in Section 4.5. The lateral stiffness obtained from lateral shear tests are presented in Section 4.6, while the withdrawal stiffness results determined from the tensile tests are provided in Section 4.7. Finally, comparisons between the lateral test results and Eurocode 5 (CEN, 2004) are presented in Section 4.8.

4.2. Material and test instruments

4.2.1. Material

The types of joints tested in this study reflect typical fastener sizes and connection layouts used in construction. It should be noted that variability is expected in the parameters of the connection types investigated in this study, and the effect of such variability has been investigated and discussed in Chapter 3. Variability may arise from the choice of different wood species, which may affect the density, or the use of different nail or screw fasteners, all of which may have an effect on the joint stiffness. The dimensions of the fasteners tested in the current study are summarized in Table 4.1.

Table 4.1 Fastener dimensions used in experimental testing

Fastener Type	**Length**		**Diameter (mm)**	
	in	mm	in	mm
Common Nail	3	76.2	0.15	3.76
Common Nail	3-1/2	88.9	0.16	4.11
SIMPSON SDW22 Screw	6-3/4	171	0.22	5.58

The 3-inch long nail is used in sawn lumber connections because the actual size of a 2-inch nominal lumber lamination is 1.5 inch (38.1 mm), which allows the 3-inch nail to penetrate fully the two laminations. Similar logic is used when selecting the 3.5-inch nail (round-head nail) is used to connect LVL with a lamination thickness of 1.75 inches. It should be noted that according to the design standard, penetration in the point-side member can be limited to $5d_F$ (where d_F is the fastener's nominal diameter), and as such full penetration into the member is not required. It is

assumed that any penetration length beyond $5d_F$ is considered sufficient to develop the intended behavior and provide the needed stiffness.

There is currently no established procedure in the current design standard (CSA O86, 2019) for joining multiple laminates in built-up beams. The connection could be done by joining together two laminates at a time using shorter nails, or three or more laminates using longer nails. The choice of investigating the 6-3/4 inch screw is meant to illustrate the case where multiple laminates (in this case four) are joint together with a single fastener. Figure 4.1 shows the fasteners investigated in the current study.

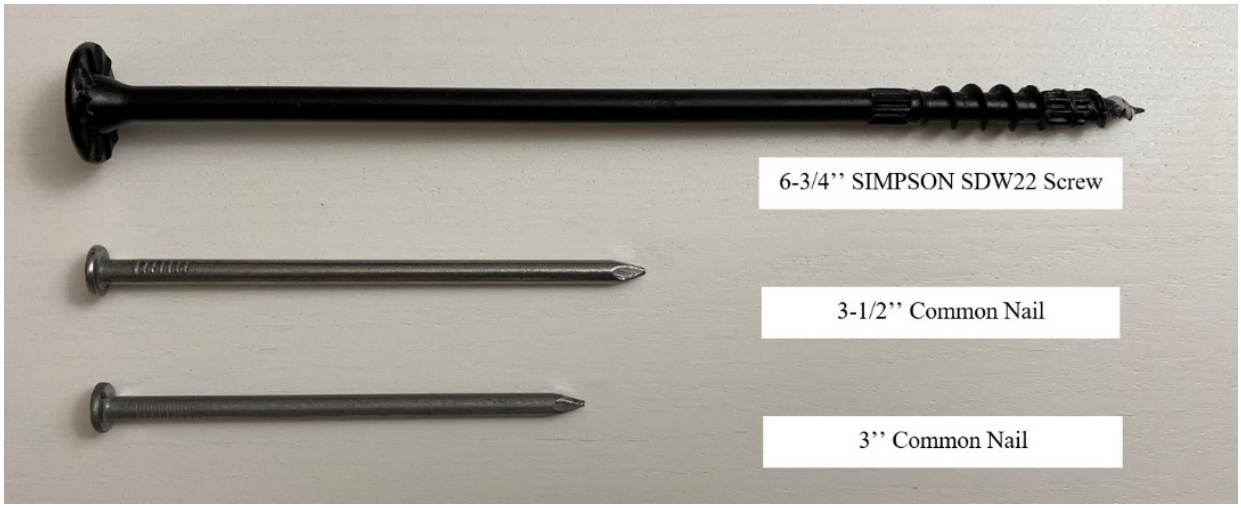

Figure 4.1 Fasteners tested in this study

The wood used in the joint level tests consists of SPF lumber and Laminated Veneer Lumber (LVL) members, with respective densities of 407 kg/m^3 and 550 kg/m^3 (COV of 4.0 % and 8.5 %) that were measured during the experiments.

4.2.2. Test instrument

Both the lateral and axial withdrawal tests are conducted with the GALDABINI testing machine at the University of Ottawa's structural laboratory. The testing apparatus applies a load using a hydraulic jack at a rate of 2.54 mm/min, in accordance with ASTM D1761. This displacement-controlled loading rate ensures that the test is completed in approximately 10 minutes, which avoids any creep effects. The loading process is ended when the ultimate displacement in the joint reached a value of 15 mm (ASTM D1761). The load and displacement of the joints are recorded using a load cell and two wire-gauge transducers. The transducers measure the relative displacements between the laminations and thereby the slip in the fastener.

4.3. Lateral test setup

The cross-section of SPF and LVL plies used in the lateral joint tests are 2''×8'' and 2''×10'', respectively and both had a length of 9'', based on similar dimensions used in the literature (Pellicane and Boding, 1984).

The lateral tests are conducted in the directions parallel and perpendicular to grain since the buckling behavior of the built-up beam is expected to induce slip in the joints in these two directions. It should be noted that typically design standards do not distinguish between these two directions for relatively slender dowel type fasteners such as nails and screws, since the disturbance of the fibers is much less than that obtained when bolted connections are used.

The test material for the lateral loads is provided in Table 4.2, where the wood material, number of plies, and the type and number of mechanical fasteners used in each connection test are indicated.

Table 4.2 Tests matrix for the lateral tests in parallel and perpendicular to grain directions

Wood Type	Number of Plies	Type of Mechanical Fastener	Number of Mechanical Fastener
SPF	3	3'' Common Nail	4
LVL	3	3-1/2'' Common Nail	4
LVL	4	6-3/4'' SIMPSON SDW22 Screw	2

As shown in Figure 4.2, the specimen consisted of outer plies resting on the base of the loading machine, while the inner plies are intentionally placed one inch higher to allow for the slip between the laminations to be measured. The lateral stability of the specimen is ensured by providing angle brackets that anchor the outer laminations to the base of the loading machine, as shown in Figure 4.2.

Two nails are driven pneumatically with palm nailer from each side to connect the outer laminations to the center laminations. The spacing between the two nails is chosen to be 4'' to satisfy the minimum fastener spacing ($16d_F$) found in the Canadian timber design standard (CSA O86, 2019).

In addition, the nails are positioned such that the minimum end distance parallel to grain ($12d_F$), and the minimum edge distance perpendicular to grain ($4d_F$) are satisfied. The 3'' nails are driven directly into solid sawn lumber laminations, while a lead hole, equal to 1/8'' in diameter is used to drive the 3-1/2'' nails into the LVL laminates, in order to avoid wood splitting. It is ensured that the nail head is flush with the surface of the wood lamination. Also, a pre-drilled lead hole with a diameter of 3/16'' is used prior to installing the 6-3/4'' screws into the LVL laminates.

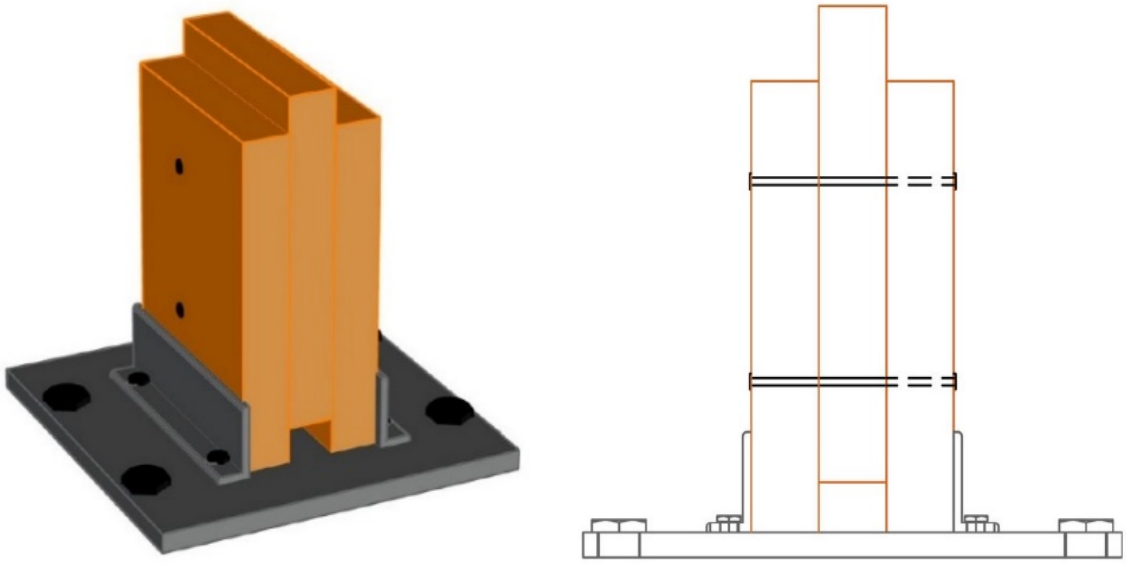

(a) (b)

Figure 4.2 Lateral tests of nails (a). Configuration; (b). Cross-section view

The lateral test setup for the parallel and perpendicular to grain joints are shown in Figure 4.3 and Figure 4.4 for the lumber and LVL specimens, respectively.

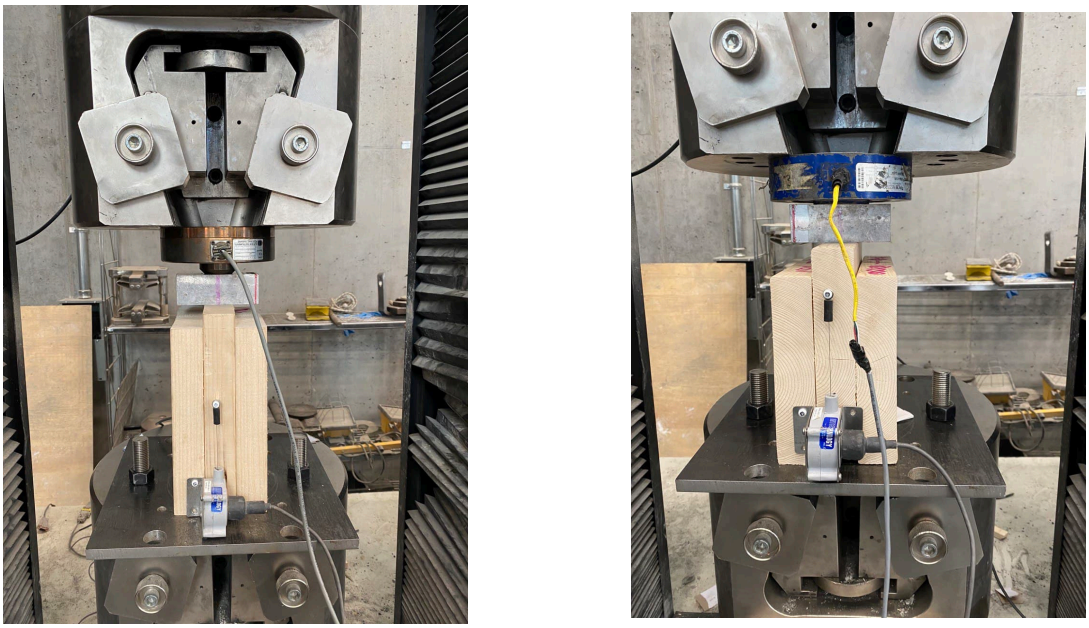

(a) (b)

Figure 4.3 Lateral test setup of 3’’ nails in (a). parallel to grain direction; (b). perpendicular to grain direction

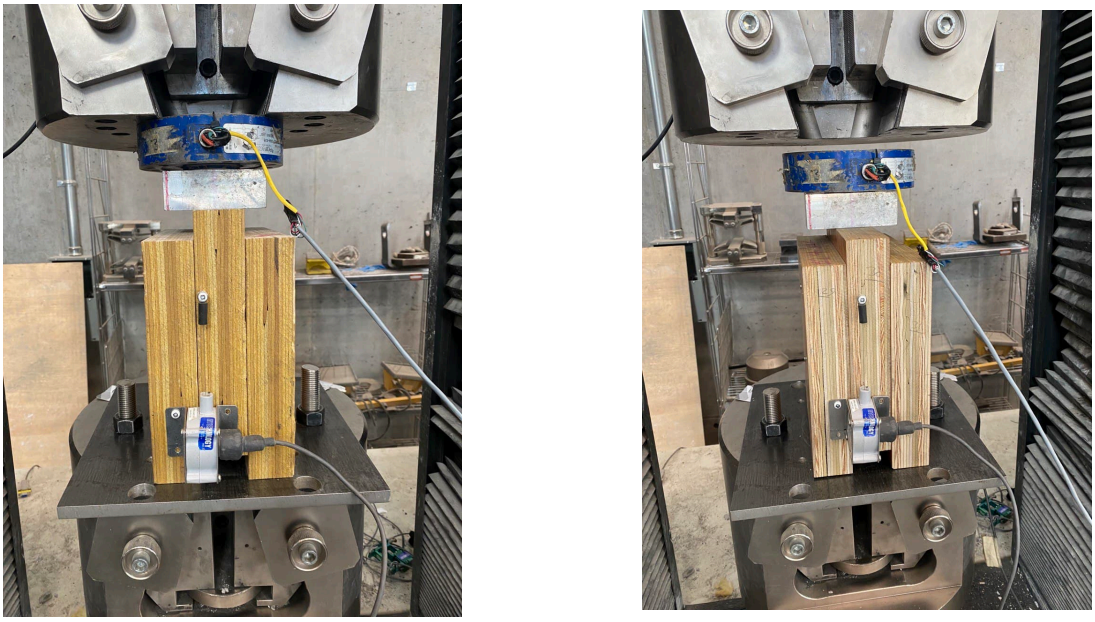

(a) (b)

Figure 4.4 Lateral test setup of 3-1/2’’ nails in (a). parallel to grain direction; (b). perpendicular to grain direction

The test setup for the 6-3/4’’screws used to join the four LVL laminates are slightly different in that the load is applied to the two middle laminates while the two outer laminates are supported. Only two screws are driven from one side of the beam with spacing consistent with that described above for nails. Due to the configuration of the test setup, the obtained test results represent the stiffness corresponding to two shear planes. The test setup is illustrated in Figure 4.5, while Figure 4.6 shows the test setup for the lateral tests in parallel and perpendicular to grain directions.

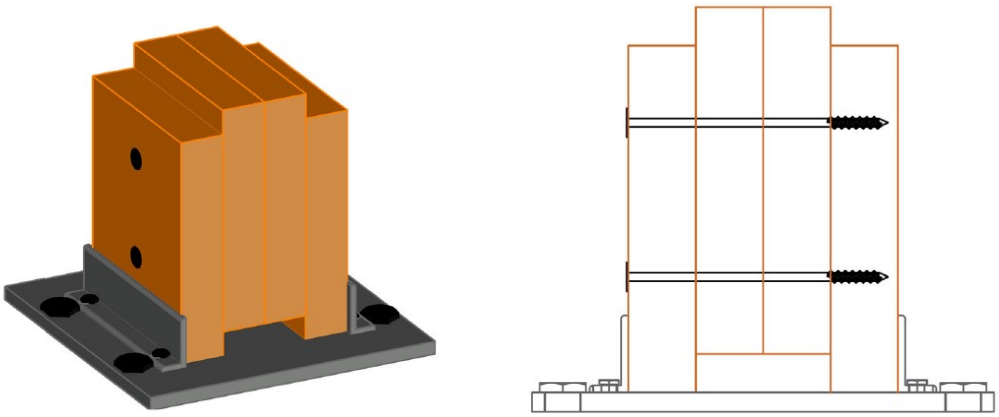

(a) (b)

Figure 4.5 Lateral tests of screws (a). Configuration; (b). Cross-section view

(a) (b)

Figure 4.6 Lateral Test setup of 6-3/4'' screws in (a). parallel to grain direction; (b). perpendicular to grain direction

4.4. Withdrawal test setup

The test configuration and loading procedure for the withdrawal tests followed the ASTM D1761 standard (2012), and is illustrated in Figure 4.7. For testing the withdrawal stiffness of 3'' nails, two pieces of SPF lumber with a width of 1.5'', depth of 2'' and length of 4'' and 8'', respectively, are used. The 3-1/2'' nails and 6-3/4'' screws are driven in the LVL piece that has the dimensions of 1.75'' in width, 2'' in depth and 8'' in length. The 3-1/2'' nails and 6-3/4'' screws are inserted in predrilled holes with a diameter of 1/8'' and 3/16'', respectively.

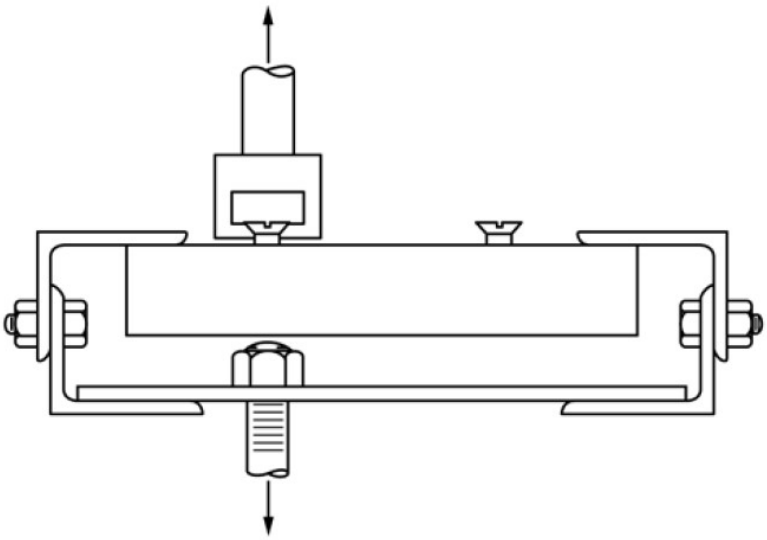

Figure 4.7 Withdrawal test configuration (ASTM D1761, 2012)

The test matrix for the withdrawal tests is provided in Table 4.3.

Table 4.3 Test matrix of the withdrawal tests

Wood Type	**Number of Plies**	**Type of Mechanical Fastener**	**Number of Mechanical Fastener**
SPF	2	3'' Common Nails	1
LVL	1	3-1/2'' Common- Nails	1
LVL	1	6-3/4'' Long SIMPSON	1

The specimens were clamped to the testing machine by means of steel plates and a withdrawal force was applied through the gripping device on the fastener heads as shown in Figure 4.8 and Figure 4.9. Like lateral tests, all fasteners were driven pneumatically with palm nailer.

No initial measures were intentionally taken in order to promote a failure in nail or screw withdrawal. It is conceivable that failure could occur in nail or screw head pull through, especially for screw connectors due to their relatively higher withdrawal capacity.

Figure 4.8 Test setup of the withdrawal tests for 3’’ nail

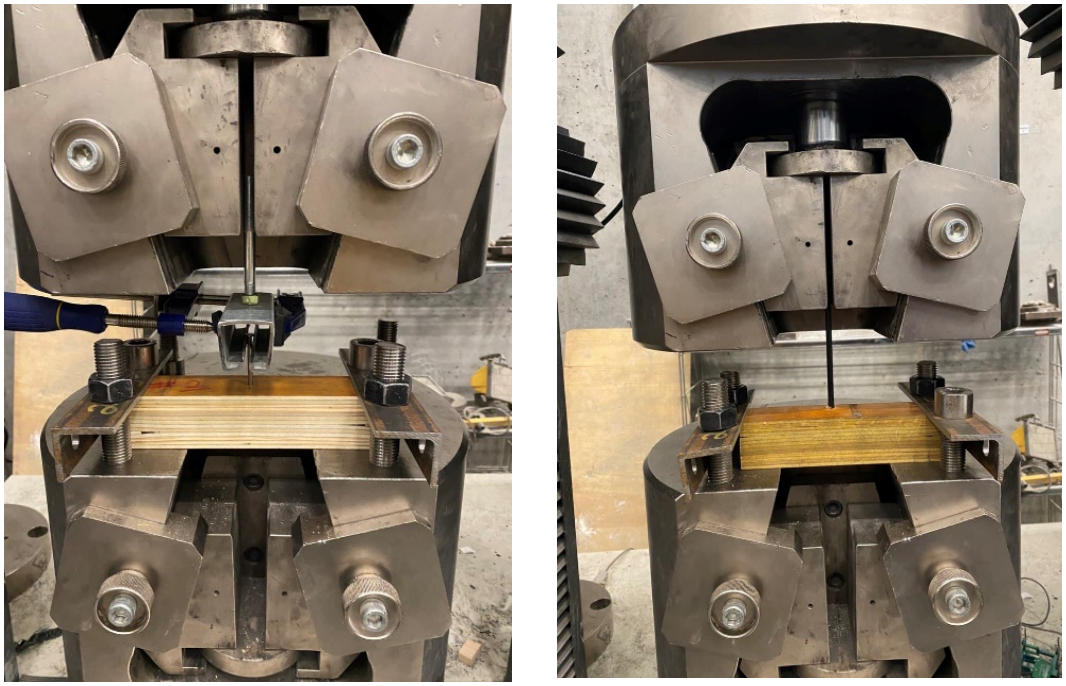

(a) (b)

Figure 4.9 Test setup of the withdrawal tests for (a). 3-1/2’’ nail; (b). 6-3/4’’ screw

4.5. Stiffness calculation method

The material available in the literature regarding initial stiffness calculation is typically meant to represent an approximation to the stiffness which in wood is non-linear in nature, even at relatively low load levels. No information was found in the literature that discusses what would be an appropriate load level to estimate the initial stiffness, which would be suitable for beam buckling. As mentioned earlier, this is an important concept that should be further investigated but is outside the scope of the current study. In the current project, the stiffness was calculated using a secant on the load-displacement curve corresponding to 10% and 40% of the ultimate load. The omission of the lower 10% is intended to eliminate behaviour dominated by factors that may be unrelated to the actual stiffness of the fastener being considered, but rather features related to the test setup, specimen details, boundary conditions, loading machine etc.

The upper limit of 40% is selected to limit the stiffness value to that representative of initial elastic stiffness before yielding in the joint is initiated. This approach is consistent with various loading protocols and research work (e.g., Winistorfer & Soltis, 1994, Sawata et al., 2013). Although the tested connection consisted of multiple fasteners (see Table 4.1), the stiffness of a single fastener is obtained by simply dividing the load by the number of fasteners and shear planes.

4.6. Lateral stiffness test results

4.6.1. Parallel to grain direction

The test procedure outlined in Section 4.3 was repeated on five duplicate specimens in order to establish some level of variability within each joint group. The number of replicates reflects the intended goal of conducting these joint tests, namely as inputs in the numerical model to obtain

realistic values for the buckling moment. If the aim is to establish performance characteristics for each fastener, then the number of replicates would need to be significantly higher, and the joints should have included other wood species and grades as well as other types of fasteners. As mentioned before, the current study is limited to typical joint configurations and materials used to construct built-up beams in light-frame construction.

Figure 4.10, Figure 4.11, Figure 4.12, Figure 4.13, and Figure 4.14 illustrate examples of the repeat 1 to 5 of the test on a specimen with SPF lumber and 3" nail and include the methodology of determining the initial stiffness using the secant method described above. The curves also show the two LVDT sensors on each side of the specimen and the average curve taken based on the data obtained from the two sensors. It can be seen that in general, the vertical movement of the specimen is even on both sides and the difference between the two curves is reasonably small.

As expected, the shape of the curves is non-linear even in the elastic region. The beginning of the curves can be characterized by a relatively linear-elastic portion that deviates from linearity before the yield point. It can also be observed that the yield point is not well-defined. This is primarily caused by the combined behaviour represented by bending in steel fastener and crushing in the wood. The curves seem to be ductile, as would be expected for fastener of this type with high slenderness (i.e. ratio of length to diameter). All joints seemed to attain their ultimate displacement just before the anticipated maximum displacement of 15 mm. Although the portion of the curve beyond the yield point is not of interest to the current study, it is presented here to provide a complete depiction of the joint behaviours.

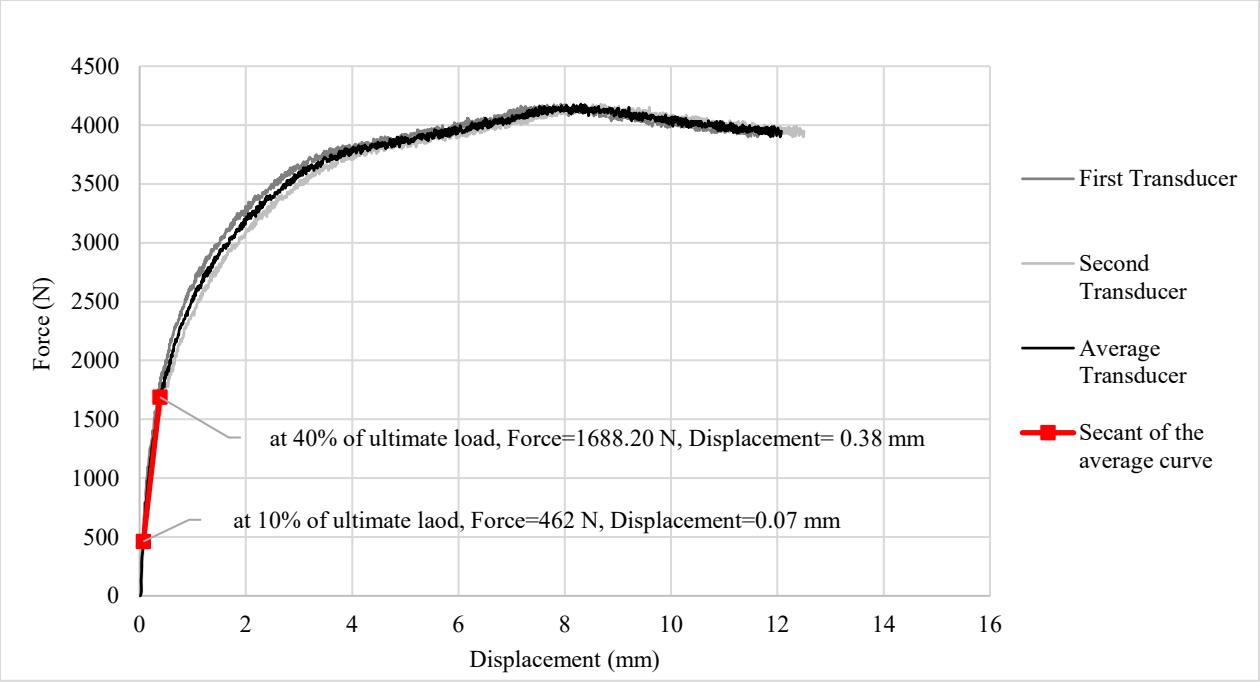

Figure 4.10 Load-Displacement curve of the first parallel to grain test with SPF lumber and 3'' nail

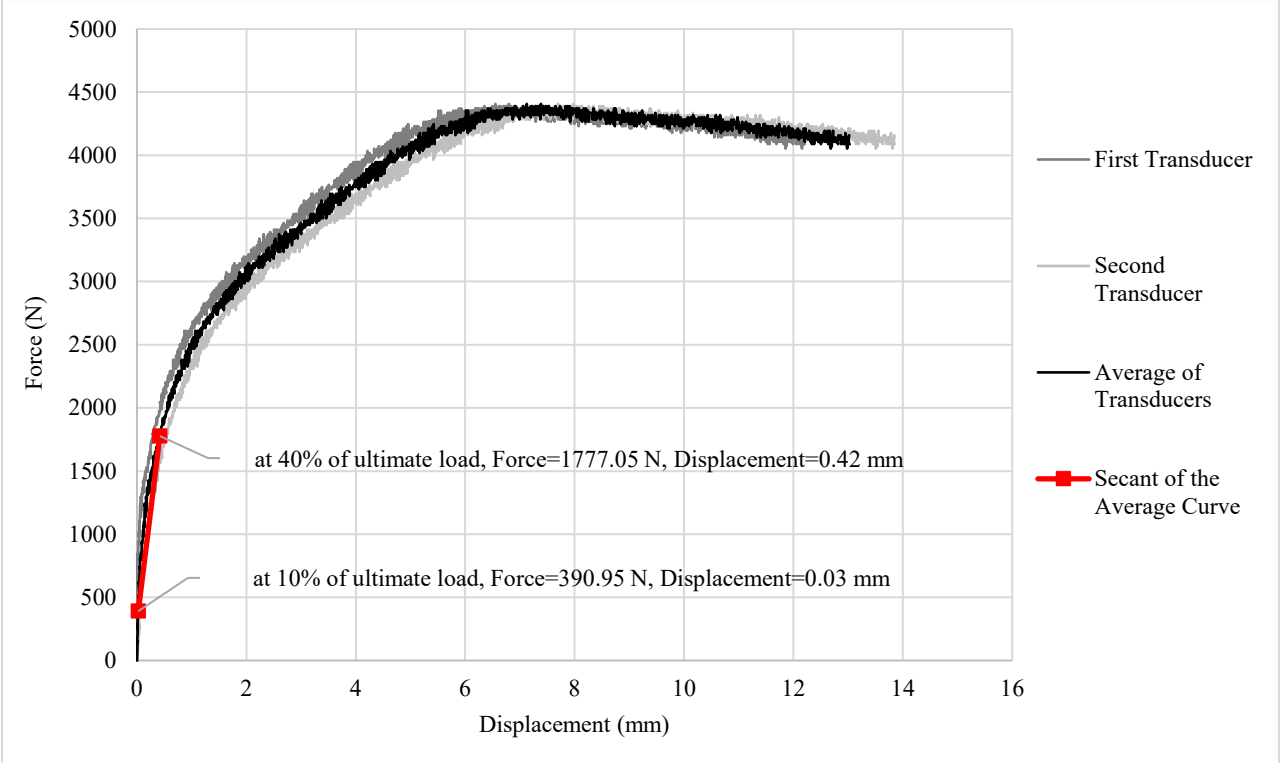

Figure 4.11 Load-Displacement curve of the second parallel to grain test with SPF lumber and 3'' nail

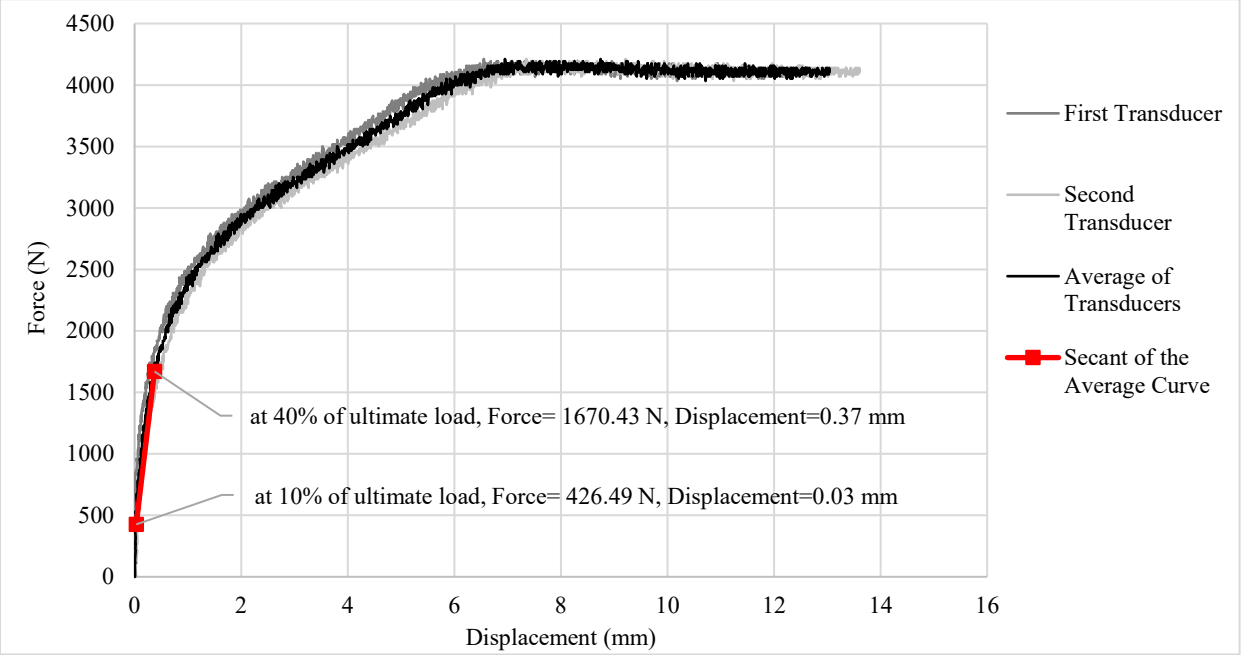

Figure 4.12 Load-Displacement curve of the third parallel to grain test with SPF lumber and 3'' nail

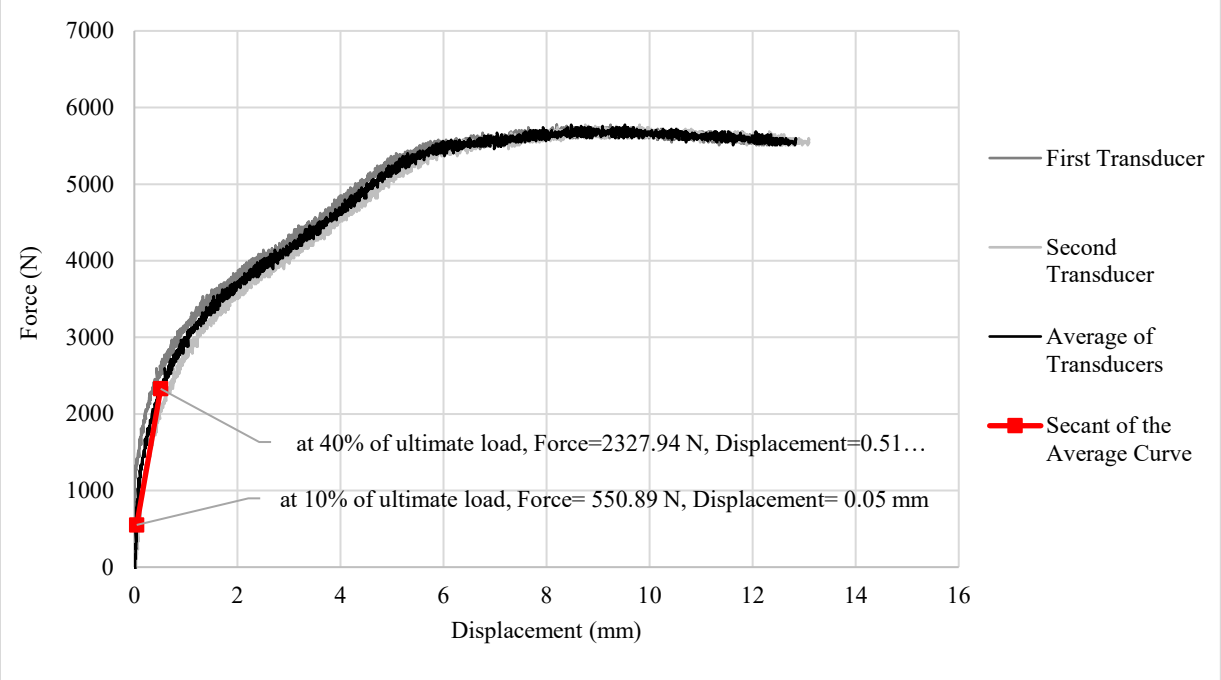

Figure 4.13 Load-Displacement curve of the fourth parallel to grain test with SPF lumber and 3'' nail

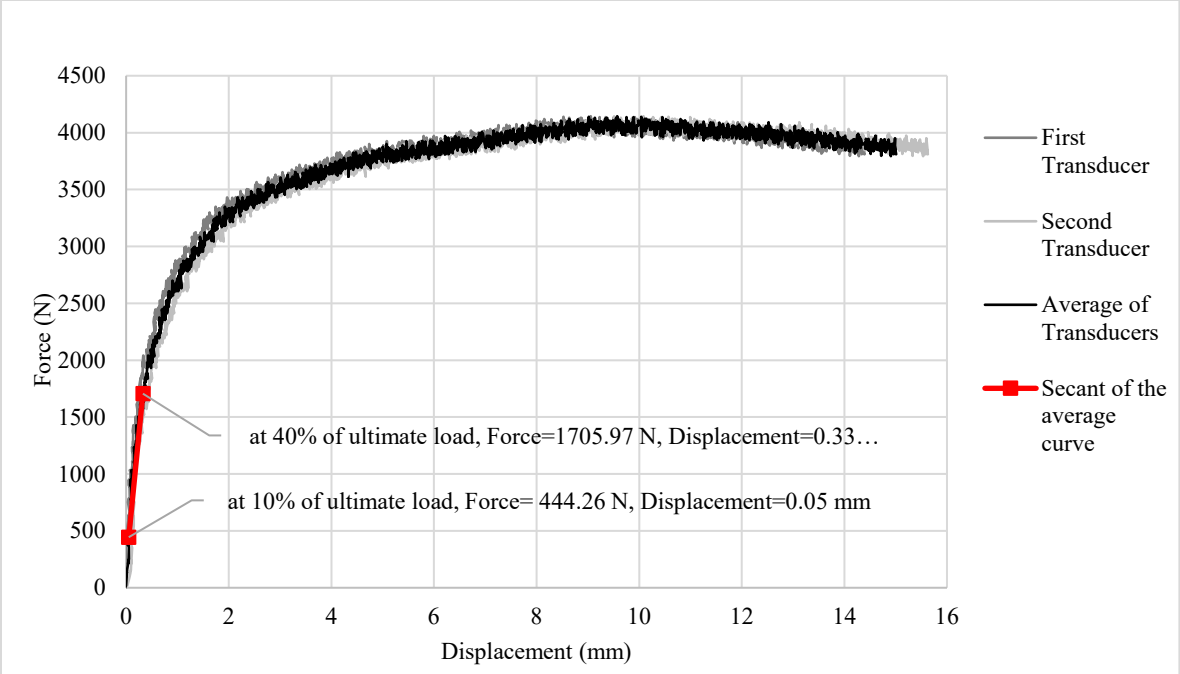

Figure 4.14 Load-Displacement curve of the fifth parallel to grain test with SPF lumber and 3'' nail

Figure 4.15 shows the average curve obtained from the five repeats.

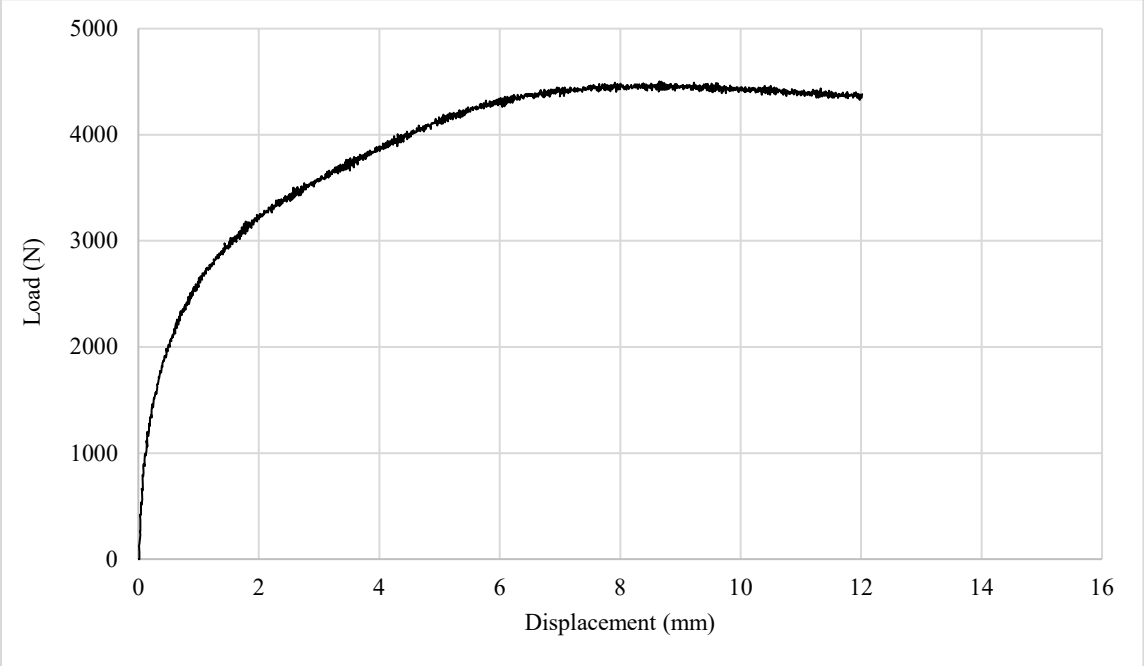

Figure 4.15 Average Load-Displacement curve of 3'' nail in SPF lumber in the parallel to grain test

The formula of the secant method for calculation of the stiffness is given in Equation 4.1.

$$K_{Par} = \frac{F_{40\%} - F_{10\%}}{\Delta_{40\%} - \Delta_{10\%}} \quad (4.1)$$

Where K_{Par} is the lateral stiffness in parallel to grain direction, $F_{40\%}$ and $F_{10\%}$ are 40% and 10% of ultimate load, $\Delta_{40\%}$ and $\Delta_{10\%}$ are the displacements corresponding to $F_{40\%}$ and $F_{10\%}$, respectively. The lateral stiffness value in parallel to grain direction, K_{Par}, for the joint of 3'' nail in SPF lumber from each test, as well as the average value, are calculated and given in Table 4.4.

Table 4.4 Experimental results of K_{Par} for 3'' nails in SPF lumber

Test Specimen	**K_{Par} (N/mm)**
1	983
2	898
3	909
4	954
5	1143
Average value	977
COV (%)	10.1

Based on the obtained results, the average stiffness for 3" nail in SPF lumber is calculated to be 977 N/mm with a COV of 10.1% for the cases presented above. The average load-displacement curve for the 3-1/2'' nail connecting LVL laminates is presented in Figure 4.16. The curve is in principle similar to that obtained for SPF using 3" nails (Figure 4.15). The average stiffness obtained from this test series is equal to 1906 N/mm with COV of 7.25%.

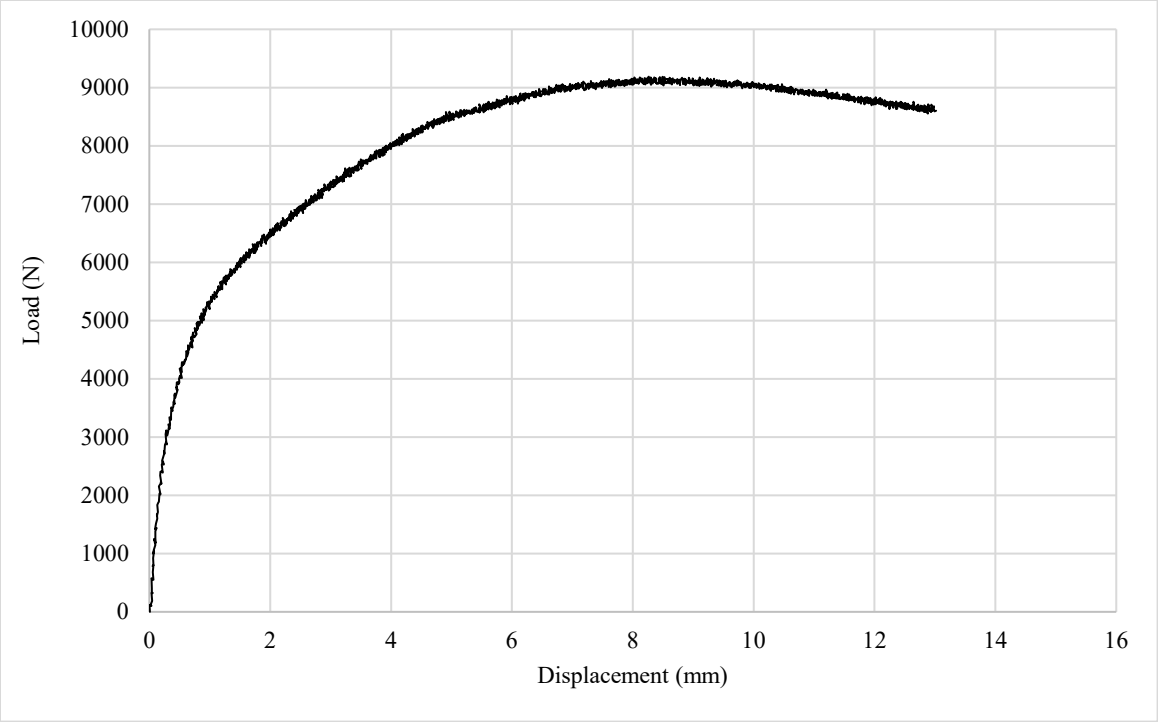

Figure 4.16 Average load-displacement curve of 3-1/2'' nails in LVL for parallel to grain direction

It can be seen that the stiffness value obtained for this group is significantly higher than that obtained for solid sawn lumber (nearly double). The significant increase in stiffness obtained for the 3-1/2'' nail relative to the 3" nail can be attributed to the larger diameter (4.11 mm versus 3.76 mm) and the higher relative density associated with LVL compared to SPF (550 kg/m^3 versus 407 kg/m^3). These factors also significantly affect the ultimate strength of the joint, where it can be seen that the peak load for the 3-1/2'' is also almost double that found for the 3".

The average load-displacement curve for the 6-3/4'' screw joint connecting LVL laminates is shown in Figure 4.17. The average stiffness is calculated to be 2022 N/mm with COV of 9.17%. The average stiffness value for this screw is only marginally higher than that obtained by the 3-1/2'' nail, which is primarily driven by the density in the material.

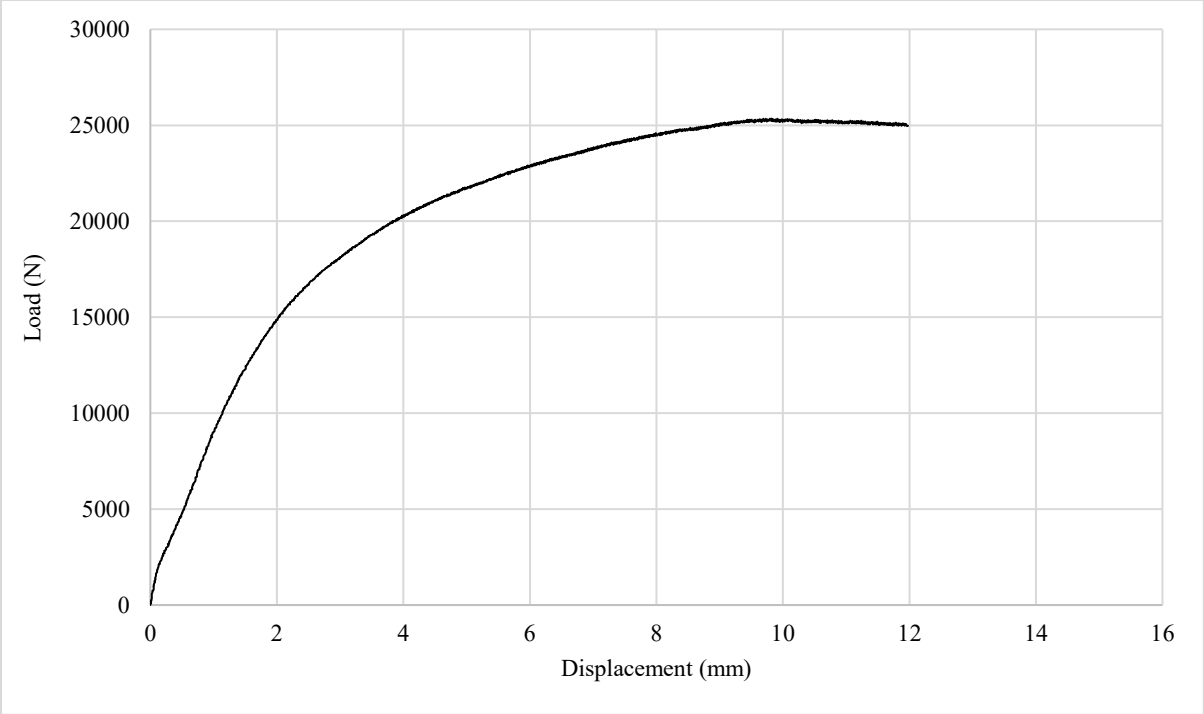

Figure 4.17 Average load-displacement curve of 6-3/4'' screws in LVL for parallel to grain direction

A summary of all the results is provided in Table 4.5 for the stiffness values obtained in the parallel to grain direction. Further details on the test results are provided in Appendix A.

Table 4.5 Summary of lateral test results of stiffness in parallel to grain direction

Fastener Type	**Average value of K_{Par} (N/mm)**	**COV (%)**
3'' Common Nail	977	10.1
3-1/2'' Common Nail	1906	7.25
6-3/4'' SIMPSON SDW22 Screw	2022	9.17

4.6.2. Perpendicular to grain direction

Lateral shear tests were conducted for the same three mechanical fasteners in the perpendicular to grain direction, K_{per}, in a similar manner as those described for the parallel to grain direction in

Section 4.3. The average load-displacement curves for the 3'' nail, 3-1/2'' nail and 6-3/4'' screw are shown in Figure 4.18, Figure 4.19 and Figure 4.20, respectively, with corresponding average stiffness values of 1195 N/mm (20.4%), 1574 N/mm (6.88%) and 1290 N/mm (4.95%). Table 4.6 provides a summary of the results and more detailed results can be found in Appendix A.

In general, the shape of the graph obtained in the perpendicular to grain direction is not very different from that obtained for the parallel to grain direction. However, the stiffness values in the perpendicular to grain direction seem to be generally lower than those obtained in the parallel to grain direction. Since the fasteners are the same, this observation could be attributed to the crushing resistance of wood in the two directions. It is well known from design standards that the crushing strength of wood (embedment strength) is significantly smaller in the perpendicular to grain direction compared to the parallel to grain direction, with a ratio (i.e. perpendicular to parallel) of embedment strength of approximately half. Whether the same applies to stiffness cannot be concluded explicitly based on the available results, but certainly the tendency point in the direction of smaller stiffness.

Table 4.6 Summary of lateral test results of stiffness in perpendicular to grain direction

Fastener Type	**Average value of K_{Per} (N/mm)**	**COV (%)**
3'' Common Nail	1195	20.4
3-1/2'' Common Nail	1574	6.88
6-3/4'' SIMPSON SDW22 Screw	1290	4.95

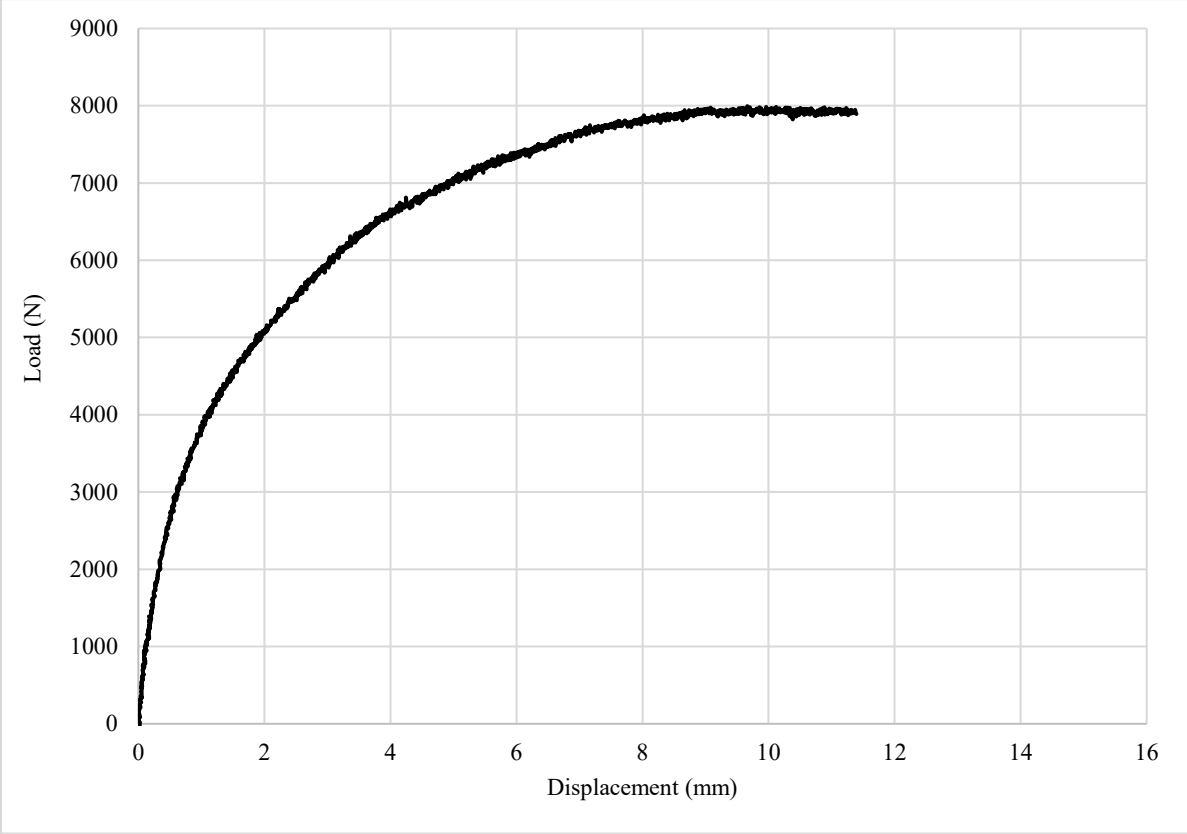

Figure 4.18 Average load-displacement curve of 3'' nails in SPF lumber in perpendicular to grain direction

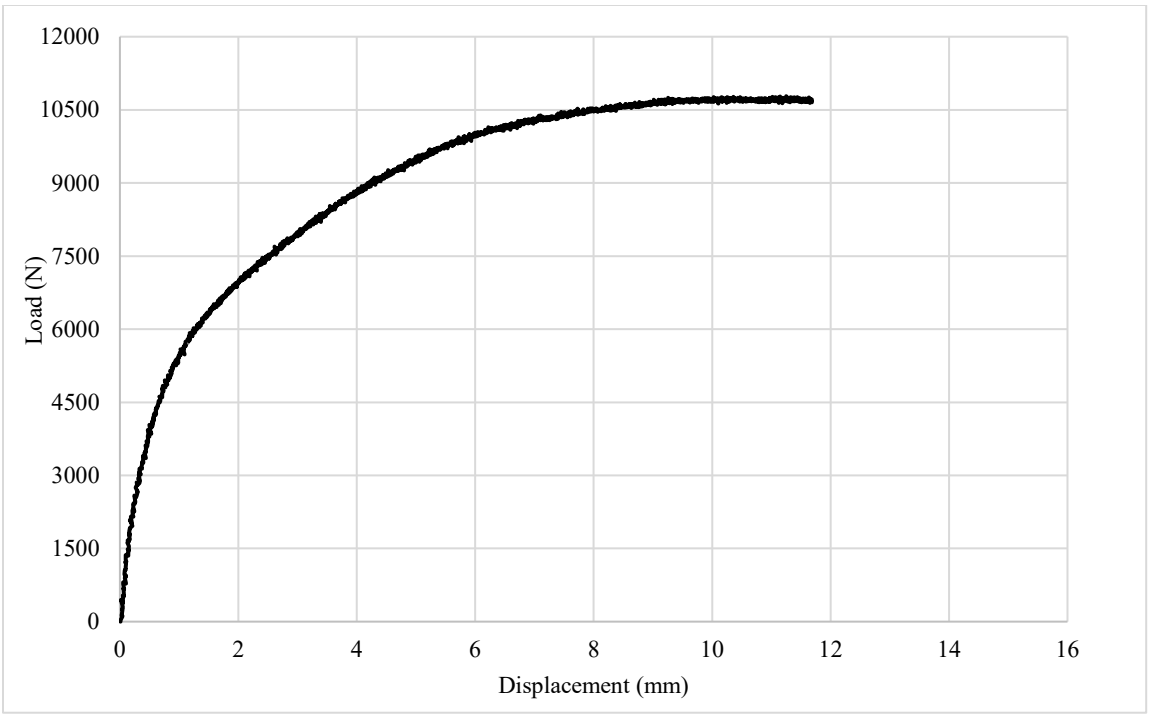

Figure 4.19 Average load-displacement curve of 3-1/2'' nails in LVL in perpendicular to grain direction

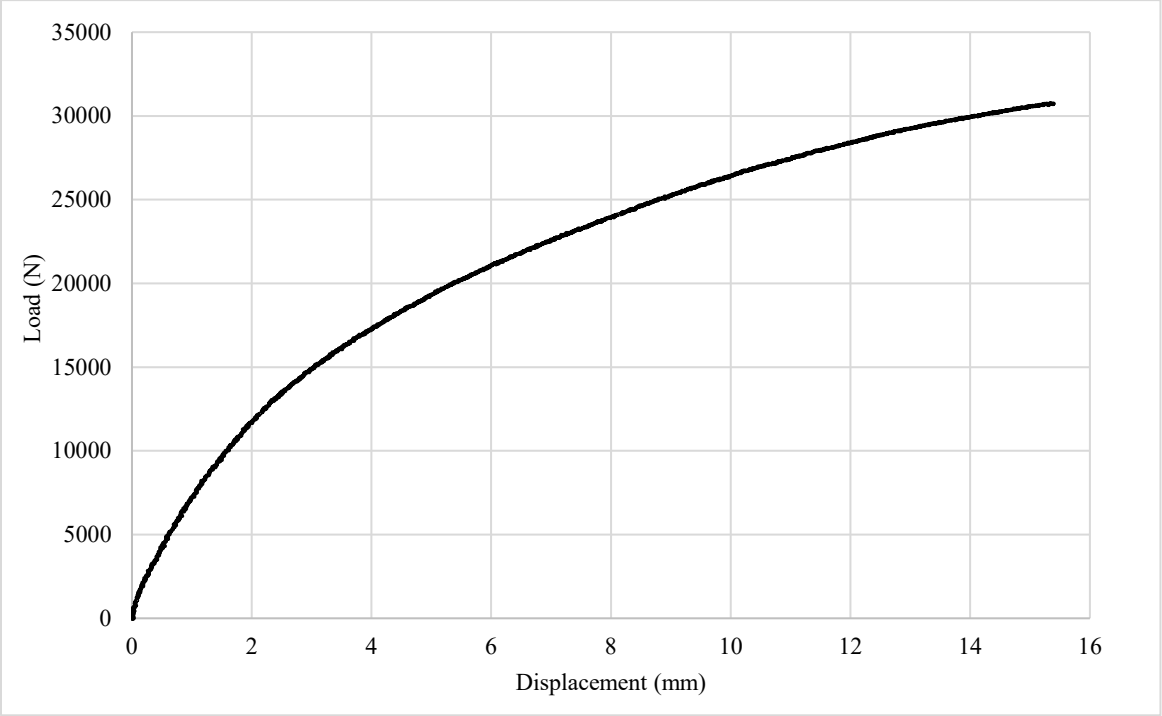

Figure 4.20 Average load-displacement curve of 6-3/4'' screw in LVL in perpendicular to grain direction

4.7. Withdrawal stiffness

This section presents the average load-displacement curves for the five replicate tests conducted for each mechanical fastener and the calculated withdrawal stiffness, denoted as K_w. The average load-displacement curve of the tensile test for 3'' nail, 3-1/2'' nail, and 6-3/4'' screw are illustrated in Figure 4.21, Figure 4.22, and Figure 4.23. The average stiffness obtained from each group of test replications based on the secant method outlined in Section 4.5 is provided in Table 4.7. Further details are provided in Appendix A.

Table 4.7 Summary of tensile test results

Fastener Type	**Average value of K_w (N/mm)**	**COV (%)**
3'' Common Nail	1154	16.2
3-1/2'' Common Nail	1876	20.6
6-3/4'' SIMPSON SDW22 Screw	4074	16.1

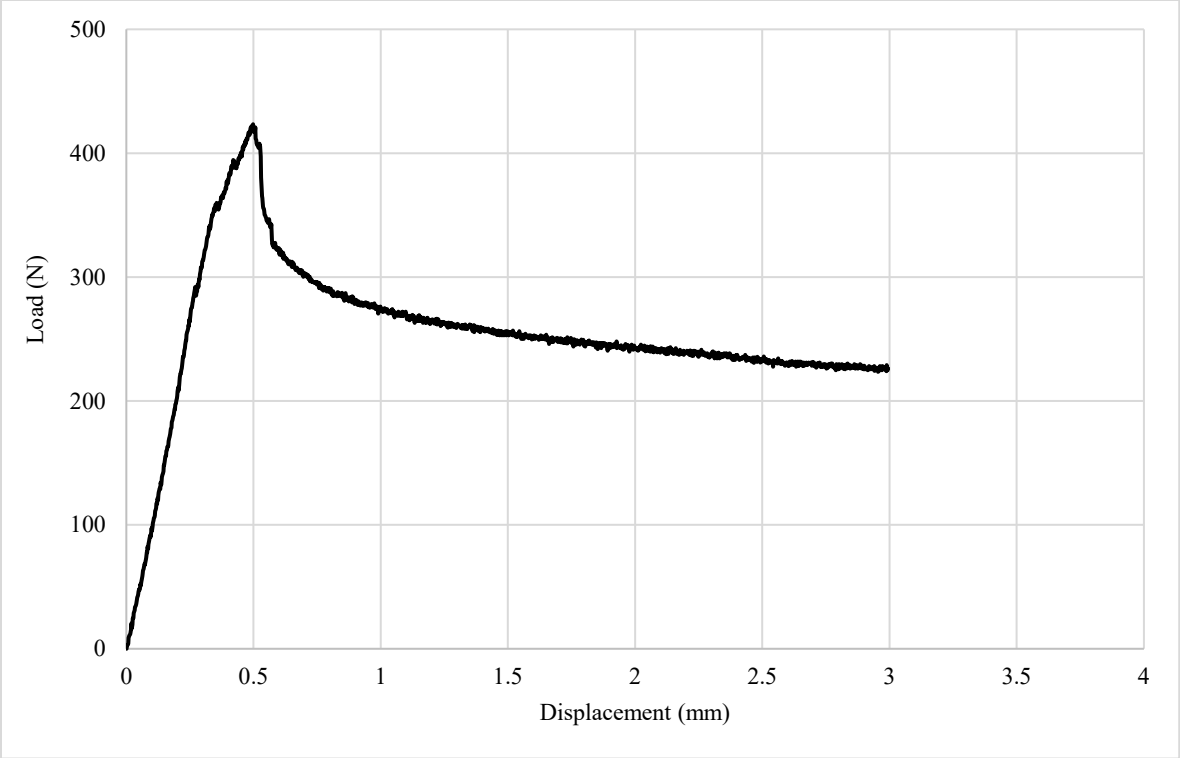

Figure 4.21 Average load-displacement curve of tensile test for 3’’ nails in SPF

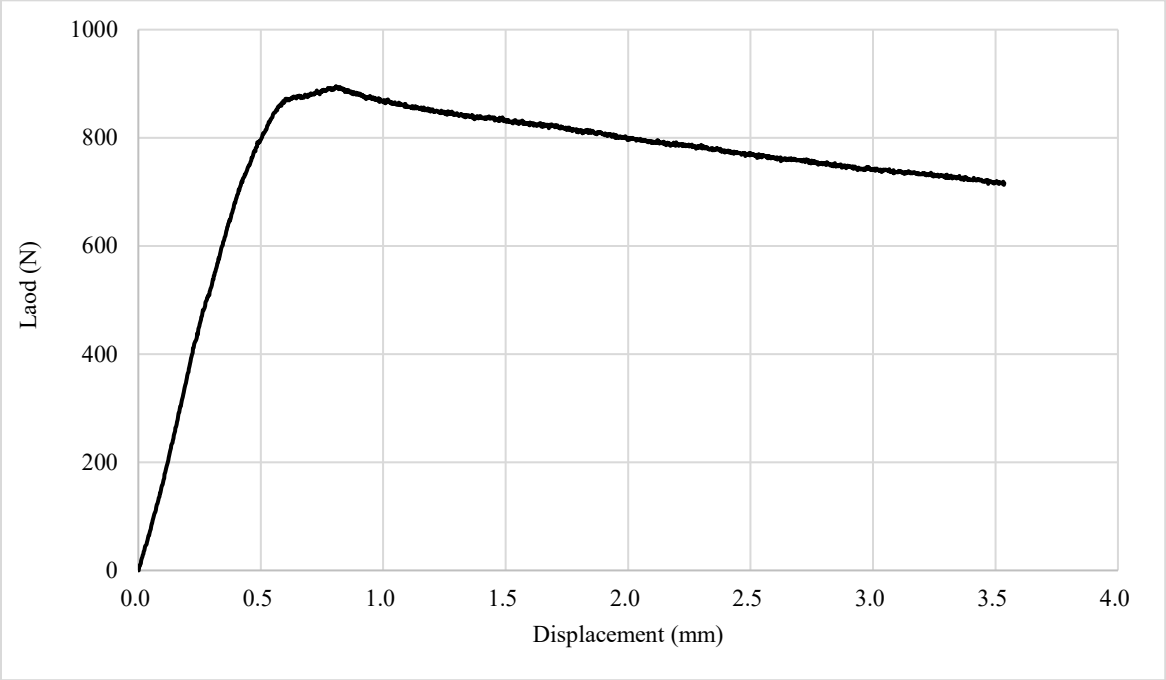

Figure 4.22 Average load-displacement curve of tensile test for 3-1/2’’ nails in LVL

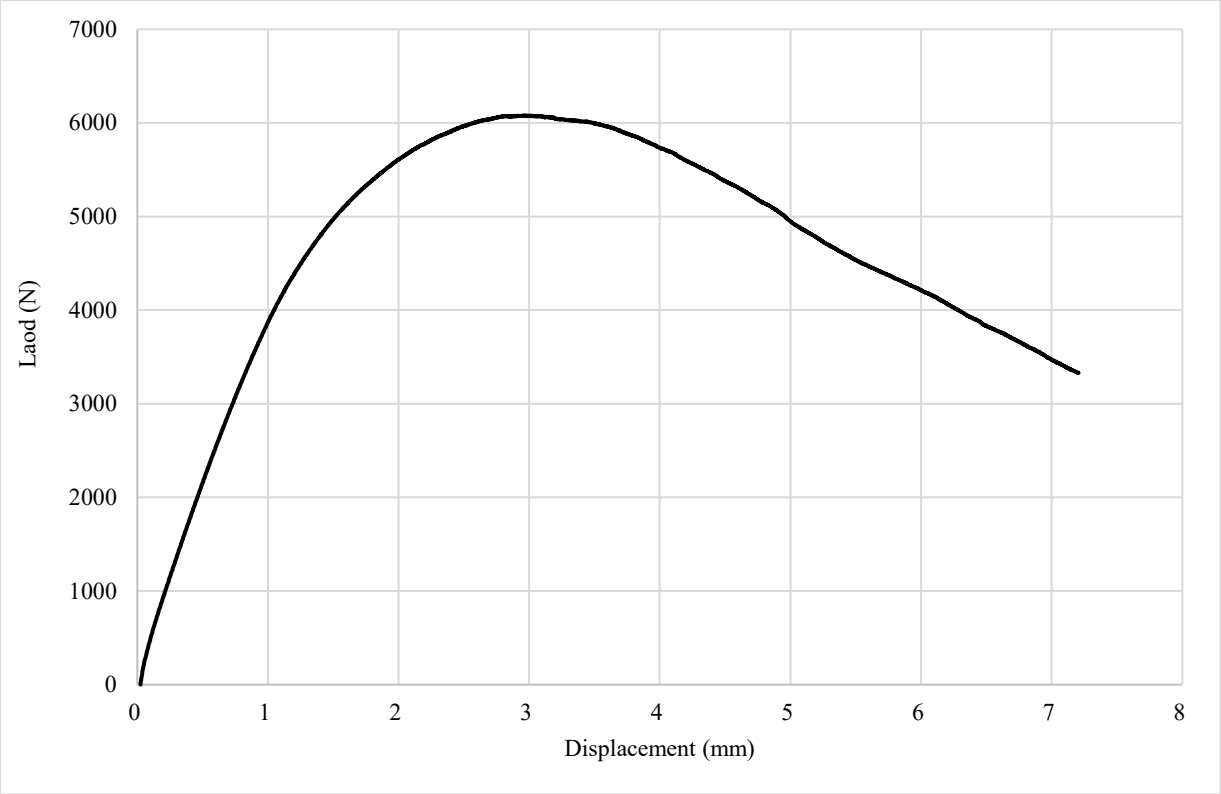

Figure 4.23 Average load-displacement curve of tensile test for 6-3/4'' screws in LVL

The initial portion of the graphs obtained from the withdrawal tests seems better defined and close to a linear behaviour than those observed in the lateral stiffness tests. It can also be observed that the yield as well as the ultimate displacement are significantly lower in the withdrawal tests. Although the post-peak region of the graphs is not directly relevant in this study, the behaviour of the nails and screws in withdrawal seem more brittle. Also, although the value of withdrawal stiffness was found to be almost insignificant in the sensitivity analysis in Chapter 3, it is noteworthy to indicate the very significant difference between nails and screws regarding the ultimate capacity and stiffness. In particular, the stiffness of the screw fasteners is around 2-4 times that of the nails. This can be attributed to several factors, but chiefly the screw threads that provide a much better grip between the screw fastener and the wood material. Whereas the nail fasteners'

withdrawal stiffness is mainly related to the friction created between the nail and wood when the nail was driven between the fibres. Withdrawal of screws involve some tearing of the mechanical connection created between the threads and the wood fibers.

It should be noted that only withdrawal tests in the direction perpendicular to grain were performed because these are reflective of the joint behaviour when the beam undergoes lateral torsional buckling failure.

It is also observed from Table 4.7 that the variability found in the withdrawal stiffness results is significantly higher than those found in the lateral test results. The variability is not expected to have any major effect on the results since, again, the LTB capacity of a built up beam is not sensitive to change in withdrawal stiffness of the fasteners connecting its laminations.

4.8. Comparison between test results and available analytical expressions

The elastic lateral stiffness of connections with mechanical fasteners for the serviceability limit state (SLS) is provided in Eurocode 5 (CEN, 2004), and referred to as slip modulus K_{ser}. This stiffness values corresponds to the secant of a load-displacement curve at load level equivalent to 40% of the ultimate load. Formulas for the slip modulus, K_{ser}, per shear plane per fastener for the nails and screws are reproduced in Table 4.8.

Table 4.8 Elastic stiffness of timber-to-timber connections per shear plane per fastener (N/mm) (CEN, 2004)

Fastener Type	K_{ser} (N/mm)
Screws Nails (with pre-drilling)	$\frac{{\rho_m}^{1.5} d}{23}$
Nails (without pre-drilling)	$\frac{{\rho_m}^{1.5} d^{0.8}}{30}$

In the formula, d (mm) is the fastener diameter and ρ_m (kg/m^3) is the mean density of the wood material. Accordingly, the lateral stiffness of the mechanical fasteners obtained from the test results can be compared with the values estimated by the above formulas.

As described earlier in this chapter, the 3'' nails were tested without pre-drilling, whereas the 3-1/2'' nails were tested with pre-drilling. Using the appropriate formula for each fastener from Table 4.8, the lateral stiffness can be calculated and compared to those obtained from the experimental results found in this study, as shown in Table 4.9. As mentioned before the code formula do not distinguish between the parallel and perpendicular to grain directions, while the current testing showed that some differences could be observed.

Table 4.9 Comparison of lateral test results with Eurocode estimation

Fastener	K_{ser} (N/mm)	K_{Par} (N/mm)	K_{Per} (N/mm)	$\frac{K_{Par}}{K_{ser}}$	$\frac{K_{Per}}{K_{ser}}$
3" common nail	792	977	1195	1.23	1.51
3-1/2" common nail	2308	1906	1574	0.83	0.68
6-3/4'' SIMPSON SDW22 screw	3139	2013	1290	0.64	0.41

The results show that significant differences can be found between the obtained results and those estimated using the code equations. The variability is mainly related to the natural variability found in wood in general.

Since the impact of the fastener stiffness is only moderate (see Chapter 3), it was decided to show the difference between the LTB moment obtained using the stiffness values from Eurocode (CEN, 2004) and test results. Three built-up beams, connected with 3'', 3.1/2'' nails and 6-3/4'' screws, are analyzed by the FEM described in Chapter 3. Table 4.10 shows the results of the comparison between the critical moments.

Table 4.10 Comparison of critical moment of built-up beams analysed with Eurocode and test stiffness

Ply dimension	Wood type	Number of plies	Fastener type	$M_{cr,Eurocode}$ (kN.m)	$M_{cr,Test}$ (kN.m)	$\frac{M_{cr,Eurocode}}{M_{cr,Test}}$
2''×6''×8'	SPF	2	3" common nail	7.19	7.27	0.98
2''×8''×10'	LVL	2	3-1/2" common nail	21.9	21.2	1.03
2''×8''×10'	LVL	4	6-3/4'' SIMPSON SDW22 screw	59.3	52.7	1.13

$M_{cr,Eurocode}$ and $M_{cr,Test}$ indicate the critical moments of the built-up beams analysed by taking the Eurocode and test values as the fasteners stiffness, respectively. In general, it can be seen that the difference between using the test results and the code formula would yield the same results for nail connections, whereas the difference seems more pronounced (13% difference) when screws were used. The variability in general seems reasonable, and it is recommended that limited test program should be sufficient to evaluate whether the code stiffness equation is suitable to be used in assessing the joint stiffness for the purpose of LTB capacity.

As noted earlier (e.g., Section 3.5.1 in Chapter 3), the LTB capacity of built-up beams is not sensitive to the withdrawal stiffness of the mechanical fasteners, as long as the withdrawal stiffness is above a certain threshold value. Table 4.11 demonstrate this by essentially yielding the same LTB capacity for a 4-Ply SPF built-up beam equal to 19.4 kN.m while using different withdrawal stiffness values representing the range found during the experimental testing phase (Table 4.7).

Table 4.11 4-Ply SPF built-up beam analyzed with different K_w

Ply dimension	**Wood type**	**Number of plies**	**K_w (N/mm)**	**M_{cr} (kN.m)**
2’’×6’’×8’	SPF	4	1154	19.4
			1876	
			4074	

Chapter 5- Proposal for prescriptive design approach for timber built-up beams

5.1. General

Based on the analysis conducted in this thesis, it is clear that the buckling capacity of timber built-up beams, constructed using mechanical fasteners, is less than a solid beam with equivalent length and cross-sectional area. The reduced capacity of the built-up beam can be expressed as a ratio of the solid beam capacity, similar to what is currently the case for built-up column provisions in the Canadian timber design standard (CSA O86, 2019). The reduction factor is intended to represent the partial composite action developed between the beam laminations and its magnitude is expected to be dependent on the number of plies, fastener types and diameters, as well as the spacing between fasteners. The pattern of fastener layout is also expected to play an important role; however, for the purpose of this proposal, this variable is not considered. The types and patterns of joints presented in this chapter are in no way comprehensive but it provides a framework for a possible approach to develop design provisions that are simplified and adequate for a design standard.

The need for this work is best demonstrated by considering the current provisions for built-up beams, as outlined in Clause 6.5.3.2.4 of the CSA O86 Standard (2019). The provision states that

> "*For built-up beams consisting of two or more individual members of the same depth, the maximum ratio permitted in Clause 6.5.3.2.1 for laterally-unsupported members may be based on the total width of the beam, provided that the individual members are fastened together securely at intervals not exceeding four times the depth*".

In other words, the provision allows the use of buckling capacity for built-up beams equivalent to a solid beam with the same cross-sectional dimensions, if the built-up beam plies are fastened securely at intervals not exceeding four times the beam depth. The standard does not quantify what the phrase ''securely fastened'' means, and this has and will continue to cause confusion since it can be interpreted as either properly fastened (i.e., following typical fastening procedures) or that the point of connection is expected to provide full restraint points. In reality, none of those interpretations ensure that the built-up beam performance and buckling capacity is near that of a solid section.

The methodology employed in this section to assess the reduction factors that could be used in the design of built-up beams relies on a limited number of beam configurations that are typically used in construction of light-frame wood buildings. Included in these configurations are the most typical lumber species (i.e., SPF) and engineered wood product species (i.e., LVL) and fastener types (i.e., nails and screws). It also includes 2-4 ply beams, since these represent the most commonly used layouts.

It is very important to emphasize that the proposed methodology of using a reduction factor has an obvious limitation, whether the depth to width ratio of the built-up beam is less than unity. In this case the buckling capacity tends towards infinity and buckling failure mode is no longer applicable. As such, using a reduction factor would not be appropriate in this case. This indicates

that further development to assess the actual buckling capacity based on the dimension of the individual laminations and the stiffness of the laminations and connections is important and recommended in future research effort.

Table 5.1 and Table 5.2 provide the dimensions of the SPF and LVL beams, respectively, that are analysed in this study. The type of mechanical fasteners used to create the built-up beams are indicated in Table 5.3.

Table 5.1 Dimension of SPF beams

Cases	Depth (mm)	Beam length, 18d (mm)	Number of plies
1	140	2515	2, 3 and 4
2	184	3315	2, 3 and 4
3	235	4229	2, 3 and 4
4	286	5144	2, 3 and 4

Table 5.2 Dimension of the LVL beams

Cases	Depth (mm)	Beam length, 18d (mm)	Number of plies
1	184	3315	2, 3 and 4
2	241	4343	2, 3 and 4
3	298	5372	2, 3 and 4
4	356	6401	2, 3 and 4
5	406	7315	2, 3 and 4
6	457	8230	2, 3 and 4
7	508	9144	2, 3 and 4
8	610	10973	2, 3 and 4

The logic behind using 3'' and 3-1/2'' nails to construct the SPF and LVL built-up beams, respectively, is that the width of the individual lumber lamination is 1-1/2'', while for LVL the laminate width is 1-3/4''. This ensures that a single nail fully penetrates the two laminations in each beam type. For 3-ply beams, the nails are driven from each side to ensure two single-shear connections. The CSA O86 (2019) requires a minimum penetration into the point-side element of

five times the nail diameter, which for the 3” and 3.5” nails used here would be equivalent to 18.8 mm and 20.6 mm, respectively. The 6’’ and 6-3/4’’ screws are used to construct the 4-ply SPF and LVL built-up beams, respectively. Since the fasteners are long enough to penetrate all laminates (e.g., 6” = 4 × 1-1/2”), it is only necessary to drive the screws from one side of the beam.

Table 5.3 Mechanical fasteners used to connect built-up beams

Wood type	**Number of plies**	**Mechanical fasteners**
SPF	2 and 3	3’’ nails
SPF	4	6’’ screws
LVL	2 and 3	3-1/2’’ nails
LVL	4	6-3/4’’ screws

The nailing pattern presented in this chapter also considers the most commonly used layout in construction and was developed in consultation with practicing engineers, as shown in Figure 5.1. More patterns could have been developed but as was demonstrated in Section 3.5.2, the increase in number of fasteners only marginally increases the buckling capacity due to the limitation in the nail stiffness. The nail spacing parallel to the grain (along the beam length) is selected to be 300 mm (nominal 1 foot), while the nail spacing in the perpendicular direction (along the beam depth) is chosen to be equal to 75 mm.

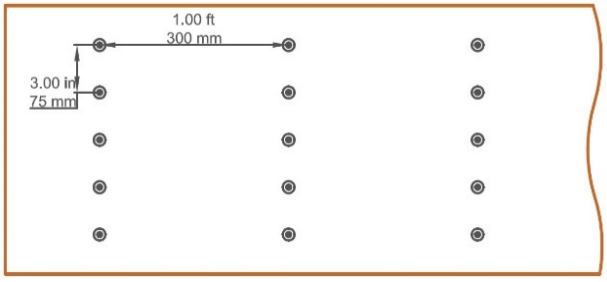

Figure 5. 1 Fastener pattern

5.2. Buckling capacity of built-up beams based on reduction factor

5.2.1. SPF Built-up Beams

Built-up beams consisting of SPF lumber and with dimensions provided in Table 5.1 and nailing provided in Table 5.3 with pattern indicated in Figure 5.1 are modelled in ABAQUS, as described in Chapter 3. The obtained lateral torsional buckling mode for the 4-ply built-up beams is illustrated in Figure 5.2.

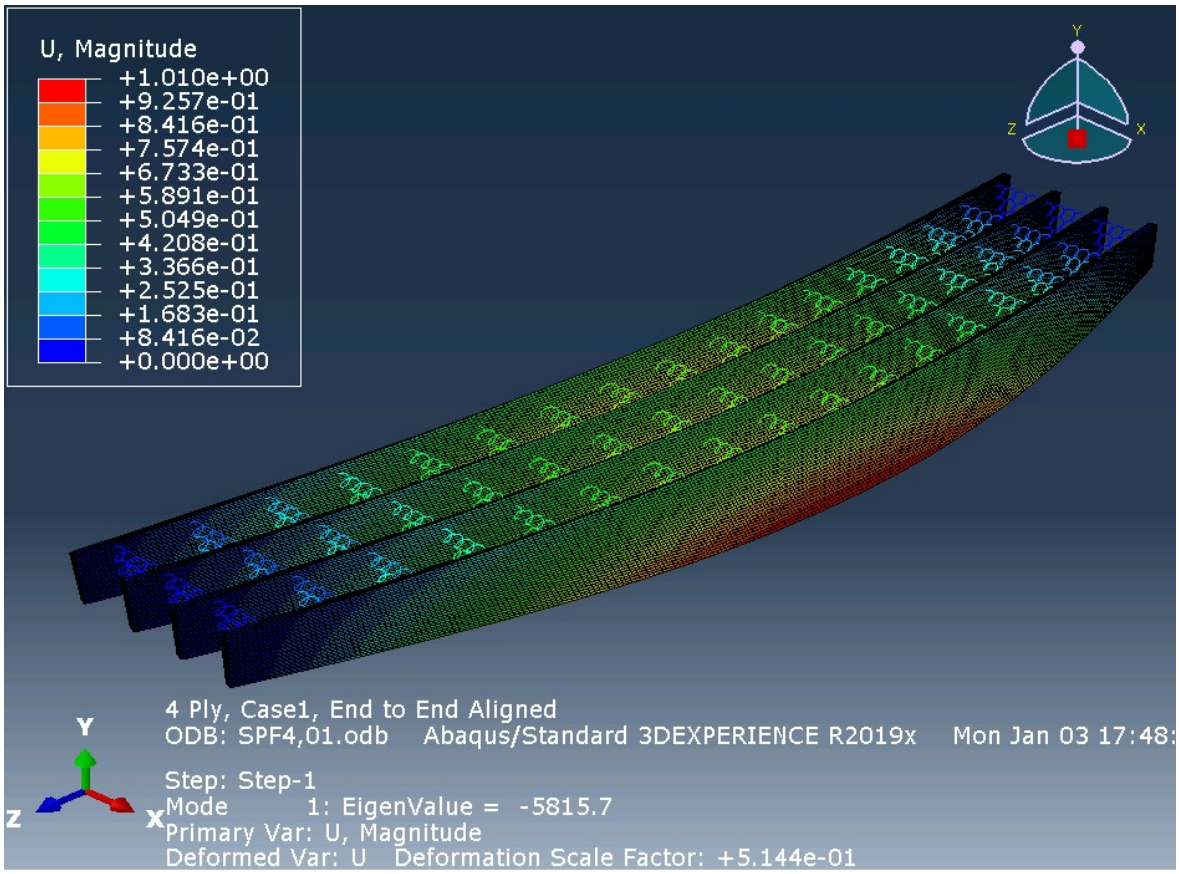

Figure 5.2 Buckling mode of SPF 4-ply built-up beam

The degree of composite action is calculated by dividing the critical moment obtained from the ABAQUS built-up beam model by those obtained from solid section with the same cross-sectional

area. The results are summarized in Table 5.4. Cases 1-4 represent the SPF beam dimensions presented in Table 5.1, where the width of the beam is kept constant but the length and depth are varied at a constant ratio of 18. All cases provided in Table 5.4 are modelled according to Chapter 3.

Table 5.4 Ratio of buckling capacity of SPF built-up to solid beam

Case	2-Ply Built-up beams			3-Ply Built-up beams			4-Ply Built-up beams		
	Critical Moment (kN.m)		Ratio (2)/(1)	Critical Moment (kN.m)		Ratio (2)/(1)	Critical Moment (kN.m)		Ratio (2)/(1)
	Solid beam (1)	Built-up beam (2)		Solid beam (1)	Built-up beam (2)		Solid beam (1)	Built-up beam (2)	
1	19.64	7.37	0.38	67.68	12.14	0.18	124.04	19.41	0.16
2	21.53	8.40	0.39	75.14	14.33	0.19	151.52	24.16	0.16
3	22.88	9.11	0.40	81.06	15.39	0.19	168.28	26.23	0.16
4	23.75	10.05	0.42	85.04	18.13	0.21	178.24	32.26	0.18

It can be observed from Table 5.4 that although the reduction factors are reasonably consistent within the number of plies, beams with more plies tend to have smaller levels of composite action. It can also be observed that decreasing the beam depth, while maintaining the constant length-to-depth ratio, tends to slightly reduce the composite action.

Although the spacings between fasteners for the analyzed beams are significantly smaller than those specified in the CSA O86 Standard (2019), the highest ratio of composite action obtained in the analysis is equivalent to less than half the full solid section capacity. This confirms that the current provisions are not adequate to ensure the safety of built-up beams when buckling capacity

is considered. Based on the analysis, the following general recommendations can be made for the design provision for nailed SPF built-up beams based on the smallest obtained value from Table 5.4:

Bending moment resistance of a built-up beam consisted of 4 or less plies fastened together with nails or spikes may be taken as 15% of the resistance of an equivalent solid beam, provided that the spacing of nails along the member length does not exceed 300 mm and spacing perpendicular to the member length does not exceed 75 mm.

More detailed requirements, based on number of built-up plies could also be provided as follows:

The factored bending moment resistance of a built-up beam may be taken as the following:

a) For 2-ply built-up beams: 37% of the bending moment resistance of an equivalent solid SPF beam, when fastened with 3'' nails from one side with spacing along the member length not exceeding 300 mm and spacing perpendicular to the member length not exceeding 75 mm.
b) For 3-ply built-up beams: 18% of the bending moment resistance of an equivalent solid SPF beam, when fastened with 3'' nails from both sides with spacing along the member length not exceeding 300 mm and spacing perpendicular to the member length not exceeding 75 mm.
c) 4-ply built-up beams: 16% of the bending moment resistance of an equivalent solid SPF beam, when fastened with 6'' wood screws from one side with spacing along the member length not exceeding 300 mm and spacing perpendicular to the member length not exceeding 75 mm.

5.2.2. LVL Built-up Beams

The same procedure as described in Section 5.1 was employed to estimate the composite action for LVL built-up beams, and the results are shown in Table 5.5. The same general observations can be made, where the variability of ply dimensions has a relatively small impact on the built-up beam buckling capacity when compared with changes in the number of plies.

Table 5.5 Composite action of LVL built-up beams

Case	2-Ply			3-Ply			4-Ply		
	Critical Moment (kN.m)		Ratio (2)/(1)	Critical Moment (kN.m)		Ratio (2)/(1)	Critical Moment (kN.m)		Ratio (2)/(1)
	Solid beam (1)	Built-up beam (2)		Solid beam (1)	Built-up beam (2)		Solid beam (1)	Built-up beam (2)	
1	59.74	21.18	35.45	185.11	36.13	19.52	356.60	52.73	14.79
2	66.35	22.51	33.93	205.45	38.95	18.96	415.56	57.32	13.79
3	56.96	26.00	45.64	219.41	47.39	21.60	448.00	71.67	16.00
4	59.12	28.59	48.36	229.28	54.11	23.60	470.36	83.49	17.75
5	60.54	29.25	48.32	195.54	55.96	28.62	482.29	86.92	18.02
6	61.56	31.35	50.93	213.17	59.69	28.00	492.53	98.06	19.91
7	62.44	33.76	54.07	223.45	69.12	30.93	500.63	111.72	22.32
8	63.97	35.84	56.02	198.30	75.74	38.19	512.52	125.04	24.40

Based on Table 5.5, the following recommendations can be made:

Bending moment resistance of a LVL built-up beam consisted of 4 or less plies and fastened together with nails or spikes may be taken as 14% of the resistance of an equivalent solid beam, provided that the spacing of nails along the member length does not exceed 300 mm and spacing perpendicular to the member length does not exceed 75 mm.

More detailed requirements, based on the number of LVL built-up plies could also be provided:

The factored bending moment resistance of a built-up beams may be taken as the following:

a) For 2-ply built-up beams: 34% percentage of the bending moment resistance of an equivalent solid LVL built-up beam, when fastened with 3-1/2'' nails from one side with spacing along the member length not exceeding 300 mm and spacing perpendicular to the member length not exceeding 75 mm.
b) For 3-ply built-up beams: 19% percentage of the bending moment resistance of a solid LVL beam, when fastened with 3-1/2'' nails from both sides with spacing along the member length not exceeding 300 mm and spacing perpendicular to the member length not exceeding 75 mm.
c) For 4-ply built-up beams: 14% percentage of the bending moment resistance of an equivalent solid LVL beam, when fastened with 6-3/4'' wood screws from one side with spacing along the member length not exceeding 300 mm and spacing perpendicular to the member length not exceeding 75 mm.

CHAPTER 6- Conclusions and Recommendations

6.1. Summary and Conclusions

The main conclusions drawn from this study are summarized as follows:

1. The sensitivity analysis performed by FEM indicated that the LTB capacity of timber built-up beams is moderately sensitive to the lateral stiffness of the mechanical fasteners, but not sensitive to the withdrawal stiffness. As expected, the LTB capacity of timber built-up beams increased when the number of mechanical fasteners connecting their laminations was increased. However, the relationship between the LTB capacity and the number of mechanical fasteners was not proportional.
2. Although the stiffness for nails and screws obtained from published code values in Eurocode 5 differ from the stiffness obtained from test results for certain joint configurations, the difference between LTB capacities obtained from the test results and the code equations did not differ significantly for nails fasteners. However, some differences were observed for screw fasteners. Also, since the behaviour of built-up beams is not sensitive to the withdrawal stiffness, an assumed value, based on published tests or formula, may be used in the analysis.
3. The analysis assessing the degree of composite action in timber built-up beams showed that the reduction factor, representing the capacity relative to that of a solid section, decreases when the number of beam lamination increases and when the depth of the beam decreases.

4. One of the key outcomes of this study is the verification that the CSA O86 Standard (2019) provisions regarding fastener spacing for built-up beams to ensure full composite action is not adequate when beam buckling analysis is considered.
5. Reduction factors are developed and presented for typical design cases following consultation with designers. Reduction factors in the range of 0.14 to 0.42 were found for beams with 2 to 4 plies and fastener spacing not exceeding 300 mm along the member length and 75 mm perpendicular to the member length.

6.2. Recommendations for future research

1. The current study focussed on traditional fasteners, such as nails and screws, to join the beam laminations. Other connection types, like bolts and split rings, could be investigated since these types of connections are expected to provide significantly greater shear stiffness and better clamping action. Also, fasteners like self-tapping screws could also be used on an angle since this provides significant improvement in stiffness by engaging the screws in withdrawal.
2. The current study is limited to connection tests and FEA on full-scale beam elements. Conducting buckling test on full-scale beam elements would be a logical next step to validate some of the findings obtained in this study.
3. The current study analyzed the effect of stiffness (shear and withdrawal) as well as the number of fasteners. An analysis of the pattern of mechanical fasteners while keeping identical number of fasteners could be beneficial to develop optimized solutions for fastening built-up beam elements.

4. Analysing other loading conditions including uniformly distributed load and mid-span concentrated load.

References

Ahmadi, H. (2017). *Lateral torsional buckling of anisotropic laminated composite beams subjected to various loading and boundary conditions*. Kansas State University.

Amadio, C., & Bedon, C. (2010). Buckling of laminated glass elements in out-of-plane bending. *Engineering Structures*, *32*(11), 3780–3788. https://doi.org/10.1016/j.engstruct.2010.08.022

Amana, E. J. (1967). Theoretical and experimental studies on nailed and glued plywood stressed-skin components, Part I. Theoretical study. *J. of the Institute of Wood Sci.*, *4*(1), 43-69.

American Forest and Paper Association. (2003). Technical Report 14: *Designing for lateral-torsional stability in wood members*. Washington, D.C.

ASTM D1761-12 *Standard Test Methods for Mechanical Fasteners in Wood*. ASTM International.

Burow, J. R., Manbeck, H. B. and Janowiak, J. J. (2006). Lateral Stability of Composite Wood I-joists under Concentrated-load Bending. *American Society of Agricultural and Biological Engineers*, Vol. 49, pp 1867-1880.

Canadian Commission on Building and Fire Codes- National Research Council of Canada. (2015). *National Building Code of Canada*, 14th ed., 1412. Ottawa, Canada: Natural Resources Canada (NRCan).

European Committee for Standardization. Eurocode 5. (2004). *Design of timber structures. Part 1-1: General – Common rules and rules for buildings*. EN 1995-1-1. Brussels: British Standards Institution (BSI). 124 p.

Challamel, N., & Girhammar, U. A. (2011). Boundary-layer effect in composite beams with interlayer slip. *Journal of Aerospace Engineering*, 24(2), 199-209.

Challamel, N., & Girhammar, U. A. (2012). Lateral-torsional buckling of vertically layered composite beams with interlayer slip under uniform moment. *Engineering Structures*, *34*, 505–513. https://doi.org/10.1016/j.engstruct.2011.10.004

Canadian Standards Association. (2019). *Engineering Design in Wood*. (CSA), 240.

Du, Yang, et al. (2016). *Lateral Torsional Buckling of Wooden Beam-Deck Systems*. University of Ottawa.

Du, Y., Mohareb, M., & Doudak, G. (2016). Nonsway Model for Lateral Torsional Buckling of Wooden Beams under Wind Uplift. *Journal of Engineering Mechanics*, *142*(12), 04016104. https://doi.org/10.1061/(ASCE)EM.1943-7889.0001172.

Du, Y., Mohareb, M., & Doudak, G. (2019, June). Sway Model for the Lateral Torsional Buckling Analysis of Wooden Twin-beam-deck Systems. In *Structures* (Vol. 19, pp. 19-29). Elsevier. Forest Products Laboratory. (2010): Wood Handbook-Wood as an Engineering Material. Madison, USA.

Forchheimer, P. _1892_. "Ueber zusammengesetzte Balken." *Z. Ver. Dtsch. Ing.*, 36, 100–103.

Galambos, T. V. (2008). *Structural stability of steel concepts and applications for structural engineers*. John Wiley & Sons. https://doi.org/10.1002/9780470261316.

Girhammar, U. A., & Gopu, V. K. A. (1993). Composite Beam-Columns with Interlayer Slip—Exact Analysis. *Journal of Structural Engineering*, *119*(4), 1265–1282. https://doi.org/10.1061/(ASCE)0733-9445(1993)119:4(1265).

Girhammar, U. A., & Pan, D. H. (2007). Exact static analysis of partially composite beams and beam-columns. *International Journal of Mechanical Sciences*, *49*(2), 239–255. https://doi.org/10.1016/j.ijmecsci.2006.07.005.

Granholm, H. (1949). *On composite beams and columns with special regard to nailed timber structures* (No. 88). Chalmer University of Technology, Goteborg, Sweden (in Swedish).

Trahair. E. & F. N. Spon (1993). Flexural, Torsional, Buckling of Structures.

Hindman D. P., Harvey, H. B. and Janowiak, J. J. (2005a). Measurement and Prediction of Lateral Torsional Buckling Loads of Composite Wood Materials: Rectangular Section. *Forest Products Journal*, Vol. 55, No. 9, pp 42-47.

Hindman D. P., Harvey, H. B. and Janowiak, J. J. (2005b). Measurement and Prediction of Lateral Torsional Buckling Loads of Composite Wood Materials: I-joist sections. *Forest Products Journal*, Vol. 55, No. 10, pp 43-48.

Hooley, R. F., & Madsen, B. (1964). Lateral stability of glued laminated beams. *Journal of the Structural Division*, *90*(3), 201-218.

Hu, Ye. (2016). *Lateral Torsional Buckling of Wooden Beams with Mid-Span Lateral Bracing*, University of Ottawa.

Hu, Y., Mohareb, M., & Doudak, G. (2017). Lateral torsional buckling of wooden beams with midspan lateral bracing offset from section midheight. *Journal of Engineering Mechanics*, *143*(11), 04017134.

Hu, Y., Mohareb, M., & Doudak, G. (2018). Effect of eccentric lateral bracing stiffness on lateral torsional buckling resistance of wooden beams. *International Journal of Structural Stability and Dynamics*, *18*(02), 1850027.

Leupold, J. (1726). *Theatrum pontificiale, or showplace for bridges and bridge construction: that is clear instructions on how not only to get across ditches, brooks and rivers in various ways, but also how to be in need of water with certain machines and a special habit Can Save Lives.*. (Vol. 7). Can be found with the author and Joh. Friedr. Gleditschen's seel. Son.

LP SolidStar Laminated Veneer Lumber (LVL). *Technical Guid 2900F_b- 2.0E.* https://lpcorp.com/media/1367/lp-solidstart-lvl-technical-guide-english.pdf.

Machado, S. P. (2010). Interaction of combined loads on the lateral stability of thin-walled composite beams. *Engineering structures*, *32*(11), 3516-3527.

Mahan, D.H. (1886). *A treatise of civil engineering*, John Wiley & Sons, New York.

Rankine, W.J.M. (1889). *A manual of civil engineering,* 17th Edition. Charles Griffin & Company, London.

Miller, J. F. (2009). *Design and analysis of mechanically laminated timber beams using shear keys*. Michigan Technological University.

Newmark, N., Siess, C., & Viest, I. (1951). Tests and analysis of composite beams with incomplete interaction. *Proc Soc Exp Stress Anal*, *9*(1), 75–92.

Pelletier, Benoit, and Ghasan Doudak. (2017). *Investigation of the Lateral Torsional Buckling Behaviour of Engineered Wood I-Joists with Varying End Conditions*. University of Ottawa.

Pelletier, B., & Doudak, G. (2019). Investigation of the lateral-torsional buckling behaviour of engineered wood I-joists with varying end conditions. *Engineering Structures*, *187*, 329-340.

Pellicane, P. J., & Bodig, J. (1984). Comparison of nailed joint test methods. *Journal of testing and evaluation*, *12*(5), 261-267.

Pleshkov, P. F. (1952). Theoretical studies of composite wood structures. *Soviet Union (In Russian)*.

Sapkás, Á., & Kollár, L. P. (2002). Lateral-torsional buckling of composite beams. *International Journal of Solids and Structures*, *39*(11), 2939–2963. https://doi.org/10.1016/S0020-7683(02)00236-6.

Sawata, K., Shigemoto, Y., Hirai, T., Koizumi, A., & Sasaki, Y. (2013). Shear resistance and failure modes of nailed joints loaded perpendicular to the grain. *Journal of wood science*, *59*(3), 255-261.

Simulia. (2011), *ABAQUS analysis user's manual (Version 6.11)*, Dassault Systemes.

Snow, J.P. (1895). Wooden bridge construction on the Boston and Maine railroad, *Journal of the Association of Engineering Societies*, 14:500-512.

St-Amour, Rémi, and Ghasan Doudak. Lateral Torsional Buckling of Wood I-Joist. Université d'Ottawa / University of Ottawa, 2016.

St-Amour, R., & Doudak, G. (2018). Experimental and numerical investigation of lateral torsional buckling of wood I-joists. *Canadian Journal of Civil Engineering*, *45*(1), 41-50.

Stussi, F. (1947). Zusammengesetze vollwandtra¨ ger. *International Association for Bridge and Structural Engineering (IABSE)*, *8*, 249–269.

Suryoatmono B. and Tjondro A. (2008). *Lateral-torsional Buckling of Orthotropic Rectangular Section beams.* Department of Civil Engineering, Parahyangan Catholic University, Bandung, Indonesia.

Wang, P., Huang, X., Wang, Z., Geng, X., & Wang, Y. (2018). Buckling and Post-Buckling Behaviors of a Variable Stiffness Composite Laminated Wing Box Structure. *Applied Composite Materials*, *25*(2), 449–467. https://doi.org/10.1007/s10443-017-9643-3.

Winistorfer, S. G., & Soltis, L. A. (1994). Lateral and Withdrawal Strength of Nail Connections for Manufactured Housing. *Journal of Structural Engineering*, *120*(12), 3577–3594. https://doi.org/10.1061/(ASCE)0733-9445(1994)120:12(3577).

Xiao, Q., et al. (2014). *Lateral Torsional Buckling of Wood Beams.* University of Ottawa.

Xiao, Q., et al. (2017). Numerical and experimental investigation of lateral torsional buckling of wood beams. *Engineering Structures*, *151*, 85-92.

Zahn, J. J. (1973). Lateral stability of wood beam-and-deck systems. *J. Struct. Div.,* 99(7), 1391-1408.

Zahn, J. J. (1984). Bracing requirements for lateral stability. *J. Struct. Eng.,* 10.1061/(ASCE)0733-9445(1984)110:8(1786), 1786–1802.

Ziemian, R. D. (2010). *Guide to Stability Design Criteria for Metal Structures*. John Wiley & Sons.

APPENDIX A- Joint Level Test Results of All Replications

This Appendix provides the load-displacement curve and stiffness obtained from repeat 1 to 5 of lateral and withdrawal experimental programs. Also, the average load-displacement curve of the 5 test replications, obtained by calculating the average of the displacements and the loads of the 5 tests replications, is provided.

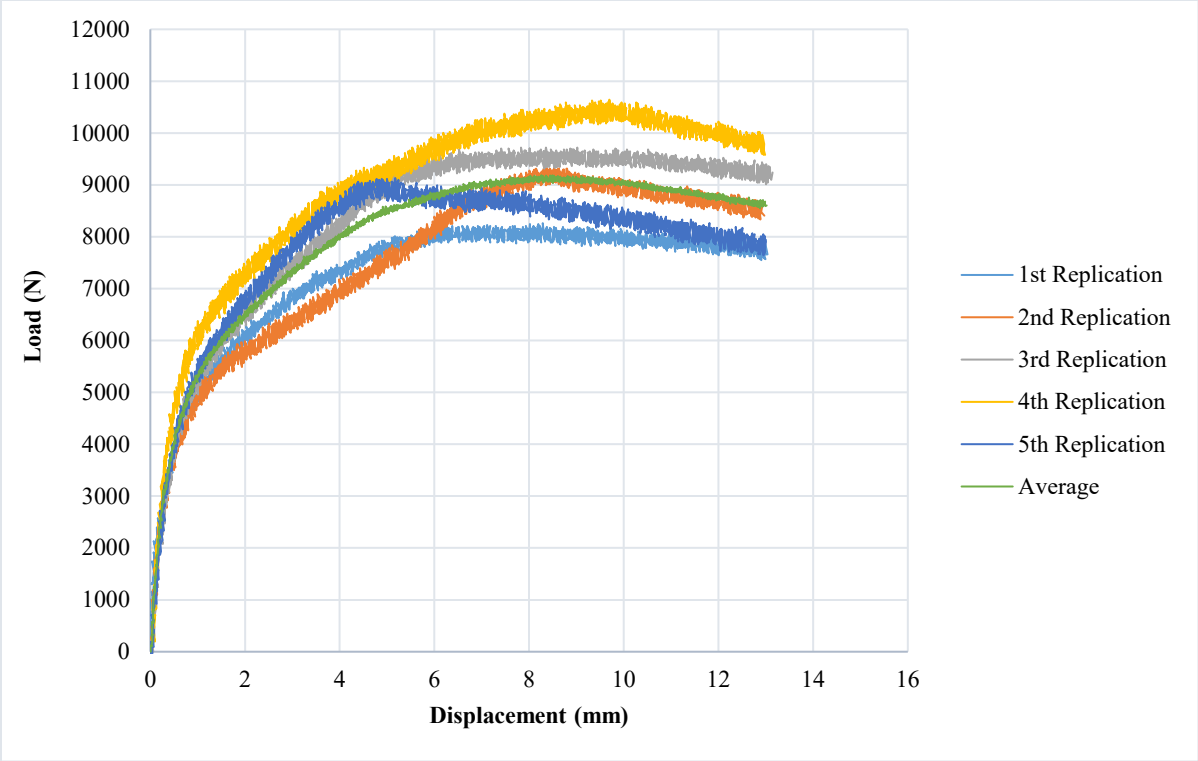

Figure A.1 Load-Displacement curves of replications 1 to 5 and their average for lateral test in parallel to grain of 3-1/2'' nails in LVL

Table A.1 Experimental results of replications 1 to 5 of K_{Par} for 3-1/2'' nails in LVL

Test Specimen	**K_{Par} (N/mm)**
1	1937
2	1842
3	1902
4	2113
5	1737
Average value (N/mm)	1906
COV %	7.25

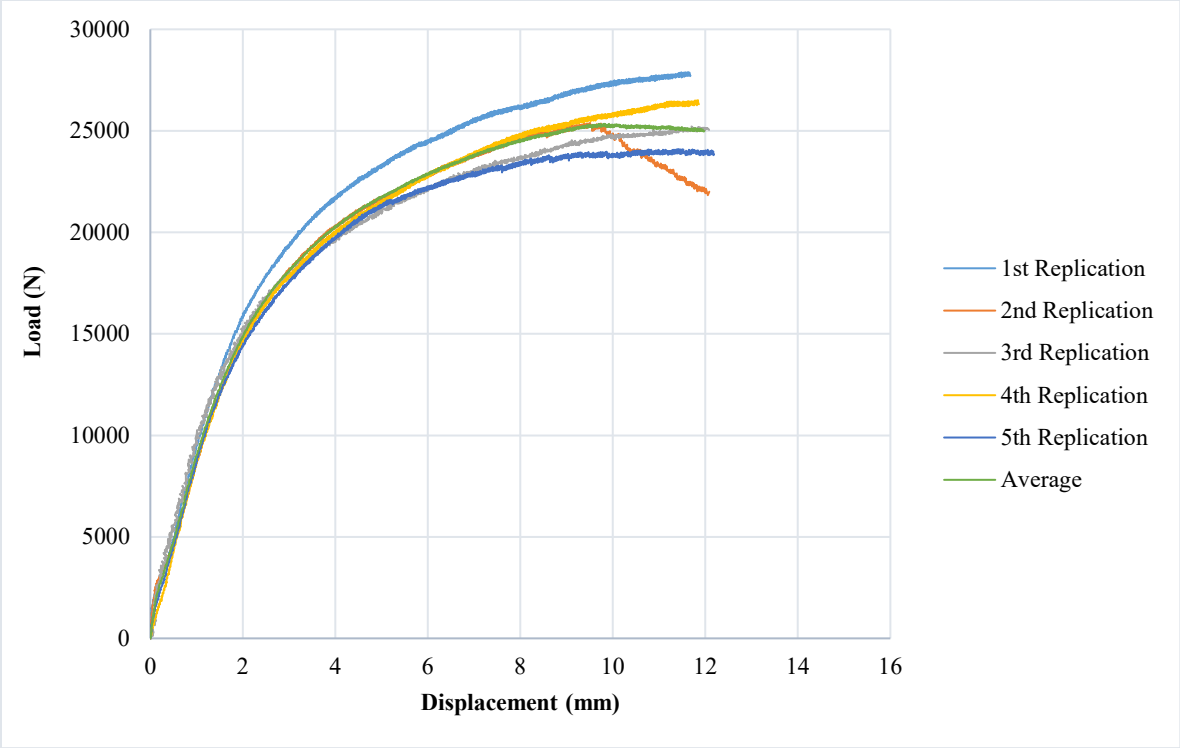

Figure A.2 Load-Displacement curves of replications 1 to 5 and their average for lateral test in parallel to grain of 6-3/4'' screws in LVL

Table A.2 Experimental results of replications 1 to 5 of K_{Par} for 6-3/4'' screws in LVL

Test Specimen	**K_{Par} (N/mm)**
1	2029
2	1743
3	2257
4	2058
5	1977
Average value (N/mm)	2013
COV %	9.17

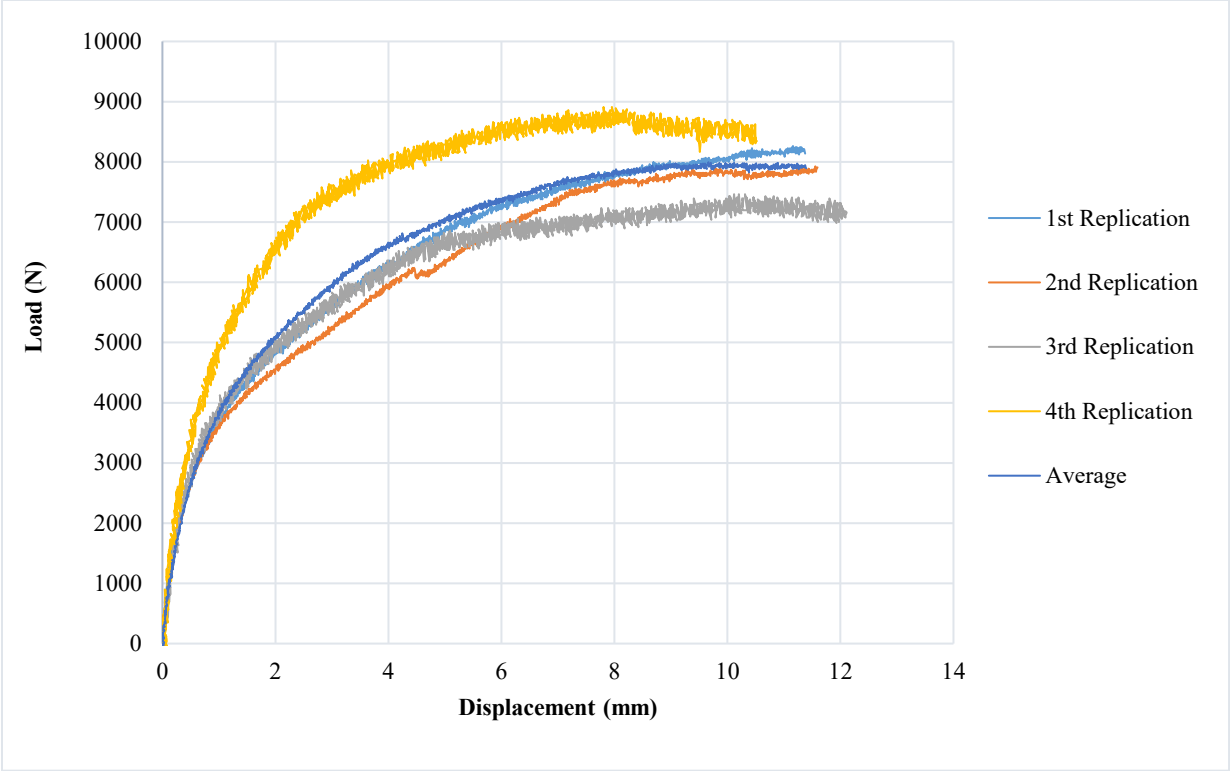

Figure A.3 Load-Displacement curves of replications 1 to 5 and their average for lateral test in perpendicular to grain of 3'' nail in SPF

Table A.3 Experimental results of replications 1 to 5 of K_{Per} for 3'' nails in SPF

Test Specimen	**K_{Per} (N/mm)**
1	1065
2	917.3
3	1418
4	1379
5*	-
Average value (N/mm)	1195
COV %	20.36

* There was an issue with the instrument

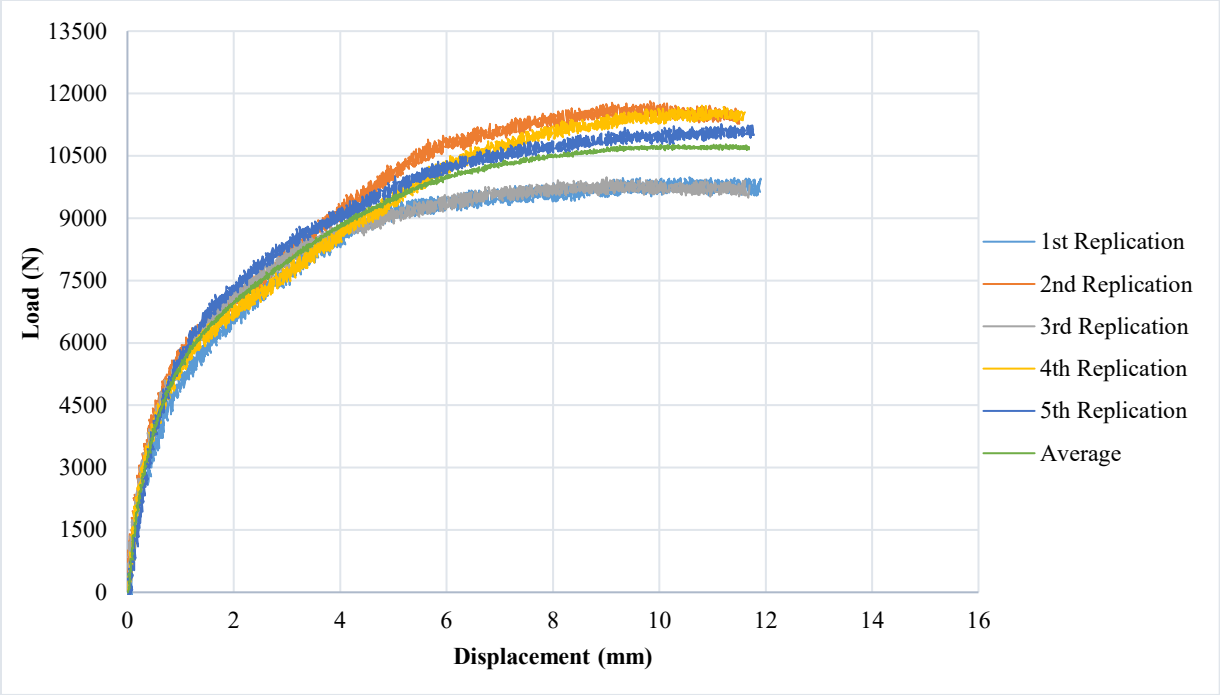

Figure A.4 Load-Displacement curves of replications 1 to 5 and their average for lateral test in perpendicular to grain of 3-1/2'' nails in LVL

Table A.4 Experimental results of replications 1 to 5 of K_{Per} for 3-1/2'' nails in LVL

Test Specimen	**Stiffness (N/mm)**
1	1649
2	1486
3	1698
4	1441
5	1596
Average value (N/mm)	1574
COV %	6.88

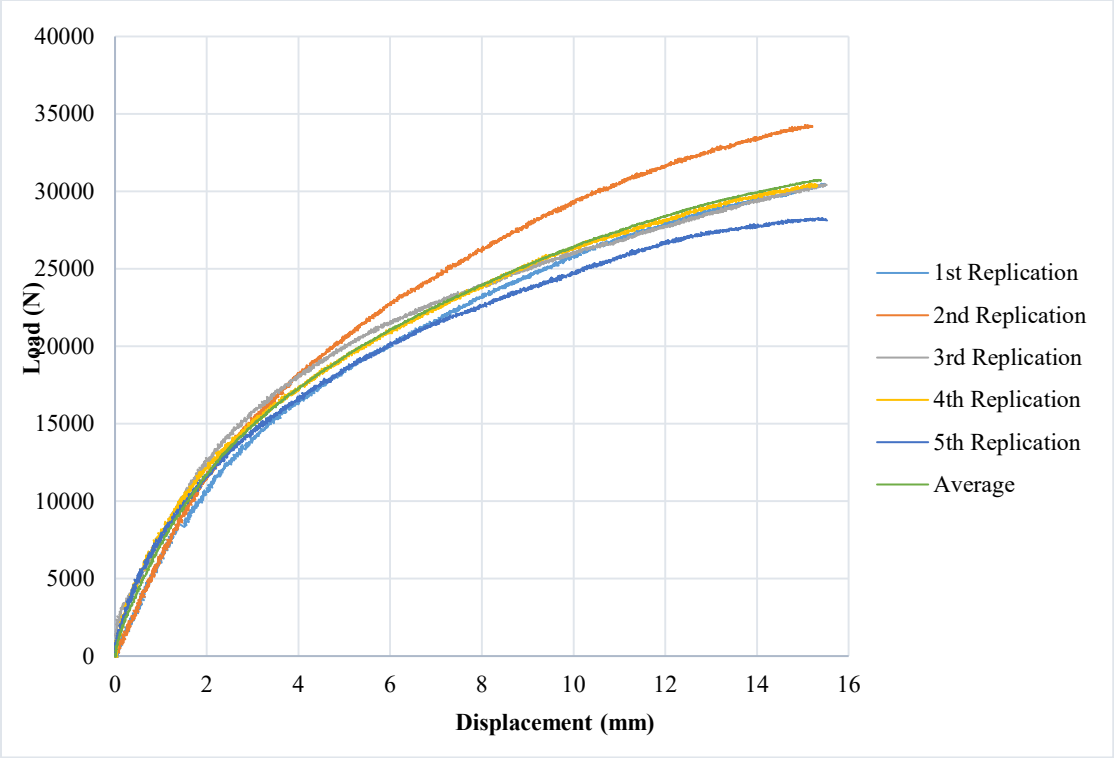

Figure A.5 Load-Displacement curves of replications 1 to 5 and their average for lateral test in perpendicular to grain of 6-3/4'' screw in LVL

Table A.5 Experimental results of replications 1 to 5 of K_{Per} for 6-3/4'' screws in LVL

Test Specimen	**K_{Per} (N/mm)**
1	1204
2	1268
3	1364
4	1342
5	1271
Average value (N/mm)	1290
COV %	4.95

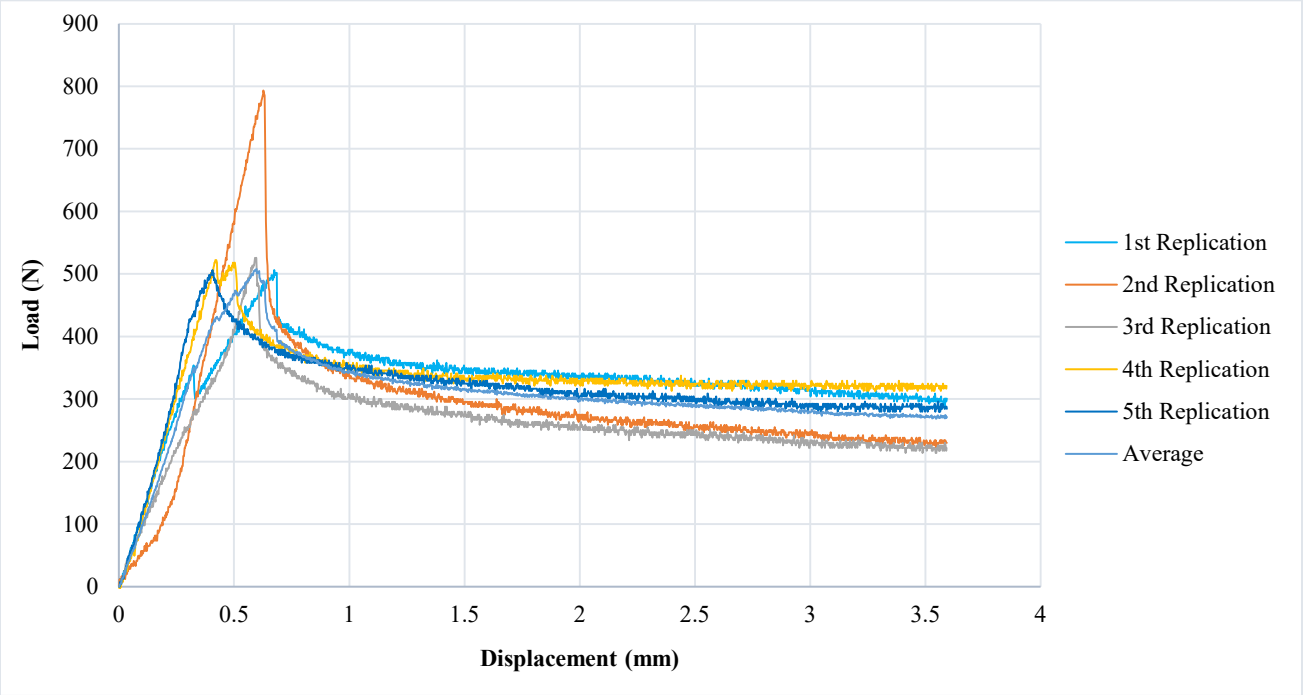

Figure A.6 Load-Displacement curves of replications 1 to 5 and their average for withdrawal test of 3'' nails in SPF

Table A.6 Experimental results of replications 1 to 5 of K_w for 3'' nails in SPF

Test Specimen	**K_w (N/mm)**
1	1198
2	1245
3	828
4	1295
5	1202
Average value (N/mm)	1154
COV %	16.15

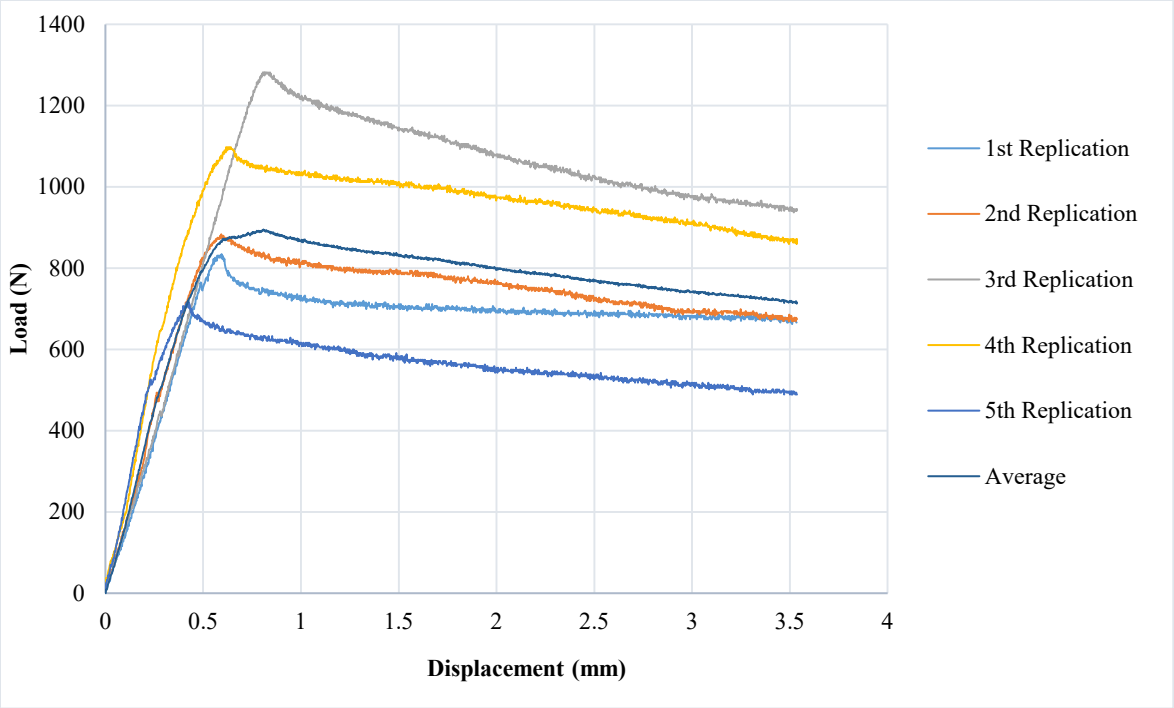

Figure A.7 Load-Displacement curves of replications 1 to 5 and their average for withdrawal test of 3-1/2'' nails in LVL

Table A.7 Experimental results of replications 1 to 5 of K_w for 3-1/2'' nails in LVL

Test Specimen	**K_w (N/mm)**
1	1511
2	1703
3	1584
4	2330
5	2253
Average value (N/mm)	1876
COV %	20.59

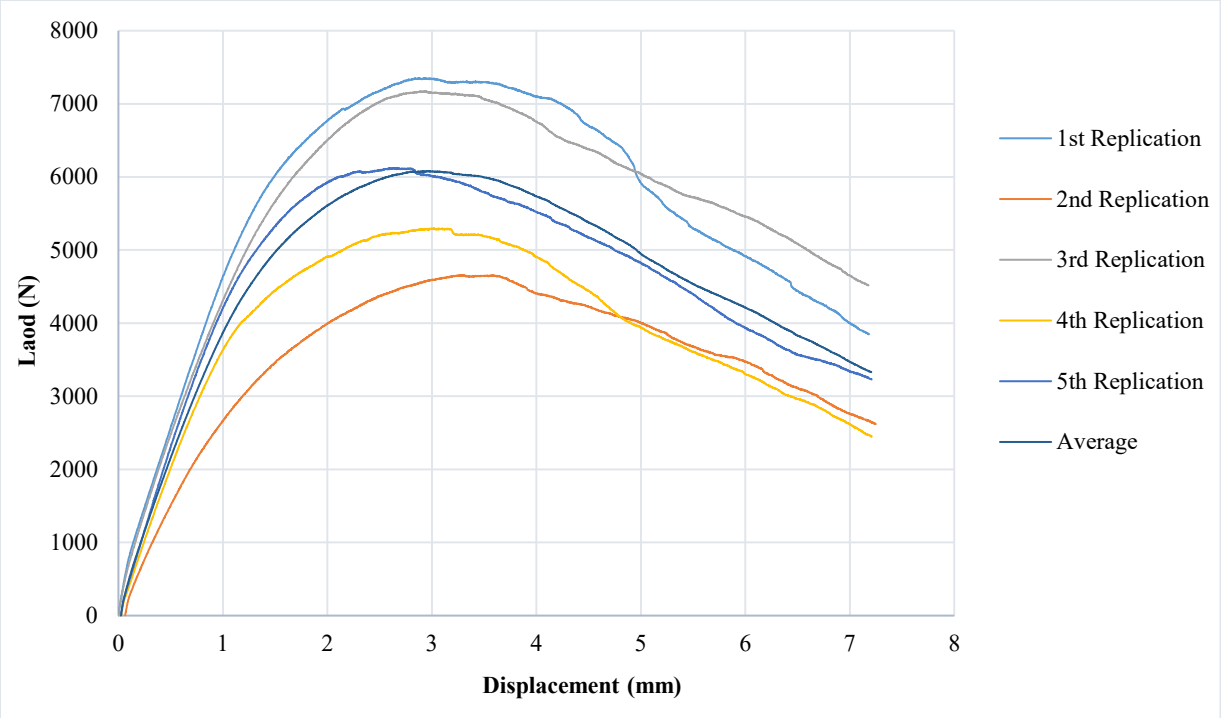

Figure A.8 Load-Displacement curves of replications 1 to 5 and their average for withdrawal test of 6-3/4'' screws in LVL

Table A.8 Experimental results of replications 1 to 5 of K_w for 6-3/4'' screws in LVL

Test Specimen	**K_w (N/mm)**
1	4469
2	2954
3	4306
4	4052
5	4588
Average value (N/mm)	4074
COV %	16.14

APPENDIX B- Input File Prepared with PYTHON Programme for Built-up Beam Model

The input file written for a 2-ply SPF built-up beam case 1 (Table 5.4) analyzed in Chapter 5.

```
*HEADING
2-Ply SPF built-up beam, case1
units (kg, m, s, N)
*PARAMETER
############################
Lb=2.515          #Beam length
################################
b=0.0381
h=0.14
bhalf=b/2
hhalf=h/2
e=7*b
c=8*b
f=14*b
g=15*b
################################
Nx=4          #Number of elements in x direction
Ny=16         #Number of elements in y direction
Nz=132        #Number of elements in z direction (longitudinal direction)
Q=Nx*Nz       #Number of elements in a layer
################################Species combination SPF
EbL=9500000000
EbT=646000000
EbR=646000000
GbLR=437000000
GbLT=437000000
```

```
GbRT=47500000
vbLR=0.347
VbLT=0.347
VbRT=0.469
################################
******AXIS 1
FIRSTAXIS1=1001                #FIRST NODE OF AXIS 1
LASTAXIS1=FIRSTAXIS1+1000000*Ny   #LAST NODE OF AXIS 1
******AXIS 2
FIRSTAXIS2=FIRSTAXIS1+Nz         #FIRST NODE OF AXIS 2
LASTAXIS2=FIRSTAXIS2+1000000*Ny   #LAST NODE OF AXIS 2
******AXIS 3
FIRSTAXIS3=FIRSTAXIS1+Nz+10000*Nx         #FIRST NODE OF AXIS 3
LASTAXIS3=FIRSTAXIS3+1000000*Ny           #LAST NODE OF AXIS 3
******AXIS 4
FIRSTAXIS4=FIRSTAXIS1+10000*Nx         #FIRST NODE OF AXIS 4
LASTAXIS4=FIRSTAXIS4+1000000*Ny        #LAST NODE OF AXIS 4
******AXIS 9
FIRSTAXIS9=100001001                #FIRST NODE OF AXIS 9
LASTAXIS9=FIRSTAXIS9+1000000*Ny       #LAST NODE OF AXIS 9
********AXIS 10
FIRSTAXIS10=FIRSTAXIS9+Nz           #FIRST NODE OF AXIS 10
LASTAXIS10=FIRSTAXIS10+1000000*Ny     #LAST NODE OF AXIS 10
*********AXIS11
FIRSTAXIS11=FIRSTAXIS9+Nz+10000*Nx         #FIRST NODE OF AXIS 11
LASTAXIS11=FIRSTAXIS11+1000000*Ny          #LAST NODE OF AXIS 11
```

********AXIS12

FIRSTAXIS12=FIRSTAXIS9+10000*Nx #FIRST NODE OF AXIS 12

LASTAXIS12=FIRSTAXIS12+1000000*Ny #LAST NODE OF AXIS 12

**********DEFINE CENTRAL NODES IN FIRST AND LAST SECTION,IN ORDER TO ENFORCE BOUNDARY CONDITIONS

E=FIRSTAXIS1+10000*Nx/2+1000000*Ny/2

EE=FIRSTAXIS2+10000*Nx/2+1000000*Ny/2

F=FIRSTAXIS9+10000*Nx/2+1000000*Ny/2

FF=FIRSTAXIS10+10000*Nx/2+1000000*Ny/2

**********DEFINE NODES FOR ENFORCING BOUNDARY CONDITIONS

******DEFINE HORIZONTAL AIXS IN THE FIRST END (AXIS AB, GH)

A=FIRSTAXIS4+Ny*1000000/2

B=FIRSTAXIS1+Ny*1000000/2

G=FIRSTAXIS12+Ny*1000000/2

H=FIRSTAXIS9+Ny*1000000/2

******DEFINE VERTICAL AIXS IN THE FIRST END (AXIS CD, IJ)

C=FIRSTAXIS1+10000*Nx/2

D=LASTAXIS1+10000*Nx/2

I=FIRSTAXIS9+10000*Nx/2

J=LASTAXIS9+10000*Nx/2

*******DEFINE HORIZONTAL AIXS IN THE LAST END (AXIS AABB, CCDD, GGHH, IIJJ)

AA=FIRSTAXIS3+Ny*1000000/2

BB=FIRSTAXIS2+Ny*1000000/2

CC=FIRSTAXIS2+Nx*10000/2

DD=LASTAXIS2+Nx*10000/2

GG=FIRSTAXIS11+Ny*1000000/2

HH=FIRSTAXIS10+Ny*1000000/2

II=FIRSTAXIS10+Nx*10000/2

JJ=LASTAXIS10+Nx*10000/2

*NODE

<FIRSTAXIS1>,<bhalf>,-<hhalf>,0

<LASTAXIS1>,<bhalf>,<hhalf>,0

<FIRSTAXIS2>,<bhalf>,-<hhalf>,-<Lb>

<LASTAXIS2>,<bhalf>,<hhalf>,-<Lb>

<FIRSTAXIS3>,-<bhalf>,-<hhalf>,-<Lb>

<LASTAXIS3>,-<bhalf>,<hhalf>,-<Lb>

<FIRSTAXIS4>,-<bhalf>,-<hhalf>,0

<LASTAXIS4>,-<bhalf>,<hhalf>,0

*NODE

<FIRSTAXIS9>,<c>,-<hhalf>,0

<LASTAXIS9>,<c>,<hhalf>,0

<FIRSTAXIS10>,<c>,-<hhalf>,-<Lb>

<LASTAXIS10>,<c>,<hhalf>,-<Lb>

<FIRSTAXIS11>,<e>,-<hhalf>,-<Lb>

<LASTAXIS11>,<e>,<hhalf>,-<Lb>

<FIRSTAXIS12>,<e>,-<hhalf>,0

<LASTAXIS12>,<e>,<hhalf>,0

**********DEFINE THE AXIS FOR ENFORCING UNIFORM MOMENT

*NGEN,NSET=AXIS5

<FIRSTAXIS1>,<FIRSTAXIS4>,10000

*NGEN,NSET=AXIS6

<FIRSTAXIS2>,<FIRSTAXIS3>,10000

*NGEN,NSET=AXIS7

<LASTAXIS2>,<LASTAXIS3>,10000

*NGEN,NSET=AXIS8

<LASTAXIS1>,<LASTAXIS4>,10000

*NGEN,NSET=AXIS13

<FIRSTAXIS9>,<FIRSTAXIS12>,10000

*NGEN,NSET=AXIS14

<FIRSTAXIS10>,<FIRSTAXIS11>,10000

*NGEN,NSET=AXIS15

<LASTAXIS10>,<LASTAXIS11>,10000

*NGEN,NSET=AXIS16

<LASTAXIS9>,<LASTAXIS12>,10000

**********GENERATE NODES ALONG AXIS 1-4

*NGEN,NSET=AXIS1

<FIRSTAXIS1>,<LASTAXIS1>,1000000

*NGEN,NSET=AXIS2

<FIRSTAXIS2>,<LASTAXIS2>,1000000

*NGEN,NSET=AXIS3

<FIRSTAXIS3>,<LASTAXIS3>,1000000

*NGEN,NSET=AXIS4

<FIRSTAXIS4>,<LASTAXIS4>,1000000

*NGEN,NSET=AXIS9

<FIRSTAXIS9>,<LASTAXIS9>,1000000

*NGEN,NSET=AXIS10

<FIRSTAXIS10>,<LASTAXIS10>,1000000

*NGEN,NSET=AXIS11

<FIRSTAXIS11>,<LASTAXIS11>,1000000

*NGEN,NSET=AXIS12

<FIRSTAXIS12>,<LASTAXIS12>,1000000

**********GENERATE BOUNDARY AXIS (AB, CD, HG, IJ, AABB, CCDD, HHGG, IIJJ)

*NGEN,NSET=AXISAB

<B>,<A>,10000

*NGEN,NSET=AXISCD

<C>,<D>,1000000

*NGEN,NSET=AXISAABB

<BB>,<AA>,10000

*NGEN,NSET=AXISCCDD

<CC>,<DD>,1000000

*NGEN,NSET=AXISGH

<H>,<G>,10000

*NGEN,NSET=AXISIJ

<I>,<J>,1000000

*NGEN,NSET=AXISGGHH

<HH>,<GG>,10000

*NGEN,NSET=AXISIIJJ

<II>,<JJ>,1000000

****

*NFILL,NSET=FIRSTENDSECTION1

AXIS1,AXIS4,<Nx>,10000

*NFILL,NSET=SECONDENDSECTION1

AXIS2,AXIS3,<Nx>,10000

*NFILL,NSET=BEAMINTERNAL1

FIRSTENDSECTION1,SECONDENDSECTION1,<Nz>,1

*NFILL,NSET=FIRSTSECTION2

AXIS9,AXIS12,<Nx>,10000

*NFILL,NSET=SECONDSECTION2

AXIS10,AXIS11,<Nx>,10000

*NFIL,NSET=BEAMINTERNAL2

FIRSTSECTION2,SECONDSECTION2,<Nz>,1

**********DEFINE FIRST C3D8 ELEMENT

*ELEMENT,TYPE=C3D8

1,1001,1002,11002,11001,1001001,1001002,1011002,1011001

*ELEMENT,TYPE=C3D8

8449,100001001,100001002,100011002,100011001,101001001,101001002,101011002,101011001

*ELEMENT,TYPE=SPRING2,ELSET=SPG1

16897,4041003,104001003

*ELEMENT,TYPE=SPRING2,ELSET=SPG2

16915,4041003,104001003

*ELEMENT,TYPE=SPRING2,ELSET=SPG3

16933,4041003,104001003

*SPRING,ELSET=SPG1

1,1

1153560

*SPRING,ELSET=SPG2

2,2

1194870

*SPRING,ELSET=SPG3

3,3

977310

*ELGEN,ELSET=BEAMELEMENT1

1,<Nz>,1,1,<Nx>,10000,<Nz>,<Ny>,1000000,<Q>

*ELGEN,ELSET=BEAMELEMENT2

8449,<Nz>,1,1,<Nx>,10000,<Nz>,<Ny>,1000000,<Q>

*ELGEN,ELSET=SPG1

16897,9,16,1,1,1,1,2,9000000,9

*ELGEN,ELSET=SPG2

16915,9,16,1,1,1,1,2,9000000,9

*ELGEN,ELSET=SPG3

16933,9,16,1,1,1,1,2,9000000,9

*SOLID SECTION,ELSET=BEAMELEMENT1,MATERIAL=MBEAM,ORIENTATION=MBEAM

*SOLID SECTION,ELSET=BEAMELEMENT2,MATERIAL=MBEAM,ORIENTATION=MBEAM

*MATERIAL,NAME=MBEAM

*ELASTIC,TYPE=ENGINEERING CONSTANTS

<EbL>,<EbT>,<EbR>,<vbLR>,<VbLT>,<VbRT>,<GbLR>,<GbLT>

<GbRT>

*ORIENTATION,NAME=MBEAM,SYSTEM=RECTANGULAR

0,0,1,0,1,1

*BOUNDARY

AXISAB,2

AXISCD,1

AXISAABB,2

AXISCCDD,1

<E>,1,3

<EE>,1,2

AXISGH,2

AXISIJ,1

AXISGGHH,2

AXISIIJJ,1

<F>,1,3

<FF>,1,2

*STEP

*BUCKLE

10,,,150

*CLOAD

AXIS5,3,1

AXIS6,3,-1

AXIS7,3,1

AXIS8,3,-1

AXIS13,3,1

AXIS14,3,-1

AXIS15,3,1

AXIS16,3,-1

*END STEP